PHYSICAL OCEANOGRAPHY OF THE BAIE DES CHALEURS, GULF OF ST. LAWRENCE

BY

CORINNE LE QUÉRÉ

DEPARTMENT OF ATMOSPHERIC AND OCEANIC SCIENCES,
MCGILL UNIVERSITY,
MONTRÉAL.

JULY 1992

A THESIS SUBMITTED TO THE FACULTY OF GRADUATE STUDIES AND RESEARCH IN PARTIAL FULFILLMENT OF THE REQUIREMENTS FOR THE DEGREE OF MASTER IN SCIENCE.

TABLE OF CONTENTS

RÉSUMÉ

Les remontées d'eau profonde le long de la côte nord de la Baie des Chaleurs ont été analysées à l'aide de séries temporelles de température et de salinité. Ces événements se déplaçaient d'est en ouest, de 40 à 85 km par jour et les correlations vent/densité étaient raisonnablement élevées. Un modèle à gravité réduite a simulé les remontées d'eau profonde en utilisant deux niveaux de densité différentes, les vents oscillants, et la topographie horizontale. La fréquence dominante allait de 4.5 à 10 jours.

Trois masses d'eau décrivent de façon appropriée les caractéristiques TS telles qu'observées en 1991. La première masse d'eau se loge entre la surface et le thermocline, la seconde se situe de part et d'autre de la thermocline, et la troisième se retrouve au fond.

Une circulation générale cyclonique a été observée d'août à octobre 1990. Le sens du courant était inversé dans les deux dernières couches et en surface à deux stations.

ABSTRACT

Time series of temperature and salinity from current meters moored in 1988 and 1990 along the north shore of Baie des Chaleurs were analyzed to characterize the frequency of upwelling events. Upwelling was found to propagate cyclonically with speeds of 40 to 85 km per day. Moderate correlations between σ_t and zonal wind stress were found. The interaction of buoyancy, topography, and oscillating wind stress simulated the upwelling in a reduced gravity model. The dominant frequencies of the upwelling events were approximately 4.5 to 10 days.

Three water masses, one between the surface and the thermocline, one straddling the thermocline, and one at the bottom, were found to describe nicely the TS properties of the water column, as observed from the 1991 CTD data.

The observed circulation, from August to October 1990, was cyclonic, with baroclinicity observed in the bottom two layers, and at two stations in the top layers.

REMERCIEMENTS

Je tiens à exprimer mes plus sincères remerciements aux gens qui m'ont aidé à accomplir ce travail.

À mon supperviseur R. Grant Ingram, qui a su m'accorder sa confiance et me communiquer ses connaissances si complètes et précieuses.

À Tineke van der Baaren, Thierry Reynaud, Jianping Gan, Jean-Claude Croteau, Claude Bélanger, Paul Peltola, Lawrence A. Mysak, John Bonnardelli, et Mohamed El Sabh qui m'ont apporté leurs conseils scientifiques et techniques, et qui ont contribué fortement à l'achèvement de cette recherche dans des délais raisonnables.

À mon époux, David Aubin, qui m'a soutenu moralement au cours de cette période, et du cheminement personnel qui l'a accompagné.

Enfin à mes parents, Nicole et Pierre Le Quéré, qui m'ont, par leurs exemples de tenacité, de persévérance, et de patience, montré le chemin de la vie.

Les fonds FCAR (C.L.Q. et R.G.I.), le projet OPEN, le CRSNG (R.G.I.) et le GIROQ ont supporté financièrement cette recherche. Merci de votre appui.

CHAPTER ONE

INTRODUCTION

1.1 GOAL OF THIS RESEARCH

The main goal of this work is to characterize the temperature and salinity fields of the Baie des Chaleurs (BdC), located on the north-west Gulf of St. Lawrence (GSL) (fig.1). To achieve this goal, the main water masses are identified, their evolution in space and time is discussed, the upwelling events occurring on the north shore are described, and a tentative sketch of the circulation of the bay is inferred.

This thesis is divided in three chapters (excluding the introduction and conclusion). Chapter 2 contains a simple description of the following physical components: topography and geological history, tides, runoff, ice cover, climatology, classification of the estuary and continuity between the BdC and the GSL. The aim of this chapter is to give an overview of useful, and often necessary information to understand the physical oceanography of the bay. Some of the results presented in chapter 2 were obtained from the literature. In chapter 3, the upwelling characteristics are described. Time series and Fourier analysis are used to enlighten the relationship between density and wind stress. The data set covers the north shore of the bay. In chapter 4, CTD and current meter data from 1990 and 1991 are analyzed to describe the water masses.

This work is part of a larger project, the Ocean Production Enhancement Network (OPEN), one of the 15 National Centers of Excellence. Studies are being done to understand the ecosystem of the BdC, one of the sites chosen for this study. Scallops were selected as the species to be studied intensively in the bay. Messier (1976) had noted that scallop catches were high in the late 60's, but fell dramatically following this period, when catches dropped below commercial profitability. The relationship of physical oceanography and biology in the study area involves the effects of variations in temperature, salinity and circulation as a control for spawning, the subsequent motion of larvae and juvenile animals, and the impact on grazing of physical forcing such as waves and currents.

1.2 LITERATURE REVIEW

Previous work on the physical oceanography of the Baie des Chaleurs was done by the Station de biologie marine de Grande-Rivière, from 1938 to 1967. Boudreault (1968) made a complete review of all the research done from 1924 to 1967, including everything published by the Station. This extensive description of studies concerning this period will not be repeated here, but instead, the focus will be put on the most relevant work.

Weekly spring and summer temperature data were analyzed at Grande-Rivière from 1952 to 1961 (Boudreault, 1967). He described and classified the water masses at this location and defined a surface layer with T>8°C, an intermediate layer with 3°C<T<8°C, and a deep layer with T<3°C. The surface layer was observed from the surface to 25 meters depth on average. The intermediate layer straddled the thermocline. It had the steepest temperature gradient and was found approximately over the 25 to 40m depth range. Maximum surface temperatures occurred at the beginning of August, while maximum temperature occurred at the beginning of October in the intermediate layer, and two weeks later in the deep layer. The thermocline was strongest (well stratified) in mid-July, when a thin surface layer was found.

Tiphane (1965), in a study at the scale of the bay, noted that the isotherms were deepening towards the south, colder water being found on the north shore. Lambert (1982) found similar results. He observed an east-west inclination of the isopycnals during spring, with colder, brackish water at the mouth of the bay, and a north-south inclination during summer, with colder, brackish water on the north shore. Lambert applied the Jalikee and Hamilton (1977) method for classifying profiles. The method consists mainly in joining similar profiles to detect main features or water masses. He found steep vertical gradients of temperature and salinity in the surface layer (0m-10m) during spring, and a mainly homogeneous surface layer covering a second layer characterized by steep gradients of temperature and salinity (10m-30m) during summer. Higher frequency fluctuations (such as during tidal cycles), were of secondary importance. His observations fit nicely with the observations of Boudreault (1967) mentioned

above, at least qualitatively. The two authors used different definitions for boundaries but their description of the layers and their evolution in time is similar. Lambert also noted that seasonal variations were much more important than tidal fluctuations.

Lacroix and Filtreau (1969) correlated annual variations in the stocks of zooplankton with annual variations of temperature for the years of 1961 to 1964. They found high stocks were related to long, hot summers, while low stocks were related to short, late summers and cold springs.

The hypothesis that internal tides might be important was discussed by Lauzier and Filtreau (1948). They observed oscillations of the thermocline consistent with tidal forcing. Lauzier (1957) also associated erratic variations of temperature and salinity at depth with tidal fluctuations. Lacroix (1958) mentioned the presence of internal tides, with a period of about 12 hours. None of these authors considered upwelling as a possible cause of internal fluctuations. Tremblay (1943), however, noted important jumps in surface temperature at Grande-Rivière, unrelated to tides. Brunel (1959), directly associated these types of fluctuations with upwelling. Lambert (1982) observed three upwelling events along the north coast, one in mid-June, one in mid-July, and one at the beginning of August. Finally, Bergeron (1992), in a study of the Bay of Tracadigache, west of Carleton, observed three drastic temperature and salinity fluctuations during the same period.

Tremblay (1943) observed a westward current on the north shore and an eastward current on the south shore. He suggested that the circulation on the north shore could be an extension of the Gaspé current, a strong current moving along the Gaspé peninsula, and that the circulation on the south shore would be related to the discharge of the bay. Using the dynamical method, Beaugé (1956) computed the geostrophic current regime. His computations implied a cyclonic circulation in the bay. Later, Bumpus and Lauzier (1965) observed low frequency fluctuations in the circulation pattern. They observed south-east to south-west currents at the extreme north east of the bay, and east to south-east currents near Miscou Island.

Lægendre and Watt (1970) used the surface and 10m mean temperatures recorded during 6 cruises done in 1956, at 3 week intervals, to deduce the presence of a cyclonic gyre at the center of the bay, south of Paspébiac. According to geostrophic motion, a cyclonic gyre would provoke a rise of the pycnocline at its center. The position of the minimum surface temperature was assumed to be the center of a gyre. Legendre (1971) also deduced the presence of a similar gyre from weekly data recorded at two stations in 1968 and 1969. One station was offshore of Grande-Rivière and the other offshore of Gascon. A strong stratification was present at both locations during the whole summer. He observed that the surface was warmer and less saline south of Gascon, but that the opposite situation prevailed at 25m depth. His conclusions were that upwelling was present in the center of the intermediate area of the bay, but could be observed at depth greater than 25m only. The higher surface temperature at Gascon, due to more mixing, would hide the upwelling in the surface layer. High primary production was observed in upwelling regions (Legendre, 1971). Lambert did not observe a gyre at the center of the bay.

Lauzier (1967) investigated the bottom drift at the entrance of the bay. He released seabed drifters from 1961 to 1965. A fraction of 35 to 50% of the recovered drifters stayed in the water for over 12 months. The observed bottom drift was towards the west along the north coast, and towards the east on the south coast. Bottom drifters released in the center of the bay were found several kilometers west.

Recently (1990-91), extensive mooring of current meters was undertaken in the bay. Part of these data are presented in this thesis.

1.3 SIMILAR BAYS AND ESTUARIES

Many other large bays and estuaries are found around the world. Among the most studied, the Chesapeake Bay, on the east coast of the United-States, is a long (280km), narrow (30km), estuary undergoing major fluctuations at time scales of 3 to 5 days (Chuang and Boicourt, 1989). The bay is connected to the Delaware estuary by an artificial canal. The Delaware estuary is shallow (mean depth of 7m) and has important subtidal variability induced by local and remote forcing

from the ocean and from Chesapeake Bay (Wong and Garvine, 1984; Wong, 1991).

On the west coast, the Columbia River estuary has high river discharge and strong tidal currents, which induces a high stratification and variability in the current regime (Officer, 1976). South of the Columbia River, the San Francisco Bay, a shallow estuary, is characterized by an irregular salinity gradient due to the influence of several rivers (Ford et al.,1990).

Closer to the BdC, the St. Lawrence estuary is a large, deep, estuary. Low frequency fluctuations induced by buoyancy and wind stress are often observed (Tee, 1991).

An extensive description of these and other smaller scale estuaries can be found in Officer (1976) and in Kjerfve (1988).

1.4 DATA

To describe the upwelling, two sets of current meter data were analyzed. The first set of 5 instruments was moored by John Bonardelli of Université Laval along the north shore for a period of 4 months, from July to December 1988. A second set of 3 instruments was moored by OPEN along the north shore, but at different locations, for a period of 6 weeks, from July to September 1990. Hourly wind data from the western region of the bay were analyzed and investigated as a possible cause of upwelling. Various data, such as tidal levels and runoff, were furnished by governmental services.

To describe the water masses, CTD (conductivity and temperature as a function of depth) data were plotted. The data come from 7 cruises which took place from June to October 1991 (as part of OPEN). The cruises lasted 2 to 3 days and covered the whole bay, for a total of 60 casts each cruise. The motion of the water masses is inferred with the help of progressive vector diagrams from 17 current meters moored (as part of OPEN) in 1990.

Details on the treatment of the data will be given at the beginning of chapters 3 and 4.

CHAPTER TWO

PHYSICAL SETTING

2.1 TOPOGRAPHY AND GEOLOGICAL HISTORY

The Baie des Chaleurs is 140 km long by up to 40 km wide. The bottom deepens eastward gradually from 20 to 100m, excluding a depression of 150m on the north-east side (fig.1). The bay ranges from latitude 47°30" to 48°30" N and longitude 64°30" to 66°30" W. A chain of mountains (the Chic Choc) is present to the north of the bay, on the Gaspé peninsula. Smaller mountains are present on the south shore.

Following the last glaciation, the bay was flooded, possibly as early as 14 000 years ago. A subsequent temporary retraction of the waters in the western area occurred around 8 000 to 10 000 years ago. This retraction was caused by a glacial rebound (Schafer, 1976). The present sedimentation started 6 000 years ago. It consists of a mixture of gravely sand to silty clay. Fine sediments are present along a trough located near the center of the bay, on an east-west axis. Coarser sediments are found near the edges. Schafer suggests that wave turbulence and bottom currents played an important role in reworking the sediments. The result of this reworking is that coarser sediments are also observed between Bonaventure and Gascon.

Two patches of high organic carbon matter were found in the sediments of the bay (Loring and Nota, 1973). Regions of high concentration of organic carbon matter are usually found in the deepest areas, which is not the case here, the BdC being relatively shallow. Both patches were located between the two coasts, one south of Paspébiac and Bonaventure, the other south of Grande-Rivière. The retention of organic matter in sediments is related to the depositional conditions and to the rate of organic productivity, but a direct relation between high productivity and high organic matter in the sediments cannot be assumed.

2.2 TIDES

Tidal ranges vary from average values of 0.8/3.2 meters (neap/spring tide) at Campbellton, on the extreme south-west coast, to 0.3/1.3 meters at Grande-Rivière, on the north-east coast (Canada, 1990). Pingree and Griffiths (1980) modeled the M_2 component of the tide in the GSL with a 2-dimensional model. They used their model results to calculate the Simpson-Hunter stratification parameter (Simpson and Hunter, 1974), and found tidal currents were not strong enough to break down the stratification anywhere in the BdC. El Sabh and Chassé (1992) developed a 2-dimensional, vertically integrated, barotropic model of the bay. They found good results in simulating fluctuations of the sea level using the 5 principal tidal forces: M_2, S_2, N_2, K_1, and O_1. El Sabh and Chassé (1992, personal communication) also computed the Simpson-Hunter parameter. Values were always larger than 2, implying that nowhere in the bay is the tidal mixing strong enough to destroy the vertical stratification. This supports the results of Pingree and Griffiths (1980). Both models are vertically integrated, linear models.

2.3 RUNOFF

The river runoff was evaluated for the period of January 1985 to October 1988. The data were kindly furnished by the Inland Water Survey of Canada. Figs.2 and 3 represent the average runoff for all rivers exceeding 50 m^3/s for both the Québec and for the New-Brunswick shore. Secondary river imput were summed up and plotted in fig.4. Each data point represents an average of a third of a month, or approximately 10 days. The total average runoff for the four years is plotted in fig.5.

A peak is always present in April or May, reaching 2500 m^3/s on average. A second peak was observed in October 1985, in December 1987, and in a few rivers during the other two years. The average runoff is 700 m^3/s during the secondary maximum. This peak is a consequence of increased precipitation in autumn, but is not always present and is not always observed during the same month. The average total runoff for summer fluctuates around 500 m^3/s.

The Restigouche River, at the west end of the bay, is the main contributor, with

~1/3 of the total amount. Other important rivers on the north shore are the Cascapédia, Matapédia, Bonaventure and Petite Cascapédia, with maximum runoff of 100 to 300 m^3/s. On the south shore, the Nepisiquit river has a comparable runoff with a maximum of 100 m^3/s. The total runoff on the north shore is approximately twice the runoff on the south shore. Similar values were observed in 1990 (M. El Sabh, 1991, OPEN annual report). The maximum runoff computed was 4 000 m^3/s, with a secondary peak in October. The difference in the maximum runoff comes mainly from the 10 day averaging performed on the present 1985-1988 data set.

2.4 ICE COVER

Over 90% of the bay is covered by ice from mid-December to mid-April, with brief open periods (F. Déry, personal communication). The reversal of air-sea heat flux occurs around the first week of March. The data studied by Déry covers a 25 year period from 1965 to 1988. Because the bay is a semi-closed area, influenced by weaker currents than those found in the GSL, the surface becomes rapidly covered with a thin ice sheet. Lower tidal levels also contribute to the rapid development of the ice cover. This ice sheet is easily broken, often leading to large open areas of short duration in January. A later ice peak is often seen after the bay has become almost ice free, early in spring. This is due to the advection of ice from the GSL.

The presence of an ice cover diminishes the exchange between the atmosphere and the ocean (Maslanik and Barry, 1989). It also affects the wind driven circulation when pack ice is present.

Matheson (1967) studied the factors that control ice formation in the GSL. The capacity of the airflow to remove heat from the surface for a long period was found to be determinant in the development of heavy ice conditions.

2.5 CLIMATOLOGY

The region of the BdC is classified as a Humid Continental region with cool summers and no dry seasons (Loring and Nota, 1973). Boudreault (1969)

computed average winds for a 10 year period from 1955 to 1965. He found that, while north-westerlies were mostly present in winter, easterlies were almost as frequent as westerlies during the summer. Spring and autumn winds were half way between the two. He also observed an inverse correlation between frequency and strength of the easterlies, and a direct correlation between the same parameters for westerlies. When easterlies were not frequent, they were very strong. When frequent westerlies were observed, strong winds were also observed also. He explained this by noting the association of easterlies with strong depressions rapidly progressing over the GSL, leading to extreme winds of short duration.

The GSL lies under several major storm tracks (Moran and Morgan, 1991). Most of the storms affecting this area are generated in the southern United-States and in Mexico. The storms travel north-east, following the upper level winds, and fade away near the Icelandic low, adjacent to Greenland. Storms are more frequent in autumn and winter.

Typical weather patterns observed inside a storm contain roughly three parts: a cold section, a warm section, and a section with high, constant precipitation (Moran and Morgan, 1991). The warm weather is on the south-east of the storm, winds are southwesterly. The cold weather is on the south-west side of the storm, winds are northwesterly. There is a cold front between these two sections, that can be accompanied with severe weather. The third section is north of the storm. High precipitation is found and the winds are easterlies. Because of the variety of weather encountered around a storm, the exact location of the storm center may modify greatly the direction of the winds affecting a given region and the type of weather present.

2.6 CLASSIFICATION OF THE ESTUARY OF THE BDC

The BdC has the characteristics of both a bay and an estuary. There are several ways to classify estuaries (Dyer, 1973). The first one, based on topographic characteristics, includes drowned river valleys, fjords and bar-built estuaries. The second one, based on the salinity structure, includes highly stratified, partly

mixed and homogeneous estuaries. Another classification proposed by Hansen and Rattray (1966) is based on salinity and velocity fluctuations.

Under the classification based on topography, the BdC corresponds best to the drowned river valleys definition (or coastal plain estuary). The bottom of the BdC deepens and widens towards the mouth. This definition was used by Tiphane (1965). Most estuaries fall under this category. For this reason, the classification proposed by Pritchard (1955) based on salinity structure, is most widely used.

Under the classification based on salinity structure, the BdC corresponds best to the partially mixed estuary definition. In this category, the ratio of river flow to tidal flow must be small, and the flow reverses at depth (Hansen and Rattray, 1966).

The characteristics of a partially mixed estuary are (Dyer, 1973): 1) An efficient exchange of salt and fresh water between the top and bottom layers. Fresh water is only found near the mouth of the river. 2) The discharge (seaward flow) and the compensating flow (landward flow) of the estuary are considerably increased by mixing of waters. 3) Surface and bottom layers are homogeneous, with a middle layer characterized by strong gradients of salinity and temperature. The bottom layer is often missing in the shallowest part of the estuary. 4) The east-west isobars (surfaces of equal pressure) usually slope towards the sea in the upper layer, and towards the land in the bottom layer. 5) The north-south isobars are strongly affected by the Coriolis force, with outflow and inflow deflected to opposite sides.

2.7 CONTINUITY BETWEEN THE BDC AND THE GSL

A natural border for the entry of the BdC can be defined by the transect between Miscou Island and Grande-Rivière (fig.1). East of this section stands the Gulf of St. Lawrence. Although the BdC is an intrinsic part of the GSL, few large scale studies of the GSL actually include data from the BdC. Because of their proximity and their interactions, it is important to understand oceanographic conditions present in the GSL. The GSL has been studied, if not extensively, at least constantly, for over 20 years.

The GSL contains three, well defined, water masses (Dickie and Trites, 1983). The characteristics of these water masses are summarized in fig.6. The values shown are mean summer values.

The first layer is defined as the water mass located between the surface and the thermocline (Lauzier et al., 1957). These authors analyzed the thickness of the surface layer for the years of 1914 to 1948. Their conclusions were based on temperature data. They observed that the thickness of this layer varies strongly with the seasons. It is formed at the end of the winter when heating, ice melt, and river runoff all contribute to restore a surface layer. The water column becomes very stable as summer progresses. Its thickness is near 25m in May. It diminishes to a minimum of 10m in July, and then slowly increases to a thickness greater than 60m in November. The layer cools down due to intense wind mixing and to decreasing air temperature. In winter, its temperature drops to a level where it is indistinguishable from the second layer, as is observed in the spring data when no thermocline is present. Spring and summer temperatures are greater than 2°C and can reach 18°C near Georges Bay in August. Salinity varies between 27 and 31 °/oo.

The second, or intermediate layer is found between 30 and 150m, with its center around 80m deep. Its temperature varies between 2°C and -1°C while its salinity varies between 32 and 33 °/oo. As the first layer deepens during the summer, this cold layer shrinks and may entirely disappear. Past studies have suggested that this layer may be formed locally in autumn and winter when intense mixing and cooling occurs at the surface. A fraction of the cold layer (estimated to be 35% by Petrie et al., 1988) may be advected from the Labrador shelf waters (Koutitonsky and Bugden, 1991).

The third or bottom layer extends from 150m to the bottom. It is formed by a mixture of Labrador and North-Atlantic waters outside of the gulf (Bugden, 1991). Its temperature varies between 2 and 5°C and its salinity varies between 33 and 34 °/oo.

The values mentioned above are representative of the whole gulf. One particular feature of the circulation in the GSL, the Gaspé current, has a significant influence on the BdC. The Gaspé current is formed partly from the discharge of

the St. Lawrence River and of the waters upwelled along the south shore of the lower St. Lawrence estuary and western GSL (Bugden, 1981). It originates in the lower St. Lawrence estuary, moves along the Gaspé Peninsula where it leaves the coast, and continues towards the Cabot Strait.

The Gaspé current is buoyancy driven, varies strongly with season, and has important non-linear properties (Ingram and El Sabh, 1990). Strong currents (>100 cm/s) of low salinity are present in spring. From May to November the salinity increases while the intensity of the current decreases (typical values of 60 cm/s), with minimum current values in July. Mertz et al. (1991) related this minimum to changes in wind stress pattern in July. Weaker wind stress would reduce the flow of upwelled waters, therefore reducing the contribution of deeper waters to the Gaspé current. High vertical shear is present in the top layer.

The center of the current displaces itself from nearshore in spring to about 14 km offshore in autumn. Isopycnals are strongly inclined from one shore to the other. They form a front about 10 km offshore, with colder water on the Gaspé side.

Several authors suggested that an extension of the Gaspé current could enter the BdC and influence its circulation (Boudreault, 1968). No specific research on this topic has been done.

CHAPTER THREE
UPWELLING CHARACTERISTICS FOR THE NORTH SHORE

3.1 INTRODUCTION

The main goal of this chapter is to characterize the upwelling events occurring on the north shore, and their subsequent propagation within the bay. To do this, time series data recorded at five locations along the north shore were analyzed. Data from three locations in both 1988 and 1990 were examined, only one location being common to both years.

We will show the importance of wind stress and topography in generating upwelling events, and, subsequent to the initial disturbance, how upwelling propagated cyclonically around the bay, playing a potentially important role in scallop ecology (Dickie, 1955). Qualitative and quantitative comparisons will be made between σ_t time series and wind stress. The background literature relevant to upwelling, a description of the data and methods, results and discussion follow.

3.2 BACKGROUND LITERATURE RELEVANT TO UPWELLING

From the studies by Sverdrup (1938), Wyrtki (1963) and Smith (1968), the following definition of upwelling is used: ascending motion for some minimum duration and extent, by which water from subsurface layers is brought into the surface layers and is removed from the area of upwelling by horizontal flow. As a consequence of vertical motion in the water column, nutrients, which are often more abundant near the bottom, are brought up to shallower depths, modifying the environment (Ryther, 1969; Cushing, 1971; Babin et al., 1991).

Ekman transport is the dominant cause of upwelling. Steady winds blowing parallel to a coast lying to its left (right) in the northern hemisphere (southern hemisphere), will provoke mass transport offshore with the combined effects of friction and the Coriolis force. This offshore Ekman drift is balanced by coastal

upwelling, resulting in horizontal density gradients. In the geostrophic adjustment process, backward propagating internal Kelvin waves (with respect to the wind direction) are excited at the beginning of the forced region establishing alongshore variations and changing the flow completely (Philander and Yoon, 1982).

Internal Kelvin waves propagate in a stratified environment of constant depth, with the coast on their right (left) in the northern hemisphere (southern hemisphere). They are trapped within one internal Rossby radius of deformation from the coast. Gill and Clarke (1974) showed that, while the motion normal to the coast is locally determined, the density changes along the coast depend on the wind stress at earlier times and at other locations. Internal Kelvin waves can increase or decrease in amplitude depending on the local wind stress as the wave progresses along the coast. An offshore surface circulation would increase the wave amplitude when a crest is passing and decrease it when a trough is passing. The speed of propagation equals the internal gravity wave velocity. Philander and Yoon (1982) added that local forcing could double that speed.

In the presence of topography, the generated waves are hybrids between continental shelf waves and internal Kelvin waves: Coastal Trapped Waves (CTW) (Gill and Clarke, 1974). For strong stratification, the current structure and wave characteristics are similar to those of internal Kelvin waves (Mysak,1980). The effects of stratification versus topography may be quantified with the parameter $S=(NH/fL)^2$, where N is the Brunt-Väisälä frequency, H is the depth scale, L is the offshore length scale, and f is the Coriolis parameter (Huthnance et al., 1986). When S tends to infinity, the coast can be approximated as a coastal wall, while if S is close to 1, CTW must be considered. Stratification decreases the effect of friction through the inhibition of vertical motion. Waves moving in a highly stratified environment with bottom topography will propagate farther before decaying, and their speed of propagation will increase (Brink, 1982; Chapman, 1983). Gill and Clarke (1974), using a model including both stratification and topography, found that the displacement of the thermocline in the presence of bottom topography was about 75% of the value it would have had in the absence of topography. In the case for weak stratification, the generated CTW must be analyzed by decomposition into modes, and they can be observed

with sea level measurements. The sea level changes by 1cm for every 1.45m displacement of the thermocline (Gill and Clarke, 1974).

Killworth (1978) investigated the effects of coastline geometry using a 3-dimensional, linear, uniformly stratified, ocean model. His experiments showed that Kelvin waves lose a great deal of energy by scattering when passing over a ridge. This energy goes into low wave modes, explaining why mainly Kelvin waves of lower modes are found in nature. Crepon et al. (1984) also looked at the effects of coastline geometry. Using a 2-layer ocean model, they showed that Kelvin waves could be generated by wind blowing parallel to a coast of variable geometry. A ridge in the coast would be the center of backward propagating Kelvin waves leading to reverse currents.

Crepon and Richez (1982) showed that longshore variability in the wind stress could lead to similar results. For discontinuous surface stress, laboratory experiments demonstrated offshore cyclonic or anticyclonic eddies might be generated in the stress-free region with bottom topography in the form of a ridge (Narimousa and Maxworthy, 1986).

Upwelling is frequently observed around the world. One of the best known regions, the coast of Peru, was the site of the Coastal Upwelling Ecosystems Analysis Joint Experiment (Brink et al., 1980). The waters over the shelf were found to respond to local alongshore wind stress with a time lag of 0.5 to 2 days. Free CTW were found to dominate the variability of the alongshore currents in the upper 200m. Forcing of these waves was poorly related to wind stress. The main period of upwelling takes place from March to May when the winds are equatorward.

North-west Africa is another region where many studies have been completed. Barton et al. (1977) analyzed five upwelling events from February to April, when the trade winds blowing from the north-east are favorable for Ekman transport. They found upwelling occurred in response to variations in the wind pattern. Crepon et al. (1984) examined infrared satellite images of the Cape Verde region. In an application of their model discussed earlier, they showed the importance of coastline geometry in localizing the upwelling centers in this area.

Along the Australian coast, McClean-Padman and Padman (1991) studied upwelling on the inner shelf and surf zone near Sydney. They found that about half the events were produced by wind forcing of approximately 0.2 Pa (N/m^2). The wind stress led the upwelling by 1 to 2 days. The other observed events were caused by mesoscale eddy encroachment. CTW were extensively studied during the Australian Coastal Experiment (ACE). They were found to propagate along the south-east coast of the continent (Freeland et al., 1986).

On the west coast of Vancouver Island, Beak Consultants Limited (1979) completed statistical studies of upwelling. They found that upwelling events were only weakly correlated to wind stress. Although they could relate some individual events to wind forcing, several events remained unexplained. Freeland and Denman (1982) also studied upwelling off the west coast of Vancouver Island. They found that one of the larger upwelling zones was provoked by strong coastal flows passing over a canyon. Finally, CTW were analyzed by Yao et al. (1984) who found that the lowest two modes, locked in phase, were most appropriate in describing the observed signal off the coast of Vancouver Island.

Csanady and Scott (1974) observed coupled upwelling and downwelling on the north and south shores of Lake Ontario. Halpern (1974) explained that between wind impulses, the pycnocline relaxes but does not reach horizontal equilibrium before the next impulse. Upwelling events would start from a quasi-steady summer mean state characterized by a weakly inclined pycnocline. Subsequent cyclonic propagation was found. Velocities were approximately 0.5 m/s. Csanady (1983) summarized these results.

In the Gulf of St. Lawrence, Rose (1988) studied temperature fluctuations in relation to wind stress and cod migration, in the north-east sector. His main conclusions were that alongshore winds generated upwelling with periods greater than 3 days. The variations were almost synchronous over the whole region of study (150 km). Yao (1986) modeled the response of currents to local wind forcing in Trinity Bay, north-east Newfoundland. He found that internal Kelvin waves were forced by wind stress, which agreed reasonably well with observation.

3.3 DATA AND METHODS

3.3.1 OCEAN DATA

Two data sets of temperature and salinity were used. In 1988, temperature and salinity time series were obtained from five current meters moored (by John Bonardelli of Université Laval) at three locations: Gascon, Bonaventure, and Carleton (fig.1). Table 1a summarizes the depth and mooring information for each of the current meters. The deeper current meters at Gascon and Carleton were 1m above the bottom. These time series cover a 4 month period from August to December. In 1990, time series from three current meters moored (by OPEN) at again three locations were analyzed: Grande-Rivière, Paspébiac, and Bonaventure (fig.1). Table 1b summarizes the related information. The time series are six weeks long, from August to October.

a	Location	Depth(m)	Record Length	
Gascon		3	30 July	25 Nov.
Gascon		23	28 July	3 Dec.
Bonaventure		2	31 July	5 Dec.
Carleton		1	19 Aug.	14 Dec.
Carleton		11	27 July	6 Dec.

b	Location	Depth(m)	Record Length	
Gr.-Rivière		23	24 Aug.	17 Oct.
Paspébiac		18	23 Aug.	8 Oct.
Bonaventure		13	22 Aug.	13 Oct.

Table 1: Time series depth and length for 1988 (a) and 1990 (b)

The distance between Gascon and Bonaventure is approximately 55 km, slightly greater than the separation between Bonaventure and Carleton. A small bay lies between the two latter stations, in which the Caspedia River enters the BdC. Grande-Rivière and Paspébiac are separated by 85 km, Paspébiac and Bonaventure by 25 km. All 1990 stations were in the eastern half of the bay, while the 1988 stations covered the center and northwestern area.

Aanderaa RCM-4 current meters were used for all moorings. The accuracy of the sensors was ±0.05°C for the temperature, ±0.0025 S/m (Siemens/m) for the conductivity, 1% of the full scale range for the pressure, ±1 cm/s or 2% of the actual speed whichever is greater, ±7.5° in the direction for speeds from 2.5 to 5 cm/s, and ±5° for speeds over 5 cm/s. The threshold velocity was 2.5 cm/s. The original data were recorded every 15, 20, or 30 minutes.

The σ_t time series were first computed from the temperature and salinity data. The output series were smoothed, decimated to hourly, and low pass filtered using a moving average block of 36 hours. The first block of 36 hours was cut off (Godin, 1972). A spectral analysis was done to identify at which low frequency upwelling events are taking place. Finally, cross-correlations were made between the shallow time series (all locations in 1988) and the deep time series (Gascon and Carleton in 1988, Grande-Rivière, Paspébiac, and Bonaventure in 1990).

3.3.2 WIND DATA

Meteorological time series from the stations at Charlo and Miscou, located on both sides of the bay (fig.1), were furnished by the Atmospheric Environment Service of Canada. They included hourly winds at Charlo for 1988 and 1990. Wind data from Miscou were unusable for the periods of interest. Comparison was made between Miscou and Charlo wind stress for 1987 to ensure that the data set at Charlo was reliable. It was found that, although the magnitude of the wind stress was greater at Miscou (1.5 to 2 times), the maximum correlation was 0.80 at zero time lag (fig.7).

Wind data were treated like the ocean data except that no decimation was performed since the data were sampled hourly. Kinematic wind stress was first calculated and then low pass filtered with the same filter as before. The kinematic stress, F_i, was calculated from the following relation (Csanady 1983):

$$F_i=(\rho_a/\rho_w)\, C_{10} W_i\, W$$

where ρ_a is the density of the air, ρ_w is the density of the water at the interface, W_i is the magnitude of the wind vector along the coast (270°), W is the absolute magnitude of the wind, C_{10} is a drag constant with value of $1.6\text{x}10^{-3}$ for W<7m/s, $2.5\text{x}10^{-3}$ for W>10m/s and increases linearly between the two points. The

relations between the kinematic stress, the friction velocity (u_i^*), and the wind stress (τ_i) are as follows:

$$F_i = u_i^{*2}$$

$$\tau_i = \rho_w u_i^{*2}$$

The wind stress time series will be used later for cross-correlation analysis with the σ_t data.

3.4 RESULTS

Figs.8 (1988, shallow stations), 9 (1988, deep stations) and 10 (1990) show the density and wind stress time series. By examining all oceanic data sets, we see that upwelling occurred more frequently during the months of August, September and at the beginning of October. After mid-October, the events were hard to identify. The water column tends to be less stratified by mid-fall due to the increased wind mixing and decreasing air temperature. The slowly decreasing water temperature trend may be confused with weak upwelling. During this period, wind stress at Charlo oscillated from positive to negative values. The maximum amplitude of the zonal component was around 0.05 Pa until mid-October, while the amplitude of the meridional component reached 0.01 Pa. After this period, amplitudes doubled. According to the differences seen at Miscou in 1987, the magnitude of the zonal wind stress at the mouth of the bay could reach values of 0.10 Pa.

Observation of the wind stress and density pattern for 1988 showed the presence of two regimes. The first regime was active from the beginning of the series until mid-October. During that time, the wind stress at Charlo was relatively weak, the water column was well stratified and underwent severe fluctuations. The second regime was active from mid-October until the end of the series. The wind stress was relatively strong, the water column was less stratified and underwent small fluctuations. All σ_t time series varied similarly, except for Carleton (1m) which underwent severe fluctuations until the end. Time series from 1990 were too short to make similar comparisons.

Because wind driven upwelling could be clearly seen in the density time series only during the first regime, all correlations with the wind stress were done with a shortened series, ending on 22 October. All correlations with Gascon (3m) were done with a shortened series, ending 30 September. This particular station showed a drastic decrease in salinity starting in October (fig. 8). The presence of this step in the data has the effect of reducing the importance of the smaller fluctuations in density due to upwelling. This decrease in salinity may have been due to increased river runoff affecting this location. The effects of destratification on the generation of CTW will be discussed later.

Vertical velocities were calculated from the vertical migration of isopycnals at Carleton in 1988. Values ranged from 4.7×10^{-5} m/s to 8.3×10^{-5} m/s, with an average value of 6.0×10^{-5} m/s or 5.2 m/day.

3.4.1 CROSS-CORRELATIONS

The cross-correlation analysis for the three shallow locations gave the following results (fig.11a). Upwelling at Gascon (3m) was correlated to the upwelling at Bonaventure (2m) with a 11 hour lag, and a correlation coefficient of 0.74. Gascon (3m) also preceded Carleton (1m). The maximum correlation occurred at a lag of 21 hours with a coefficient of 0.45. Carleton (1m) and Bonaventure (2m) had a maximum correlation coefficient of 0.74 at zero time lag.

Cross-correlations computed between the deep stations, Gascon (23m) and Carleton (11m), showed a maximum correlation coefficient of 0.71, with Carleton following Gascon by 53 hours (fig. 11c).

At Gascon, the cross-correlation between the two levels is 0.49, with a 23 hour lag. At Carleton, it is 0.80 with a 13.5 hour lag (fig. 11i). At these two stations, the upwelling was observed in the bottom layer first.

The 95% significance level was computed using the Student-T distribution (Jenkins, 1968). It ranged from 0.27 to 0.41.

From the 1990 data, cross-correlations between Grande-Rivière and Paspébiac were maximum with Grande-Rivière leading by 21.5 hours, with a correlation coefficient of 0.64. Grande-Rivière also led Bonaventure with a time lag of 37

hours and a correlation coefficient of 0.50. Finally, Paspébiac led Bonaventure with a time lag of 10 hours and a correlation coefficient of 0.91. The 95% significance level was 0.34 for all these correlations (fig. 11f).

a	Gascon (23m)		Carleton (11m)		Gascon (3m)		Bonaventure (2m)		Carleton (1m)	
Zonal Stress	0.54	-10	0.60	16.5	0.52	14.5	0.70	27.5	0.74	29
Meridional Stress	0.40	88	0.23	148						
Gascon (23m)			0.71	53	0.49	23				
Carleton (11m)									0.80	13.5
Gascon (3m)							0.74	11	0.45	21
Bonaventure (2m)									0.74	0

b	Grande-Rivière(23m)		Paspébiac (18m)		Bonaventure (13m)	
Zonal Stress	0.36	-60	0.53	1.5	0.58	10.5
Meridional Stress	0.45	28	0.38	47	0.26	57
Gr.-Rivière(23m)			0.64	21.5	0.50	37
Paspébiac (18m)					0.91	10

Table 2: Cross-correlation values for 1988 (a) and 1990 (b). The first number is the magnitude of the maximum correlation and the second number is the corresponding time lag. Positive values imply that the station to the left leads the station on top.

Correlations with the wind stress were as follows: In 1988 for the shallow stations, the zonal wind stress correlated best with Gascon (3m), Bonaventure (2m) and Carleton (1m), with values of 0.52, 0.70 and 0.74, for time lags of 14.5, 27.5 and 29 hours (fig. 11b). Significance levels are 0.60 for Gascon (3m), 0.32 and 0.25 for Bonaventure (2m) and Carleton (1m), respectively. For deeper stations, the zonal component correlated best with Gascon (23m) and Carleton (11m) with values of 0.54 and 0.60, time lags of -10 and 16.5 hours, and significance levels of 0.33 (fig. 11d). Negative lags imply the upwelling preceded wind stress. An explanation for this result will be given in the discussion. In 1990, for Grande-Rivière, Paspébiac, and Bonaventure correlations with the zonal

wind stress had maximum values of 0.36, 0.53 and 0.58, for time lags of -60, 1.5 and 10.5 hours (fig. 11g). Correlations between the meridional component of the wind and σ_t for all stations were low (fig. 11 d and h).

All correlations between density time series exceeded the 95% confidence level. All correlations between zonal wind stress and density time series exceeded the 95% confidence level except at Gascon (3m) in 1988. Only Grande-Rivière and Paspébiac in 1990 were above the 95% significance level for their correlation with meridional wind stress. Table 2a (1988) and 2b (1990) summarize these results.

3.4.2 SPECTRAL ANALYSIS

From the Fourier analysis of the σ_t truncated series with 10 degrees of freedom, two significantly different peaks in 1988 were observed (fig. 12 and 13). The first one, the most energetic, was around 10 days. This peak was also seen at Carleton (11m), and at Gascon (23m) with a slight shift to higher frequencies, and in the zonal wind stress. The second peak was around 4.5 days. It was seen at the same stations and was present in the meridional wind stress spectra. The shallow stations showed more disparate spectra but with most of the energy still at lower frequencies. In 1990, most of the energy was found in the lower frequencies, but no distinct peaks were observed (fig. 14).

The energy associated with the principal lunar tide, 0.52 days, is indicated with an arrow on each density spectrum. It was one to two orders of magnitude less than the energy associated with low frequencies. Stronger values were at Carleton, which has the highest recorded tidal levels in the BdC. The energy associated with the diurnal tides was weak and did not show on most of the plots. The energy associated with the day/night cycle, 1.0 days, is indicated with an arrow on each wind spectra. It was more important than the low frequencies only in the meridional wind stress spectrum in 1988. In the other wind stress spectrum, it was 5 to 10 times less energetic than the low frequencies. The day/night cycle was not always clear, as it was contamined by high frequencies.

3.5 DISCUSSION

The most important thing to note is the correspondence of almost every upwelling event at Gascon (23 m) and Carleton (11 m) in 1988 (fig. 9). Five major events ($\Delta\sigma_t/\Delta t$ >1 kg/m^3) occurred between the end of July and the first week of September, followed by one minor event and a sixth major event around 20 September. Following this period, density oscillated at all locations, with smaller amplitudes. These oscillations were partly due to fresh water input, as a consequence of increased precipitation in autumn. The same kind of direct correspondence was present in 1990, where four major events occurred at all stations (fig. 10). There was also a one to one relation between upwelling events and the positive zonal wind stress. The amplitude of the upwelling was greater in 1988 than in 1990, as was the amplitude of the zonal wind stress.

3.5.1 THE PROPAGATION OF THE UPWELLING

From a visual inspection of the density data, as well as from σ_t correlations, cyclonic propagation of upwelling events within the bay was clearly seen. We will first discuss this result and then speculate on the initial causes of the perturbation.

Until mid-October, the environment was highly stratified and S>>1. The propagating wave is treated as a simple internal Kelvin wave and topography is considered a perturbation. When mixing increased by mid-October, the wave pattern became more complex and should be decomposed into modes and modeled with topographic effects included. In order to make accurate predictions of the upwelling around the bay, a more extensive study should include modal decomposition of the signal, and individual events should be followed around the bay.

Only one set of correlations did not clearly show cyclonic propagation of upwelling. In 1988, Bonaventure (2m) and Carleton (1m) were highly correlated with one another but with a zero lag. Compared with the 53 hour lag for the deeper instruments, it is a significant difference. Several factors may explain this difference: 1) An intensifying wind stress was accompanied by more mixing which led to a surface layer with higher density. 2) The shallow instruments were more subject to meteorologically driven perturbations (temperature, radiation,

etc.) and fresh water input. 3) Time lags and duration varied between events and between locations depending on the stratification of the water column prior to one specific event. Shallow instruments were more affected since they were above the thermocline. The fact that upwelling was observed in the bottom before the surface at Gascon and Carleton tends to confirm the importance of mixing at the surface. For these reasons, the deeper instruments are thought to be more reliable for computation of travel speeds. All other correlations between density time series showed cyclonic propagation. Using these lags, the speed of propagation can be measured.

In 1988, the speed of propagation of the perturbations around the bay was 0.55±0.01 m/s. In 1990, three values can be calculated: 0.83 m/s between Grande-Rivière and Bonaventure; 1.10 m/s between Grande-Rivière and Paspébiac; and 0.69 m/s between Bonaventure and Paspébiac. The average velocity was 0.90±0.01 m/s. The theoretical two layer internal gravity wave velocity for shallow water is (Pond and Pickard, 1983):

$$C = \sqrt{\left(\frac{g(\rho_2 - \rho_1)}{\rho_2}\right)\left(\frac{h_1 h_2}{h_1 + h_2}\right)}$$

where ρ_1 is the density of the first layer, ρ_2 is the density of the second layer, h_1 is the depth of the first layer, and h_2 is the depth of the second layer. In the western area of the bay, the estimated values are ρ_1=1022 kg/m^3 , ρ_2=1024 kg/m^3 (from chapter 4), h_1=15m, and h_2=15m. The related velocity is C=0.46 m/s. On the eastern side of the bay the depth of the second layer is estimated to be 85 m. Theoretical velocity increases to 0.61 m/s. We see in the data that the actual speeds of propagation were greater in the eastern region. The speeds of propagation were also greater than the theoretical value, which is similar to the corrections suggested by Philander and Yoon (1982). The local wind stress acted as a reinforcement for the progressing wave, enhancing its motion and increasing its velocity. It is also in agreement with the modifying action of topography in a highly stratified environment, which will increase the phase speed of the wave. Note that when the wave reaches the south shore, if wind stress is still westerly, then its speed should decrease considerably. The wind stress would then force

downwelling on the south shore and therefore reduce the amplitude of the wave and decrease its velocity.

3.5.2 THE GENERATION OF THE UPWELLING

The correlations of the density time series at the observation sites further suggests that the perturbations, upwelling or downwelling, would have been generated at the extreme north-east of the bay. The correlations with the zonal wind stress were reasonably high and above the 95% significance level. Lags also increased as one moved further inside the bay. The correlations with the meridional wind stress were low and fell under the 95% significance level at Bonaventure in 1990, and everywhere in 1988. Although lags would then be appropriate, it is not likely that meridional wind stress would have generated Kelvin waves.

The negative time lags at Gascon (23m) in 1988 and at Grande-Rivière in 1990 may be explained by combining wind stress, buoyancy and horizontal topography. The zonal wind stress oscillated between positive and negative values with a period of approximately 10 days. The symmetry of the bay along the east-west axis suggests that, if positive wind stress induced upwelling on the north shore, negative wind stress must have induced upwelling on the south shore. To respect continuity, upwelling on the north shore should be coupled with downwelling on the south shore and vice versa. The same kind of coupled upwelling and downwelling was observed in Lake Ontario (Csanady and Scott, 1974) and in Trinity Bay (Yao, 1986), where basins are of comparable dimensions with the BdC. In the case of reversing wind stress, a period of upwelling would be followed by a recovery period which would be followed by downwelling, or vice versa. When the wind stress was zero, just before it reversed, the isopycnals were out of equilibrium. Buoyancy would act to force water masses back to their original location. When recovering their equilibrium after downwelling, the isopycnals rose, similar to upwelling. Therefore, for that period, at a fixed location for sinusoidal wind stress, density increased and provoked an upwelling signal (as by the definition used herein) before the wind stress was appropriate.

3.5.2.1 THE REDUCED GRAVITY MODEL

This hypothesis was tested in a 2-layer reduced gravity model using realistic horizontal geometry of gridscale 2km x 1km and constant depth (Greatbatch and Otterson, 1991). Open boundary conditions were applied at the mouth of the bay, permitting Kelvin waves to propagate out of the region modeled. This was done by extending the coastline out to sea. Forcing from the GSL was ignored. Real wind stresses from August 13 to 20 1988, were used (fig.15). The wind was westerly for the first three days, followed by reverse winds for another three days, and then westerlies again. The model had reached steady state prior to the first plot showed in fig.16 (Le Quéré et al., ms. in prep.). The lines show the distance of the thermocline from equilibrium, with 0.2m spacing. Full lines are downwelling, dashed lines are upwelling.

Fig.16a shows the time of maximum downwelling on the north shore, 5 days after the wind was turned on. Downwelling is present on the entire north shore. The thermocline has deepened 3m at its maximum excursion. Fig.16b shows the state of the bay just before the winds reversed. Winds were too weak to sustain downwelling on the north shore. The thermocline started to rise near Grande-Rivière. Fig.16c shows the bay less than 24 hours after the winds reversed. Upwelling had commenced near Grande-Rivière.

The model results show that the vertical migration of the thermocline started before the wind stress became positive. The initial rising motion of the thermocline was clearly to the north-east of the bay, as observed in the data.

3.5.3 THE DOMINANT FREQUENCY OF OCCURRENCE

Fourier analysis showed two dominant low frequencies of around 4.5 and 10 days in 1988, and a wider peak around the same frequencies in 1990, in both the zonal wind stress and the density spectrum. If a Kelvin wave was generated, the presence of these two frequencies in the density data can be related directly to wind forcing since, for a given frequency, a Kelvin wave of one single mode is generated. However, the presence of topography can modify the wave type, especially when wind mixing was intensified in autumn. From that perspective, a

speed of propagation of 0.5 to 1.0 m/s is a first order approximation which may vary with the stratification in relation to local topography and wind stress. The zonal wind stress provided a better fit with the density spectra, especially in 1988, when longer time series were in hand. Most of the energy for all time series was in the low frequency band. The Nyquist frequency associated with upwelling events is $^1/_{2.5\ days}$. Any sampling done at a lower frequency would be aliased.

Upwelling occurs within approximately one internal Rossby radius of deformation of the coast, which varies from 5 to 13 km (appendix I), as one moves from west to east. Furthermore, the wind pattern was similar throughout the year (fig.17) which suggests that, as soon as the ice melted in April, the propagating signals coupled to upwelling and downwelling events began. Marcotte (1964) plotted daily observations of surface temperature at Grande-Rivière from 1951 to 1962. Rapid temperature decreases of the order of 2°C or more were often present in May, and occasionally in April, with the largest and most frequent temperature decrease seen in June, July, and August, when the stratification is strongest. For the rest of the year, rapid temperature decreases of 2°C or more were again often present.

3.5.3 THE RELIABILITY OF THE DATA

The correlation coefficients found in this study are thought to be reliable due to the length of the time series and to the frequency of sampling. The observation that similar patterns were reproduced in 1988 and 1990 is another indication of their reliability. One discrepancy persists in relation to the wind stress. The fact that only data at the western end of the bay were available does not permit us to assess the effects of meridional wind stress. Although the observed zonal wind stress at Charlo was typically half of the observed magnitude at the mouth of the bay, it was still strong enough for the main features to be apparent. The meridional wind stress was too weak for any features to be observable. It would certainly increase the accuracy of the correlations and especially of the time lags to have an extended field of wind stress. The position of the thermocline prior to wind forcing induced great fluctuations in the response time lag to wind stress.

3.6 CONCLUSION

Upwelling on the north coast of the Baie des Chaleurs was found to occur with periods ranging from 4.5 to 10 days. The largest events showed a change in density greater than 3 kg/m^3, which corresponds to over 10 °C and 3 °/oo. Cross-correlation analysis showed a cyclonic propagation of the upwelling with velocities of 0.5 to 1.0 m/s.

Zonal wind stress coupled with buoyancy was likely to be the generator of the upwelling. When easterlies were present, downwelling was observed on the north shore. When the winds weakened, the thermocline started rising and continued to rise as westerlies began. A simple 2-layer reduced gravity model reproduced well the observed upwelling pattern. The model conditions were fixed to force the signal to propagate in the form of an internal Kelvin wave.

The predominant westerlies at these latitudes, accompanied by the strength of the zonal wind stress compared to the meridional wind stress, increased our confidence that the former were responsible for the generation of most of the wind driven phenomena observed within the bay.

Since the wind stress pattern was similar throughout the year, with two distinct periods, strong winds from October to March, with weak winds the rest of the year, the upwelling pattern described here should be present as soon as the water column is sufficiently stratified to support propagating waves. Surface temperature records from Grande-Rivière (1951-1962) support this hypothesis.

The energy associated with the upwelling and downwelling events is much larger than the energy associated with tides. Any sampling in the BdC should consider this and be done at a frequency greater than the Nyquist frequency=$^1/_{2\ 5\ \text{days}}$.

Further research could include the following:

- An extended wind field to detect the effects of stretching in the wind stress. Crepon and Richez (1982) showed that longshore variability in the wind stress could provoke upwelling. Since the magnitude of the wind stress at Miscou and Charlo were different, stretching effects could be important in the BdC.
- Correlations with density data from the south shore, mainly to find the difference in the speed of propagation of upwelling and downwelling and dissipation characteristics.

- Include bottom topography in the numerical model to observe the influence of the depression off Grande-Rivière. As mentioned before, a narrow canyon off the west coast of Vancouver Island enhanced upwelling in that region (Freeland and Denman, 1982).
- Modal decomposition of σ_t and wind stress time series.

CHAPTER FOUR

DESCRIPTION OF THE WATER MASSES AND THEIR EVOLUTION IN SPACE AND TIME

In the previous chapter, the importance of upwelling and downwelling events on the north shore of the BdC was shown. The conclusions were that the perturbations propagate cyclonically around the bay, from spring to autumn. The energy found in the low frequency band was much stronger than the energy associated to tidal (semi-diurnal or diurnal) fluctuations. In this chapter, the water masses will be described, their relative importance and variability will be characterized, and, ultimately, the circulation of the bay will be inferred.

A series of seven CTD cruises from June to October 1991, covering the entire bay, will be used to describe the water masses. A second set of CTD data composed of weekly sampling at four stations on the north shore of the bay will be analyzed to determine the stratification of the water column, and how it changes in time. The data covers the months of May to November 1991. Finally, progressive vector diagrams from moored current meters in 1990 will be related to the water masses to help deduce the motion field.

The problem of aliasing in the data will also be discussed. A description of the data and methods, results and discussion follow.

4.1 DATA AND METHODS

All the data treated in this chapter were taken as part of the OPEN project. Original station designations are used to facilitate comparisons with other research projects at a later date. Current meter data for the 1991 field season were available too late (May 1992) to be used in the present study.

4.1.1 CTD CRUISES

A series of sixty stations spread over the entire bay were visited during each cruise (fig.18, small dots). They were grouped in twelve lines of constant longitude, including two to seven casts per line. These lines will be referred to with the letters B to M, from east to west. A total of ten cruises were completed. A little less than forty-eight hours was needed to visit all the stations. Seven cruises out of these ten cruises were selected for further analysis. The other three cruises were discarded because only a small number of stations had been visited. In two cases, storms forced the ship to stop. In the other case, stations differed from the usual ones; more stations were added in the western area of the bay, and the stations in the east were not visited. The first cruise took place in June 1991. The other six cruises were done from August to October of the same year. The exact dates are given in Table 3. The prefix RH of the names stands for *Répartition horizontale*; horizontal distribution. The number refers to the cruise, 0 is for June.

CRUISE	DATE
RH0	10, 11, 12 June
RH1	21, 22, 23 Aug.
RH2	26, 27, 28 Aug.
RH5	5, 6, 7 Sept.
RH6	15, 16, 17 Sept.
RH8	29, 30 Sept., 1 Oct.
RH9	8, 9, 10 Oct.

Table 3: Dates of the seven CTD cruises done in 1991. The prefix RH of the names stands for *Répartition horizontale*; horizontal distribution. The number refers to the cruise, 0 is for June.

The casts were performed with a Seacat Profiler SBE19 (conductivity, temperature, depth recorder). The resolution of the sensors was 0.001°C for temperature, 0.0001 S/m for the conductivity, and 0.03% of the full scale range for the pressure (Sea-Bird Electronics, 1990). Only the downcast was used. The

data were averaged at 1m intervals. The uppermost 2 meters were eliminated. These data were suspect because of ship related disturbance.

Vertical contours of temperature, salinity, and sigma-t for constant longitude are plotted in figs. 19 to 25. All contours are at intervals of one unit. Data were interpolated using the software "SURFER" (Golden, 1990). A grid size of 25x95 was used. The program used the minimum curvature method for interpolation (Briggs, 1974). Values of the grid points were calculated based on the data, smoothed, and recalculated until successive changes in the values were less than 0.005. Any grid element containing a data point was fixed. Horizontal contours of density at 3m are plotted in figs. 26 to 32. A grid size of 25x25 was used for these plots. The contours of density are represented in one 3-dimensional picture for each cruise (figs.33 to 39). The purpose of these pictures is to have a quick general idea of the "synoptic" state of the bay during one cruise. Finally, TS plots were done for all transects of longitude 64.67° (fig. 40).

4.1.2 CTD WEEKLY STATIONS

Four stations on the north shore were visited every week from May to November 1991. The stations were (from east to west): Grande-Rivière, Gascon, Bonaventure, and Carleton. They were approximately 1km offshore, with bottom depth varying between 13 and 23m. Each station was always sampled at the same phase of the tide. Grande-Rivière and Bonaventure were visited at low tide, Gascon and Carleton were sampled at high tide. The dates of the visits and the correspondence between Julian days (used in the figures) and the Roman calendar are shown in fig.41. The same treatment described in the previous section was applied, with a grid size of 25x25. The contours of figs. 42 to 45 represent the time evolution of the temperature, salinity, and σ_t.

4.1.3 PROGRESSIVE VECTOR DIAGRAMS

A progressive vector diagram is an addition of arrows representing, for each data point of an Eulerian time series, the distance traveled for a given velocity. The series of progressive vectors plotted here come from current meters moored in 1990, at the stations shown in fig. 18 (large dots). The length of the series vary from 6 weeks to 3 months. Table 4 summarizes the related information.

NAME	DEPTH (m)	DATE	NAME	DEPTH (m)	DATE
O1-N2	23	26 Aug.-21 Oct.	O6-N2	35	24 Aug.-13 Oct.
O1-N3	47	26 Aug.-21 Oct.	O7-N1	7	24 Aug.-13 Oct.
O3-N1	26	13 June-24 Aug.	O7-N2	31	24 Aug.-13 Oct.
O3-N3	53	13 June-24 Aug.	O8-N1	18	25 Aug.-17 Oct.
O3-N4	93	13 June-24 Aug.	O8-N2	31	25 Aug.-17 Oct.
O4-N1*	21	16 June-12 Sept.	O8-N3	52	25 Aug.-17 Oct.
O4-N2*	34.5	16 June-12 Sept.	O9-N1	13	24 Aug.-12 Oct.
O4-N3*	58	16 June-12 Sept.	O10-N1	14.5	23 Aug.-19 Oct.
O6-N1	19	24 Aug.-7 Oct.			

Table 4. Time series depth and length for the 1990 progressive vectors. The instruments identified with a star were displaced from their original locations by fishermen.

Aanderaa RCM-4 current meters were used for all moorings. The accuracy of the sensors was described in the previous chapter. The original data were recorded every 20 minutes. The time series were smoothed with a running weight algorithm, and decimated to hourly. The resulting time series were used to compute progressive vectors (figs. 46-53). The moon phases were added on each plot (except when it confused the picture) to help relate low frequency fluctuations to the tidal cycle. The same scale was used for each level at one station, but may vary between stations. Several levels were discarded because their directions were considered doubtful.

4.2 RESULTS

This section contains a simple description of each of the figures presented.

4.2.1 DESCRIPTION OF THE TEMPERATURE, SALINITY, AND σ_t CHARACTERISTICS OBSERVED OVER THE SEVEN CTD CRUISES

4.2.1.1 VERTICAL CONTOURS

Figs.19 to 25, B to M show the vertical profiles of temperature, salinity and σ_t for constant longitude.

RH0 (figs.19 B to M): The temperature ranged from 15°C at the surface, to less than 0°C at depth. The warmest waters were found on the south shore for most of the bay, except off Carleton, where the warmest waters were at the center. A layer of isothermal water, with 0°C>T>-1°C, was present from 25 to 40m depth down to the bottom. The 0°C isotherm was inclined from south to north. The steepest gradient of temperature was found between 10 and 15m on the south shore, and between 5 and 10m on the north shore.

The salinity ranged from 21 to 24 °/oo at the surface, with the less saline waters on the south shore, increasing in salinity from west to east, to 32 °/oo at depth. A patch of relatively fresh water was observed at longitude 65.83° (J), east of the Cascapédia River. The steepest gradient of salinity was at the same depth as the steepest gradient of temperature. Slopes were similar.

The density profile was similar to the temperature and salinity profiles. Density varied from 15 to 17 kg/m^3 at the surface, again increasing from west to east, to over 25 kg/m^3 at depth. The isopycnals in the top 15m slope from north to south, while the deeper isopycnals slope from south to north, resulting in divergence around 15m on the north shore, and convergence at the same depth on the south shore.

RH1 (figs.20 B to M): This cruise was done just after hurricane "Bob" hit the GSL on 20 August. The maximum temperature at the surface was 15 to 17°C, with warmest temperatures on the south shore. The minimum temperature was less than 1°C. The slope of the isotherms vary a lot from profile to profile. For the first two profiles (B and C) most of the isotherms were inclined from south to north, with a warm pool next to the south shore. For the next four profiles (D to

G), the slope of the isotherms was not constant, wave like forms were present in the center of the bay. At the western end of the bay (H to M) the isotherms were more or less level. In some profiles, a steeper gradient of temperature was observed from 30 to 35m.

The salinity ranged from 26 to 32 °/oo, with the less saline waters on the south shore. Relatively fresh water was observed at longitude 65.50° (K) on the south shore. For the profiles B and C, the slopes were diverging from 50m on the south shore. For the other profiles, no distinct tendencies were observed in the slopes.

The density ranged from 18 to over 25 kg/m^3. For the profiles B and C, the isopycnals were diverging from 40m on the south shore. For the other profiles, although large fluctuations in the slopes of the isopycnals were present, no distinct tendency was apparent.

RH2 (figs.21 B to M): The temperature ranged from 18°C at the surface, to less than 1°C at depth. The warmest waters were again close to the south shore. A pool of isothermal water was present at depths greater than 50m, with 0°C>T>-1° C. Divergence on the north shore, and convergence on the south shore, were often observed around 25m.

The salinity ranged from 27 °/oo, with less saline water on the south shore, to over 32 °/oo at depth. Divergence on the north shore, and convergence on the south shore, were often observed around 30m.

The density ranged from 19 kg/m^3, with less dense water on the south shore and in the western end, to over 25 kg/m^3 at depth. The water was homogeneous at depths greater than 50m. Divergence on the north shore and convergence on the south shore were evident around 25m.

RH5 (figs.22 B to M): The temperature ranged from 16°C to less than 1°C. The warmest waters were not always close to the south shore, but were often in the central bay. Temperatures less than 1°C were observed deeper than 60 to 65m. The steepest gradient of temperature varied in depth, expanding from 10 to 20m in the western area, to 30 to 40m in the eastern area. In the western end, the isotherms diverged on the north shore, and converged on the south shore near 25m.

The salinity ranged from 27 to over 32 °/oo at depth. The less saline waters were not always found close to the south shore, but also often in the center. Divergence on the north shore, and convergence on the south shore were observed around 25m, in the western area.

The density ranged from 20 kg/m^3 to over 25 kg/m^3 at depth greater than 60m. In the eastern area, a thermocline was present between 30 to 60m (23 and 25 kg/m^3) while in the western area, the divergence and convergence pattern described above was present.

RH6 (figs.23 B to M): The temperature ranged from 15°C to less than 1°C at depths greater than 60m (on average). The steepest gradient of temperature was found between 30 and 50m. In the eastern end of the bay, divergence on the north shore and convergence on the south shore was present around 25m. In the western area, this situation was reversed.

The salinity ranged from 28 to over 32 °/oo. The same inclination as the isotherms was found, except near the mouth of the Restigouche River.

The density ranged from 21 kg/m^3 to 25 kg/m^3, deeper than 55m. A similar inclination of the isopycnals was again observed.

RH8 (figs.24 B to M): The temperature ranged from 12°C to less than 1°C deeper than 60-65m. The isotherms were inclined from north to south from longitude 65.17° (F) to longitude 65.83° (J), at the center of the bay. No major divergence/convergence patterns were observed. The steepest gradient of temperature was between 30 and 60m.

The salinity ranged from 28 to over 32 °/oo at depth.

The density ranged from 21 kg/m^3 to over 25 kg/m^3 deeper than 60m. The steepest gradient was found between 30 and 60m. A slight inclination of the isopycnals was observed at the center of the bay.

RH9 (figs.25 B to M): The temperature ranged from 11°C to less than 1°C at depth greater than 55 to 60m. A strong inclination (of up to 30m) of the isotherms was present, with divergence on the north shore around 40m.

The salinity ranged from 28 to over 32 °/oo at depth. Again a strong inclination was observed with divergence on the north shore.

The density ranged from 21 kg/m^3 to over 26 kg/m^3 at depth. The same inclination observed in the temperature and salinity profiles was present.

4.2.1.2 HORIZONTAL CONTOURS

Figs. 26-32 show the horizontal contours of density at the surface (3m).

RH0 (fig. 26): The horizontal gradient of density was substantial, with a difference of 4 kg/m^3 between the north and south.

RH1 (fig. 27): The density varied mainly in the east-west axis, with a difference of 3.5 kg/m^3. The densest water was to the east. There was also a less pronounced north-south gradient.

RH2 (fig. 28): The density varied both in the north-south and east-west axis, with densest water on the north-east side. The density difference reached 3 kg/m^3.

RH5 (fig. 29): Similar to RH2, with an increased density west of Carleton.

RH6 (fig. 30): A north-south gradient of density was present on the eastern side, with densest water on the north. The density difference was 1 kg/m^3 at most.

RH8 (fig. 31): A weak north-south gradient was present on the east side. The density difference was 1 kg/m^3 at most.

RH9 (fig. 32): The density varied both in the north-south and east-west axis. The density difference reached 2 kg/m^3. There was a zone of dense water close to the shore, from Bonaventure to Grande-Rivière.

4.2.1.3 TS DISTRIBUTION

Fig. 40 shows the TS distribution for all cruises. The water column was always stratified with greatest stratification observed during the first cruise, in June. Fresher water was also observed during this cruise. Cruises one to six had a similar range of salinity and of temperature. Cruises eight and nine had a reduced range of salinity and temperature.

RH0: The salinity ranged from 23 to 32.5 °/oo, and temperature ranged from -1 to 15.5 °C.

RH1, RH2, and RH5: The salinity ranged from 28 to 32.5 °/oo, and the temperature ranged from -0.5 to 16.5 °C.

RH6: The salinity ranged from 28 to 32 °/oo, and the temperature ranged from 0 to 14.5 °C.

RH8 and RH9: The salinity ranged from 28.5 to 32.5 °/oo, and the temperature ranged from 0 to 12 °C.

4.2.2 DESCRIPTION OF THE WEEKLY CTD STATIONS

GRANDE-RIVIÈRE (fig. 42): The surface temperature increased approximately 1°C every ten days until the first week of August. The temperature was constant at 15°C for three weeks, and then started to decrease. At 10m depth, two irregular decreases in temperature were observed, one at the beginning of July, and the other at mid-October.

The surface salinity increased irregularly until the third week of August. It then stayed constant, with a small decrease between mid-September and mid-October. At 10m depth, one irregular increase in salinity was observed.

Similar to salinity, the surface density increased irregularly until the third week of August. It then stayed constant, with a small increase between mid-September and mid-October.

The temperature, salinity, and density profiles were strongly stratified until the beginning of September, followed by transition to an almost completely homogeneous water column.

GASCON (fig. 43): The surface temperature at this location increased until the end of June, it then decreased for two weeks, and increased again until mid-August. The pattern was similar at 10m except for one supplementary decrease in temperature at the beginning of June.

The surface salinity increased to its maximum at mid-August, with a small decrease the third week of June. At 10m, a succession of low and high salinities were observed.

The density reflects the temperature and salinity profiles. The water column was strongly stratified until the end of August, and then became homogeneous.

BONAVENTURE (fig. 44): Similar to Gascon, the surface temperature increased until the end of June, it then decreased for two weeks, and increased again to its maximum at the end of July. At 10m, three other temperature drops were observed.

The surface salinity slowly increased until mid-September. At 10m depth, the salinity was variable. It increased until mid-July, then decreased until mid-August, and thereafter increased.

The water column remained stratified until the end of the sampling series.

CARLETON (fig.45): The surface and 10m temperatures increased and decreased successively four times. The maximum surface temperature was at the beginning of August.

The surface salinity increased until the beginning of August. Two peaks in salinity were observed at depth, one in mid-July, and one at the end of August.

The water column was stratified until the end of the series.

4.2.3 DESCRIPTION OF THE PROGRESSIVE VECTOR DIAGRAMS

STATION 1 (fig. 46): Station 1 was at the extreme north-east of the bay, approximately 5km offshore. Time series were seven weeks long. The second level (23m) and the third level (47m) had no resemblance, neither in current direction nor in low frequency fluctuations (3 to 15 days). Current reversals were sometimes (not regularly) seen over the semi-diurnal cycles, at both levels. The dominant direction of the currents at both levels varied with a low frequency time scale. These fluctuations were not related to the lunar cycles in any obvious way. The direction of the currents at the second level were east, south-west and north-east, while the direction of the currents at the third level fluctuated between east and south.

STATION 3 (fig. 47): Station 3 was approximately 15km offshore, in front of Grande-Rivière. Time series were two months long. The first level (26m) and the third level (53m) exhibited similar features. Except for the first two weeks, currents were in the same direction. Flow at the fourth level (93m) was generally in an opposite direction to that at the upper depths. Low frequency fluctuations in the direction of the flow were present at all levels and were not related to the lunar cycle in any obvious way. The currents at the first and third levels flowed to the north-west except during the month of June, when the current of the first level rotated. The current at the fourth level changed from south-east to south-west, with some variable flows.

STATION 4 (fig. 48): Station 4 was approximately 15km off Miscou Island, near the entrance to the bay. Time series were almost three months long. The first level (21m) and the second level (34.5m) were similar during the entire series. The third level (58m) showed similar low frequency fluctuations but with a shift of 30 to 45° east in the direction of the current. Current reversals were often observed at all levels over the tidal cycle. Low frequency fluctuations were obvious, with currents shifting over 90°, and were not related to the lunar cycle in any obvious way.

STATION 6 (fig. 49): Station 6 was less than 5km offshore, in front of Paspébiac. Time series were seven weeks long. The first level (19m) and the second level (35m) were similar. Current reversals were often present at both levels over the tidal cycle. The currents were constant in the south-west direction most of the time.

STATION 7 (fig. 50): Station 7 was approximately 5km offshore, in front of Grande-Anse, on the south shore. Levels one (7m) and two (31m) were not similar. Current reversals were sometimes observed, more often at the second level. Low frequency fluctuations were present at both levels, and were not related to the lunar cycle in any obvious way. The current at the first level was mostly towards the north-east. The current at the second level reversed on occasion, with long periods toward the south-west and towards the north-east.

STATION 8 (fig. 51): Station 8 was in front of Gascon, between the north and south shore. The first two levels (18m and 31m) were similar, with current

reversals observed about half the time. Low frequency fluctuations were present, causing shifts in direction, and sometimes loops in the residual current. The third level (52m) differed. It often showed current reversals during tidal cycles. The residual current changed direction with a low frequency. The dominant direction at the first two levels was north west, while the direction of the third level changed from north-east to south-west, with a mean current almost to the north.

STATION 9 (fig. 52): Station 9 was a few km offshore, in front of Bonaventure. Only one level (13m) was available. Current reversals were common. Low frequency fluctuations were present and not related to the moon phases. The main direction of the current was towards the west and south.

STATION 10 (fig. 53): Station 10 was in front of Bonaventure, half way between the north and south shore. Its only level (14m) showed frequent current reversals. Low frequency fluctuations were present and not related to the lunar cycle. The main direction of the current was south to east.

4.3 DISCUSSION

4.3.1 THE PROBLEM OF ALIASING IN THE DATA

A data set is aliased when the interval of time between two successive data samplings is greater than the Nyquist frequency, which equals half the period. For example, if the real signal is sinusoidal, with a period of 12 hours (like semi-diurnal tides), the sampling interval must be less than 6 hours. If sampling is done with an appropriate frequency, all the maximums and minimums of the signal will be seen in the data. When the frequency is inappropriate, the signal registered can show something totally different from reality, and lead to false conclusions. Fig. 54 represents some of the possible sampling errors (large dash).

Some of the data described above is aliased. The main recurring events in the BdC are the tides, upwelling, and seasonal fluctuations. The principal semi-diurnal and diurnal tidal constituents, M_2, S_2, N_2, K_1, and O_1, have periods of 12.00, 12.42, 12.66, 23.93, and 25.82 hours, respectively. Longer periods associated with tides are the lunar fortnightly, M_f, and the lunar monthly, M_m, with periods close to 14 and 28 days. From results of the previous chapter, the

typical period associated with upwelling was between 4.5 and 10 days. The annual and longer cycles are important but cannot be considered with the available data.

To account for all cycles present, ideal sampling should be performed with a time step less than six hours, lasting for over one year. This is not realistic with the available equipment (and funds), but fortunately, some conclusions can be drawn from incomplete and aliased data sets.

The set of seven CTD cruises included aliasing in several different ways. Each cruise took a little less than forty-eight hours to complete. This implies that all samples were not done at the same tidal phase. When the ship moved from one end of the bay to the other, if an upwelling event was observed, its extent or speed of propagation could not be deduced. Finally, the frequency at which the cruises were done is also less than the semi-diurnal and diurnal tides, and the upwelling Nyquist frequency. The frequency of upwelling events cannot be deduced with this data. Comments on the variability from one cruise to the other would be relevant if the effects of upwelling and of higher frequency tidal fluctuations could be removed.

The set of weekly CTD profiles were done at the same tidal phase. This limited errors due to tidal effects, and permitted observations of other kinds of variability. The period, however, was greater than that associated with the upwelling events. We saw in the previous chapter, that the energy involved in upwelling was important, as were the associated fluctuations in temperature, salinity and density. Two ways to overcome this problem are suggested. Both solutions attempt to detect upwelling events that could have occurred between two cruises.

The first solution consists in using the model described in the previous chapter, with real winds over the period of interest. This model showed good results in reproducing the depth of the thermocline with just the wind data, at least qualitatively, and for a short period of time (2 to 6 days).

The second and easiest solution is to compare the data at discrete depths with temperature and salinity data from current meters moored during the same period. By doing this, it is possible to know if upwelling or downwelling events occurred,

and at which stage of the event the ship sample was taken. Unfortunately, the current meter data from the 1991 season are not yet available.

The two methods could be used in conjunction, to test the accuracy of the model.

This data will be used to follow the stratification conditions in the water column. Upwelling events in this type of data are visible by a successive rise and fall of the thermocline. It differs from seasonal changes which occur at a longer time scale.

For the third set of data, the current meter data, there is no aliasing in regard to the semi-diurnal tides or upwelling. A shortcoming for this research is that these data come from a different year than the CTD data.

4.3.2 THE WATER MASSES

Some general comments can be made from the results of the CTD cruises:

- The salinity profiles rarely showed a distinct halocline. Salinity increased with depth, with steepest gradients close to the surface or near the coast.
- A layer of high temperature gradient was present varying in depth and extent from as little as 10m to as much as 60m.
- A mass of isothermal water was always present below depths varying between 40 and 60m and the bottom. The temperature of this layer was less than 0°C in June, and less than 1°C later in the summer and fall.
- The inclination of the isopycnals was extremely variable, with changes of up to 35m, and slopes of up to 3m/km.

A classification similar to that of Boudreault (1967) is used. He defined three distinct water masses. The first water mass was defined by the surface and the top of the thermocline. The second water mass straddled the thermocline. The third water mass ranged from the bottom of the thermocline to the bottom. The 8°C and 3°C isotherms separated the three layers.

This classification of water masses differs from the classification used in the GSL. Three water masses are also defined in the GSL, but the deepest water mass

is not present in the BdC. The top two water masses of the BdC are considered to be one water mass in the GSL.

The definition of three water masses seems appropriate for the BdC because the flow may be different in the two top layers, as during upwelling events or local river input. Some modifications are proposed to the scheme of Boudreault. The top and bottom of the thermocline are kept as frontiers between the layers but density, instead of temperature, is used to set the limits. This will include the effects of salinity as well as temperature.

From our observations, the first water mass is better defined by the 23 kg/m^3 isopycnal, which corresponds to the 10°C isotherm and a salinity of 30 °/oo.

The second water mass, straddling the thermocline, extends up to 25 kg/m^3, corresponding to 1°C and 31.5 °/oo. The 1°C isotherm marked the boundary, most of the time, where the water became quasi-homogeneous.

The third water mass has a density greater than 25 kg/m^3, corresponding to 1°C and 31.5 °/oo.

Based on this definition, the depth of the interfaces for each cruise was estimated (table 5). For each longitude, the mean depth of the 23 and 25 kg/m^3 isopycnals was computed ($^1/_2$(min. depth+max. depth)), and the average over all longitudes was performed.

The mean depth of the first interface varied between 23 and 33m, except for the first and last cruises. During the first cruise, the depth of the first interface was 19m, while in the last cruise, its depth was 14m. The shallowness of the thermocline during the first cruise can be imputed to the seasonal changes. During the last cruise, the thermocline rose to the surface on the north shore, reducing the average depth of the first interface.

The mean depth of the second interface varied between 46 and 57m, except for the first and last cruise, where it was 44 and 30m, respectively.

The maximum temperature was observed during the last week of August. The minimum salinity increased regularly until the last cruise.

One feature observed in five of seven cruises was the presence of isopycnal divergence on the north shore and isopycnal convergence on the south shore, at

depth varying from 15 to 40m. In these five cruises, the feature was observed in 90% of the profiles taken east of longitude 66°. The typical water mass distribution is represented in fig. 55.

Different forcing may cause the inclination of the isopycnals. Among them, upwelling, internal tides, geostrophic currents, with or without a surface tilt could all independently play this role. We showed in the previous chapter that upwelling was present in 1988 and in 1990 and correlated to wind stress with a correlation coefficient varying between 0.36 and 0.60. When upwelling occurs on the north shore, a northward motion at mid or bottom depth must be present to respect

	T_{min} (°C)	T_{max} (°C)	S_{min} (°/oo)	S_{max} (°/oo)	$\sigma_{t\text{-}min}$ (kg/m^3)	$\sigma_{t\text{-}max}$ (kg/m^3)	1st interface	2nd interface	comments
RH0	0	15	21	32	15	25	19	44	divergence on the north shore
RH1	1	17	26	32	18	25	33	57	
RH2	1	18	27	32	19	25	23	46	divergence on the north shore
RH5	1	16	27	32	20	25	27	57	divergence on the north shore
RH6	1	15	28	32	21	25	31	56	divergence on the north shore
RH8	1	12	28	32	21	25	23	53	
RH9	1	11	28	32	21	26	14 (0-25)	30 (30-60)	divergence on the north shore

Table 5 Summary of the minimum and maximum temperature, salinity, and density for the seven CTD cruises. The mean depth of the first and second interface as defined in this chapter was also evaluated.

continuity. Csanady (1982), using a 3-layer model, showed that during downwelling the intermediate density fluid is squeezed away from the coast while upwelling acts in the opposite way. Alternating upwelling and downwelling moves the intermediate fluid in and out of the coastal band.

The presence (or absence) of internal tides should be examined in the future.

The geostrophic currents were not computed, because the problem of the surface tilt could not be overcome. When current meter data for 1991 is available, it may be possible to pursue this calculation.

4.3.3 THE STRATIFICATION OF THE WATER COLUMN

An interesting aspect of the weekly samples is that it gives a time evolution of the stratification of the water column at one location.

Destratification of the water column was observed at Grande-Rivière and at Gascon at the beginning of September. The water column at Carleton and Bonaventure was stratified until the end of the series, which may also indicate the presence of upwelling.

Destratification at Grande-Rivière and Gascon means that the thermocline has descended below the local bottom depth; 23m at Grande-Rivière and 21m at Gascon. This comment is based on the observation that none of the TS plots show a complete destratification (fig.40).

The TS distribution at the entry of the bay showed the strongest stratification in June. The range of temperature and salinity observed, indication of the degree of stratification, decreased from mid-September to mid-October.

On the horizontal contours of density, clear north-south and east-west gradients were observed until mid-September. For the last three cruises, the surface density differences were small, with a local gradient on the north-east shore during the last cruise.

From the data available, no deepening of the thermocline occurred between August and October (table5). The stratification of the whole water column did not show any particular evolution in time (figs. 33-39), besides the spring and autumn difference, and a slight decrease in surface density.

4.3.4 THE GENERAL CIRCULATION

Table 6 summarizes the mean currents, the mean temperature, and the mean salinity associated with each of the stations and levels.

The main finding from the progressive vectors is that there is no obvious distinction between the circulation observed in the first and second layer. At stations 1, 6, 7 and 8, instruments were moored in the first two layers. Stations 1 and 7 showed a different circulation in the top two layers, while stations 6 and 8 had similar low frequency fluctuations and the mean currents. Fluctuations were present at station 7, but they did not persist for a long time.

At station 3 and 4, instruments were moored in the lower two layers. A difference was observed in the direction of the mean current and in the low frequency fluctuations, but the lower levels at stations 3 and 4 were in opposite direction.

The mean currents are plotted in fig.56, thin arrows correspond to the top layer. The instruments at stations 3 and 4 have longer time series than all others.

Cyclonic motion at the center of the bay is clear. Stations 3 and 4 have a component of the current towards the north shore, which may be a consequence of the currents induced during upwelling events. None of the low frequency fluctuations could be associated to the lunar cycle. The frequency of upwelling is appropriate for generating these kind of fluctuations. This should be looked at in further detail.

To better understand the forcing involved, we now consider two sketches representing hypothetical circulation of the bay (fig. 57). In the first sketch (fig. 57a), the circulation driven by estuarine forcing was neglected (no fresh water imput), only the forcing of the GSL was considered. It is assumed that an extension of the Gaspé current, constrained by the Coriolis force, enters the BdC on the north shore. This current would move along the north coast until friction or entrainment forces it to turn, and exit on the south shore. This would lead to cyclonic motion in the central bay.

NAME	V (cm/s)	DIRECTION (°)	TEMP. (°C)	SALINITY (°/oo)	CORRESPONDING WATER MASS
O1-N2	4.8	94.6	9.9	29.4	INTERFACE 1
O1-N3	7.1	166.8	4.0	31.3	2
O3-N1	9.2	290.9	7.6	30.2	2
O3-N3	3.6	309.2	1.4	31.1	2
O3-N4	3.7	162.3	0.2	32.6	3
O4-N1*	6.5	319.2	8.2	29.4	2
O4-N2*	5.1	312	5.2	30.2	2
O4-N3*	1.3	339.6	0.63	31.8	3
O6-N1	11.3	236.7	10.4	29.7	1
O6-N2	6.1	257.8	6.2	30.5	2
O7-N1	6.2	71	13.1	27.4	1
O7-N2	2.7	82.0	5.5	30.5	2
O8-N1	4.4	291.7	10.2	29.4	1
O8-N2	4.2	295.1	1.3	31.8	2
O8-N3	0.7	340.3	5.9	missing	2
O9-N1	5.4	236.3	10.4	29.3	1
O10-N1	4.0	134.7	11.8	29.0	1

Table 6 Mean speed, direction, temperature and salinity for the 1990 current meters. The water mass corresponding to the previous description is on the last column.

The progressive vectors at station 1 (closest to the Gaspé current and close to shore) did not enter the bay. These time series were seven weeks long, from August to October. Average currents from the other stations tend to show the presence of cyclonic motion within the bay, at least at the center and the eastern end, no data being available for the western end.

The second sketch (fig.57b) represents the circulation with only the forcing from the estuary present. As mentioned in chapter two, the BdC is a partially mixed estuary. The usual circulation for this type of estuary is composed of two layers, one deeper and heavier, which enters the estuary while the upper layer, composed of the lighter, fresher waters, exits the bay. Entrainment and mixing occurs

between these two layers. Moreover, the Coriolis effect will play a role once again in forcing the outgoing waters on the south shore, and the ingoing waters on the north shore.

From the progressive vectors available, the outward motion of the shallow layer was only observed on the south shore. The fact that the current meter were moored from August to October 1990 must be emphasized. It is possible that the outgoing water occupies a larger cross-section in spring when the runoff is more important. Two deep instruments were available. At station 3, the mean current exits the bay, and at station 4 it enters the bay.

From our observations, the cyclonic circulation in the bay was more important than the estuarine motion, from August to October. The forcing of the Gaspé current was not observed.

4.4 CONCLUSION

Three water masses, one between the surface and the thermocline, one straddling the thermocline, and one at the bottom, were found to adequately describe the TS properties in the water column.

Destratification of the water column started at the beginning of September and was observed in the top 25 to 30m only. The rest of the water column was well stratified until mid-October (end of the sampling). After this period, the entire water column is expected to become less stratified, due to increased wind mixing and cooling of the air.

The isopycnals, for most of the time, diverged from around 15 to 40m depth on the north shore, and converged on the south shore. This divergence/convergence pattern could be driven by wind induced upwelling on the north shore, though other kinds of forcing were not investigated.

A difference in speed of 3 cm/s was common between the top two layers, with significant difference in direction at station 1 and 7 only. A difference in direction between the second and third layers was observed. The circulation was cyclonic in the center and east section of the bay, during August to October 1990. In the past, it was suggested that cyclonic motion within the bay would be forced by an

extension of the Gaspé current. One current meter at the entry of the bay showed little forcing from the GSL.

Estuarine circulation (classical two layer circulation) was not observed in the progressive vector diagrams. It may be important during spring, and hidden by larger signals later in summer and autumn.

CHAPTER FIVE

GENERAL CONCLUSIONS

Different physical components of the Baie des Chaleurs were reviewed in this work.

In the third chapter, time series of temperature and salinity from current meters moored in 1988 and 1990 at different locations along the north shore were analyzed to characterize the frequency of upwelling events. All events observed during August and September 1988 were similar at Gascon and Carleton, and were associated with positive zonal wind stress. Further analysis of σ_t time series showed high correlations between the stations accompanied by cyclonic propagation of the upwelling signals with speeds of 40 to 85 km per day.

Comparisons of σ_t and zonal wind stress time series showed moderate correlations with time lags decreasing in the eastern part of the coast. Negative time lags at the mouth of the bay are explained by interaction of buoyancy, topography, and oscillating wind stress. When easterlies were present, downwelling was forced on the north shore. When wind stress weakened, the isopycnals were out of equilibrium and rose before westerlies began. This hypothesis was well simulated by a 2-layer reduced gravity model. The model results showed that the vertical migration of the isopycnals can be forced by buoyancy before the forcing of the wind stress is appropriate.

The dominant frequencies of the upwelling events were approximately 4.5 to 10 days. The energy associated with these low frequencies was at least one degree of magnitude larger than the higher frequencies. The difference in density during upwelling events could reach 3 kg/m^3, which corresponds to 10°C and 3 °/oo. The vertical velocity was 5.2m per day at Carleton.

The 1988 wind data showed strong wind stresses from October to March, with weaker winds the rest of the year. The weaker winds were appropriate to drive upwelling, suggesting that upwelling should be present as soon as the water column is stratified enough to sustain propagating waves.

In the fourth chapter, three water masses were defined. The first water mass was defined by the surface and the top of the thermocline. The second layer straddled the thermocline. The third water mass ranged from the base of the thermocline to the local bottom. Steep inclinations of the isopycnals were observed during most of the cruises, with divergence near 15 to 40m on the north shore, and convergence on the south shore. This could be provoked by upwelling on the north shore.

Destratification occurred in the surface layer between the first and second week of September. No deepening of the thermocline occurred between August and October. The range of temperature and salinity observed decreased from mid-September to mid-October, mainly due to a drop in the surface density.

Based on the studies made in the GSL (Lauzier et al., 1957), increased mixing should lead to an almost homogeneous water column during winter. The three water masses become distinct in spring when heating, ice melt, and river runoff all contribute to restore the surface layer. Though no deepening of the thermocline was observed in our data, it probably occurred in later autumn.

The mean circulation in the intermediate section of the bay, from August to October 1990, was cyclonic, with baroclinic motion observed in the bottom two layers, at station 1 almost outside the bay, and at station 7 on the south shore.

The cyclonic circulation was thought to result from forcing of the Gaspé current on the north shore. Data from the current meter closest to the Gaspé current and close to shore did not show a strong westward current, as would have been appropriate. Wind driven and/or bathymetrically driven circulation should be examined as possible causes of the cyclonic motion.

The current meter data from the 1991 field season are required to describe the long term circulation and its evolution from spring to autumn. The current data could also be used with the temperature and salinity fields (CTD) to better understand the effects of upwelling, and to reduce aliasing effects.

The effect of upwelling on the general circulation was described in a minor way. Research on this relationship could greatly ameliorate our knowledge of the physical oceanography of the BdC since much of the energy is contained and

propagated through upwelling events. The influence of upwelling on the destratification of the water column, how it forces local fluctuations in the current, dissipates, and propagates on the south shore, are all possibly important.

A model of the general circulation of the bay could help in this task. Such a model could include, by order of importance, bottom topography, multiple layers (two or three), real wind stress, fresh water imput (to take account of the river runoff), exchange of water with the GSL, and non-linear effects. The Rossby number (which gives an indication of the importance of non-linear effects) is reasonably low for most of the bay but extreme situations occur where high currents may lead to strong non-linear effects (appendix 2). Unusually high currents are seen during storms and in spring when the runoff is important.

APPENDIX ONE

INTERNAL ROSSBY RADIUS OF DEFORMATION

The internal radius of deformation is a measure of the horizontal extent of internal perturbations. For example the upward motion of water in an upwelling event occurs within approximately one radius of deformation from the coast. Assuming a 2-layer fluid, λ, the Rossby radius of deformation is:

$$\lambda = \frac{1}{f}\left[g\frac{\rho_2 - \rho_1}{\rho}D\right]^{\frac{1}{2}}$$

where the subscripts 1 and 2 refer to the first and second layers, D is the depth of the water column. With typical values of ρ_1=1022 kg/m^3 and ρ_2=1024 kg/m^3 (see chapter 4 for details), D=20 to 100 m, the Rossby radius varies from 5.6 to 13 km, from west to east. In the BdC, the internal radius of deformation is always smaller than 1/2 the width of the bay. Because of this, the circulation on both coasts may be considered independently. Thus perturbations near the coasts do not interfere with one another.

APPENDIX TWO

ROSSBY NUMBER

The Rossby number (R_0) is an indication of the importance of non-linear effects over Coriolis effects in the equation of motion. When R_0 is much less than 1, non-linear effects can be neglected. When it is close to 1, small perturbations grow rapidly and can lead to hardly predictable currents or to turbulence. For example, the intensification of the western current in the Gulf Stream is driven by non-linear effects (Charney, 1955). The equation of motion follows:

$$\frac{\partial u}{\partial t} + u\frac{\partial u}{\partial x} = -\frac{1}{\rho}\frac{\partial p}{\partial x} + fv - fw + \text{friction} + \text{tidal forces}$$

$$R_0 = \frac{\text{non} - \text{linear} \quad \text{terms}}{\text{Coriolis}}$$

$$= \frac{u^2}{L}\frac{1}{fu} = \frac{u}{fL}$$

where u and v are the horizontal velocities, w is the vertical velocity, ρ is the density, p is the pressure, f is the Coriolis parameter, and L is the width of the basin or some horizontal length scale (Pond and Pickard, 1983).

Because the width and current vary from east to west, the Rossby number is not constant over the bay. The Coriolis parameter, f, can be approximated as a constant for such small latitudinal differences; $f=2\Omega sin\varphi$, Ω is the angular velocity of the earth, φ is the latitude, for a value of 1.1×10^{-4} s^{-1}. For the center and eastern regions, the mean value of the current is 20 cm/s. Extreme values reach 60 cm/s. These values are mean RMS (root mean square) current taken from current meters moored during the summers of 1988 and 1990 (see chapter 3 for details). The width is approximately 35 km for that area. Mean Rossby number is then 0.05, small enough to neglect non-linear effects, at least as a first approximation. The largest Rossby numbers approach 0.15, when non-linear effects may not be negligible. In the western region, at the mouth of the Restigouche river, near Carleton, average velocities are 15 cm/s, extreme velocities are 30 cm/s. Width is

approximately 15 km. Mean Rossby number is now 0.09, with extreme values reaching 0.18. The mean Rossby number is larger in this area, non-linear effects are more likely.

While the mean value of the Rossby number is reasonably low for most of the bay, extreme situations occur where high currents may lead to strong non-linear effects. Unusually high currents are seen during storms and in spring when the runoff is important.

REFERENCES

Babin, M., J.-C. Therriault and L. Legendre, (1991) Potential utilization of temperature in estimating primary production from remote sensing data in coastal and estuarine waters. *Estuarine Coastal and Shelf Science*, **33**, pp 559-579.

Barton, E. D., A. Huyer and R. L. Smith, (1977) Temporal variation observed in the hydrographic regime near Cabo Corveiro in the north-west African upwelling region, February to April 1974. *Deep Sea Research*, **24**, pp 7-23.

Beak Consultants Limited, Vancouver B. C., (1979) *An examination of the variability of upwelling on the west coast of Vancouver Island and its relationship to the flushing of Alberni inlet*, **Report 793**, 54 p.

Beaugé, L., (1956) Le golfe St-Laurent. *Rev. Trav. Inst. Pêches marit.*, **20**, pp 5-39.

Bergeron P., (1992) Évaluation des paramètres de production et du potentiel de la Baie de Tracadigache (Baie-des-Chaleurs) pour l'élevage de la moule bleue sur filières flottantes. *Ministère de l'Agriculture, des Pêcheries et de l'Alimentation, Direction de la recherche scientifique et technique,* **Cahier d'information no.129**, 65 p.

Boudreault F. R., (1967) Regime thermique saisonnier d'une station pilote à l'entrée de la Baie des Chaleurs. *Naturaliste Can.*, **94**, pp 695-698.

Boudreault F. R., (1968) Revue des travaux d'océanographie physique effectués dans la Baie des Chaleurs (1924-1967). *Ministère de l'industrie et du Commerce, Station de biologie marine de Grande-Rivière*, **Cahier d'information no.47**, 24 p.

Boudreault F. R., (1969) Régime des vents à Grande-Rivière (baie des Chaleurs). *Naturaliste can* , **96**, pp 667-670.

Briggs, I. C., (1974) Machine contouring using minimum curvature. *Geophysics*, **5**, pp 39-47.

Brink, K. H., D. Halpern and R. L. Smith, (1980) Circulation in the Peruvian Upwelling Systems Near 15 °S. *J. Geophys. Res* , **85**, pp 4036-4048.

Brink, K. H., (1982) The effect of bottom friction on low-frequency coastal trapped waves. *J. Phys. Oceanogr.*,**12**, pp 127-133.

Brunel, P., (1959) Le zooplancton de la Baie des Chaleurs en 1955: Distribution horizontale quantitative et corrélations hydroclimatiques. *Contr Dépt. Pêch. Québec*, **no.73**, pp 1-65.

Bugden, G. L., (1981) Salt and heat budgets for the Gulf of St-Lawrence. *Can. J. Fish Aquat Sci* , **38**, pp 1153-1167.

Bugden, G. L., (1991) Changes in the temperature-salinity characteristics of the Gulf of St. Lawrence over the past several decades. In J.-C. Therriault (ed.) *The Gulf of St-Lawrence small ocean or big estuary?* Can. Spec. Publ. Fish. Aquat. Sci , **113**, pp 139-147.

Bumpus, D. F., and L. M. Lauzier, (1965) Surface circulation on the continental shelf off eastern North America between Newfoundland and Florida. *Serial Atlas of the Marine Environment, Amer. Geogr. Soc* , **7**.

Canada, Department of Fisheries and Oceans, Canadian Hydrographic Service, (1990) *Canadian Tide and Current Tables· Vol.5, Gulf of St. Lawrence.*

Chapman, D. C., (1983) On the influence of stratification and continental shelf and slope topography on the dispersion of sub-inertial coastally-trapped waves. *J. Phys. Oceanogr.*, **13**, pp 1641-1652.

Charney, J. G., (1955) The gulf stream as an inertial boundary layer. *Tellus*, **8**, pp 83-92.

Chuang, W.-S., and W. C. Boicourt, (1989) Resonant seiche motion in the Chesapeake Bay. *J. Geophys. Res*, **94**, pp 2105-2110.

Crepon, M., and C. Richez, (1982) Transient upwelling generated by 2-dimensional atmospheric forcing and variability in the coastline. *J. Phys. Oceanogr.*, **12**, pp 1437-1457.

Crepon, M., C. Richez, and M. Cartier, (1984) Effects of coastline geometry on upwelling. *J. Phys Oceanogr.*, **14**, pp 1365-1382.

Csanady, G. T.,(1982) On the structure of transient upwelling events. *J. Phys. Oceanogr.*, **12**, pp 84-96.

Csanady, G. T.,(1983) *Circulation in the Coastal Ocean,* D. Reidel Publishing Company, 279 p.

Csanady, G. T., and J. T. Scott, (1974) Baroclinic coastal jets in Lake Ontario within the coastal zone. *J Geophys Res*, **85**, pp 2787-2812.

Cushing, D. H., (1971) Upwelling and the Production of Fish. *Adv. mar Biol.*, **9**, pp 255-334.

Déry, F., (1992) Department of Atmospheric and Oceanic Sciences, McGill University, 805 Sherbrooke St. West, Montréal, Qc., H3A 2K6. Personal communication.

Dickie, L. M., (1955) Fluctuations in abundance of the grant scallop Placopecten Magellanicus (Gmelin) in the Digby area of the Bay of Fundy. *J. Fish. Res. Bd. Can.*, **12(6)**, pp 797-857.

Dickie, L. M., and R. W. Trites, (1983) The Gulf of St-Lawrence. In B. H. Ketchum (ed.), *Estuaries and enclosed seas*, Elsevier, Amsterdam, pp 403-425.

Dyer, K. R., (1973) *Estuaries. A Physical Introduction,* John Wiley & Sons, New York, NY, 140 p.

El Sabh, M. I., (1991) OPEN Annual Report, Dalhousie University, Halifax, N.S..

El Sabh, M. I. and J. Chassé, (1991) Département d'océanographie, Université du Québec à Rimouski, Rimouski, Qc., G5L 3A1. Personal communication.

El Sabh, M. I. and J. Chassé, (1992) Numerical modeling of tides in Baie-des-Chaleurs, in *Mesoscale Meteorology and Oceanography.* Abstract presented at the 26th Annual Congress of the Canadian Meteorological and Oceanographic Society, Université Laval, June 8-12 1992.

Ford, M., J. Wang, and R. T. Cheng, (1990) Predicting the vertical structure of tidal current and salinity in San Francisco Bay, California. *Water Resour. Res.*, **26**, pp 1027-1045.

Freeland, H. J., F. M. Boland, J. A. Church, A. J. Clarke, A. M. G. Forbes, A. Huyer, R. L. Smith, R. O. R. Y. Thompson, and N. J. White, (1986) The Australian Coastal Experiment: A Search for Coastal-Trapped Waves. *J Phys. Oceanogr.*, **16**, pp 1230-1249.

Freeland H. L. and K. L. Denman, (1982) A topographically controlled upwelling center off southern Vancouver Island. *J Mar Res.*, **42**, pp 1069-1093.

Gill, A. E. and A. J. Clarke, (1974) Wind-induced upwelling, coastal currents and sea-level changes. *Deep-Sea Research*, **21**, pp 325-345.

Godin, G., (1972) *The Analysis of Tides,* U. of Toronto Press, Toronto, 264 p.

Golden Software, Inc. (1990) *Surfer, Version 4, Reference manual,* Golden, Colorado 80402-0281 USA.

Greatbatch R. J., and T. Otterson, (1991) On the Formulation of Open Boundary Conditions at the mouth of a bay. *J Geophys. Res.*, **96**, pp 18 431-18 445.

Halpern, D., (1974) Variations in the density field during coastal upwelling. *Tethys*, **6**, pp 363-374.

Hansen, D. V., and M. Jr. Rattray, (1966) New dimensions in estuary classification. *Limn. Oceanogr.*, **11**, pp 319-326.

Huthnance, J. M., L A. Mysak, and D.-P. Wang, (1986) Coastal Trapped Waves. In *Baroclinic Processes on Continental Shelves*, N. K. Mooers (ed.), Coastal and Estuarine Sciences 3, American Geophysical Union, pp 1-18.

Ingram, R. G., and M. I. El Sabh, (1991) Fronts and mesoscale features in the St. Lawrence estuary. In *Oceanography of a Large-Scale Estuarine System. The St. Lawrence*, M. El Sabh, N. Silverberg (eds.), Coastal and estuarine studies, Springer Verlag, New York, pp 71-93.

Jalickee, J. B., and D. R. Hamilton, (1977) Objective analysis and classification of oceanographic data. *Tellus*, **29**, pp 545-560.

Jenkins, G. M., and D. G. Watts, (1968) *Spectral Analysis and its applications*, San-Francisco, Ca., 525 p.

Killworth, P. D., (1978) Coastal upwelling and Kelvin waves with small longshore topography. *J. Phys.Oceanogr.*, **8**, pp 188-205.

Kjerfve, B., (1988) *Hydrodynamics of Estuaries V.1: Estuarine physics*, CRC Press, Boca Raton, Florida, 163 p.

Koutitonsky, V. G., and G. L. Bugden, (1991) The physical oceanography of the Gulf of St. Lawrence: A review with emphasis on the synoptic variability of the motion. In J.-C. Therriault (ed.) *The Gulf of St-Lawrence: small ocean of big estuary?* Can. Spec. Publ. Fish. Aquat. Sci., **113**, pp 57-90.

Koutitonsky, V. G., and R. E. Wilson, (1988) Coastal-trapped waves in continuously stratified channels. Part I: Numerical description of behavioral properties. *J Phys. Oceanogr*, **18**, pp 652-661.

Lacroix, G., (1958) *Contribution à l'écologie des Euphausiacés du sud-ouest de golfe Saint-Laurent,* Mémoire de maîtrise, Université de Montréal, Montréal, Québec, 177 p

Lacroix, G. and G. Filteau, (1969) Les fluctuations quantitatives du zooplancton de la Baie-des-Chaleurs (Golfe du St-Laurent). 1. Conditions hydroclimatiques et analyse volumétriques, *Naturaliste can*, **96**, pp 359-397.

Lambert, J.-D., (1982) *Contribution à l'étude des communautés planctoniques de la Baie des Chaleurs,* Mémoire de maîtrise, Université du Québec à Rimouski, Rimouski, Québec.

Lauzier, L. M., (1957) Variations of temperature and salinity in shallow waters of the southwestern Gulf of St-Lawrence. *Bull. Fish. Res Bd Can*, **111**, pp 251-268.

Lauzier, L. M., (1967) Bottom residual drift on the continental shelf area of the Canadian Atlantic coast. *J Fish. Bd. Can*, **24**, pp 1845-1959.

Lauzier, L. M., and G. Filteau, (1948) Observations de température et de salinité à la station Laval 290, en 1946. *Rapp ann. Sta biol St-Laurent*, **5**, pp 69-71.

Lauzier, L. M., R. W. Trites, and H. B. Hachey, (1957) Some features of the surface layer of the gulf of St. Lawrence. *Bull. Fish. Res. Bd. Can.*, **111**, pp 195-212.

Legendre, L., (1971) Production primaire dans la Baie-des-Chaleurs (Golfe du St-Laurent). *Naturaliste can* , **98**, pp 743-773.

Legendre, L. and W. D. Watt, (1970) Travaux sur les pêcheries du Québec. *Marine Biol.*, **Vol.7**, pp 167-170.

Loring, D. H., and D. J. G. Nota, (1973) Morphology and sediments of the Gulf of St-Lawrence. *Bull. Fish. Res Bd Can.*, **no.182**, 147 p.

Marcotte, A., (1964) Observations quotidiennes de la température superficielle de l'eau de mer à Grande-Rivière (Baie des Chaleurs) 1951-1962. *Cah. Inf. Sta. Biol. mar. Grande-Rivière*, **no.20**, pp 1-4.

Maslanik J. A., and R. G. Barry, (1989) Short-term interactions between atmospheric synoptic conditions and sea ice behavior in the Arctic. *Annals Glaciol.*, **12**, pp 113-117.

Matheson, K. M., (1967), *The meteorological effects on ice in the GSL*, M. Sc. Thesis, McGill University, Montréal, Québec, 110 p.

McClean-Padman, J., and L. Padman, (1991) Summer upwelling on the Sydney inner continental shelf: The relative roles of local wind forcing and mesoscale eddy encroachment. *Cont. Shelf Res* , **Vol.11, no.4**, pp 321-345.

Mertz, G., V. G. Koutitonsky and Y. Gratton, (1991) On the seasonal cycle of the Gaspé current. In J.-C. Therriault (ed.) *The Gulf of St-Lawrence. small ocean of big estuary?* Can. Spec. Publ. Fish. Aquat. Sci., **113**, pp 149-152.

Messier, D., (1976) La pêche des pétoncles dans le golfe du St-Laurent. *Ministère de l'industrie et du commerce, direction des pêcheries maritimes, direction de la recherche*, **N.72**, 48 p.

Moran, J. M., and M. D. Morgan, (1991) *Meteorology: The Atmosphere and the Science of Weather, third edition*. Macmillan Publishing Company, 586 p.

Mysak, L. A., (1980) Recent advances in shelf wave dynamics. *Rev. Geophys.*, **18**, pp 211-241.

Narimousa, S. and T. Maxworthy, (1986) Effects of discontinuous surface stress on a model of coastal upwelling. *J. Phys. Oceanogr.*, **16**, pp 2071-2083.

Officer, C. B., (1976) *Physical oceanography of estuaries (and associated coastal waters)*, John Wiley & Sons, New York, NY, 465 p.

Petrie, B., B. Toulany, and C. Garrett, (1988) The transport of water, heat and salt through the Strait of Belle-Isle. *Atmosphere-Ocean*, **26**, pp 234-251.

Philander, S. G. H., and J.-H. Yoon, (1982) Eastern boundary currents and coastal upwelling. *J. Phys. Oceanogr.*, **12**, pp 862-879.

Pingree R. D., and D. K. Griffiths, (1980) A numerical model of the M_2 tide in the Gulf of St-Lawrence. *Oceanologica Acta*, **3**, pp 221-225.

Pond, S. and G. L. Pickard, (1983) *Introductory Dynamical Oceanography, 2nd edition*, Pergamon Press, New York, NY, 329 p.

Pritchard, D. W., (1955) Estuarine circulation patterns. *Prog. Amer. Soc. Civil Eng.*, **81**, no.717.

Rose, G. A., (1988) *Temporal and Spatial Variability in Onshore Cod (Gadus morhua).* Ph. D. Thesis, McGill university, Montréal, Québec.

Ryther, J. H., (1969) Photosynthesis and fish production in the sea. *Science*, **166**, pp 72-76.

Schafer, C. T.,(1976), Distribution and depositional history of sediments in the Baie des Chaleurs, Gulf of St-Lawrence. *Can. J. Earth Sci.*, **14**, pp 593-605.

Sea-Bird Electronics, Inc., (1990) *Conductivity, temperature, depth recorder, operating manual,* Bellevue, Washington 98005 USA.

Simpson, J. H., and J. R. Hunter, (1974) Fronts in the Irish Sea, *Nature*, **1250**, pp 404-406

Smith, L. S., (1968) Upwelling. *Oceanogr. Mar. Biol Ann. Rev.*, **6**, pp 11-46.

Sverdrup, H. U., (1938) On the process of upwelling. *J. Mar Res.*, **1**, pp 155-164.

Tee, K.-T., (1991) Meteorologically and buoyancy induced subtidal salinity and velocity variations in the St. Lawrence estuary. In *Oceanography of a Large-Scale Estuarine System: The St Lawrence*, M. El Sabh, N. Silverberg (eds.), Coastal and estuarine studies, Springer Verlag, New York, pp 51-70.

Tiphane, M., (1965) Topographie de la Baie des Chaleurs. *Cah. Inf. Stn biol mar. Grande-Rivière*, **29**, pp 1-3.

Tremblay, J. L., (1943) *Rapport général sur les activités de la Station de biologie du St-Laurent pendant les années 1936-1942*, Université Laval, Ste-Foy, Québec, **no.4**, pp 1-100.

Wong, K.-C., (1991) The response of the Delaware estuary to the combined forcing from Chesapeake Bay and the ocean. *J. Geophys. Res* , **96**, pp 8797-8809.

Wong, K.-C., and R. W. Garvine, (1984) Observations of wind-induced, subtidal variability in the Delaware estuary. *J. Geophys. Res.*, **89**, pp 10 589-10 597.

Wyrtki, K., (1963) The horizontal and vertical field in the Peru current. *Bull Scripps Instn Oceanogr.*, **8**, pp 313-346.

Yao, T.,(1986) The response of Trinity Bay, Newfoundland, to local wind forcing. *Atmosphere-Ocean*, **24**, pp 235-252.

Yao T., H. J. Freeland and L. A. Mysak, (1984) A comparison of low-frequency current observations off British-Columbia with Coastally Trapped Wave theory. *J. Phys Oceanogr.*, **14**, pp 22-34.

FIGURES

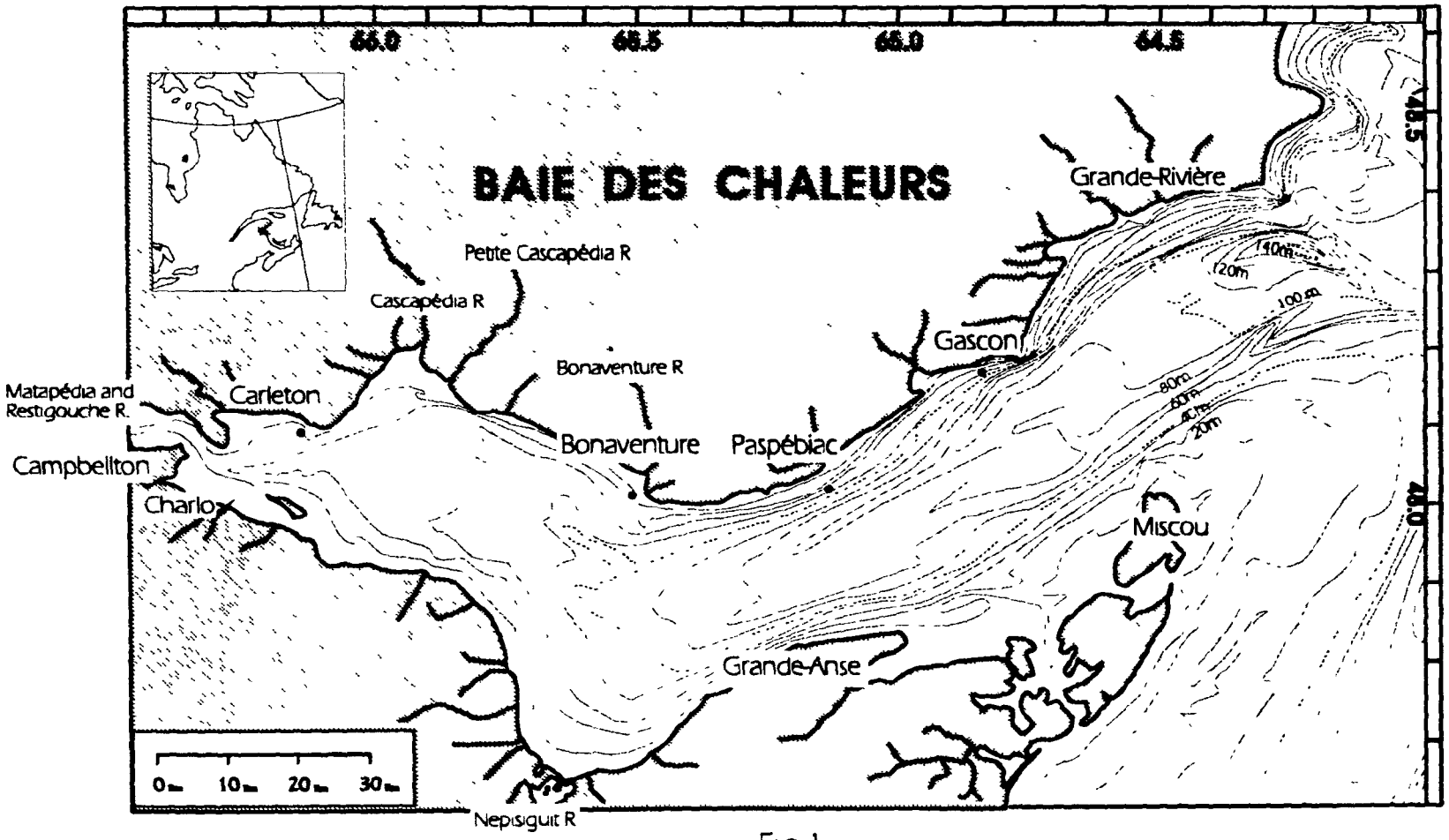
66.0
65.5
65.0
64.5
48.5
48.0
BAIE DES CHALEURS
Grande-Rivière
Petite Cascapédia R
Cascapédia R
Gascon
Bonaventure R
Matapédia and
Restigouche R.
Carleton
Bonaventure
Paspébiac
Campbellton
Charlo
Miscou
Grande-Anse
0
10
20
30
Nepisiguit R

Fig 1

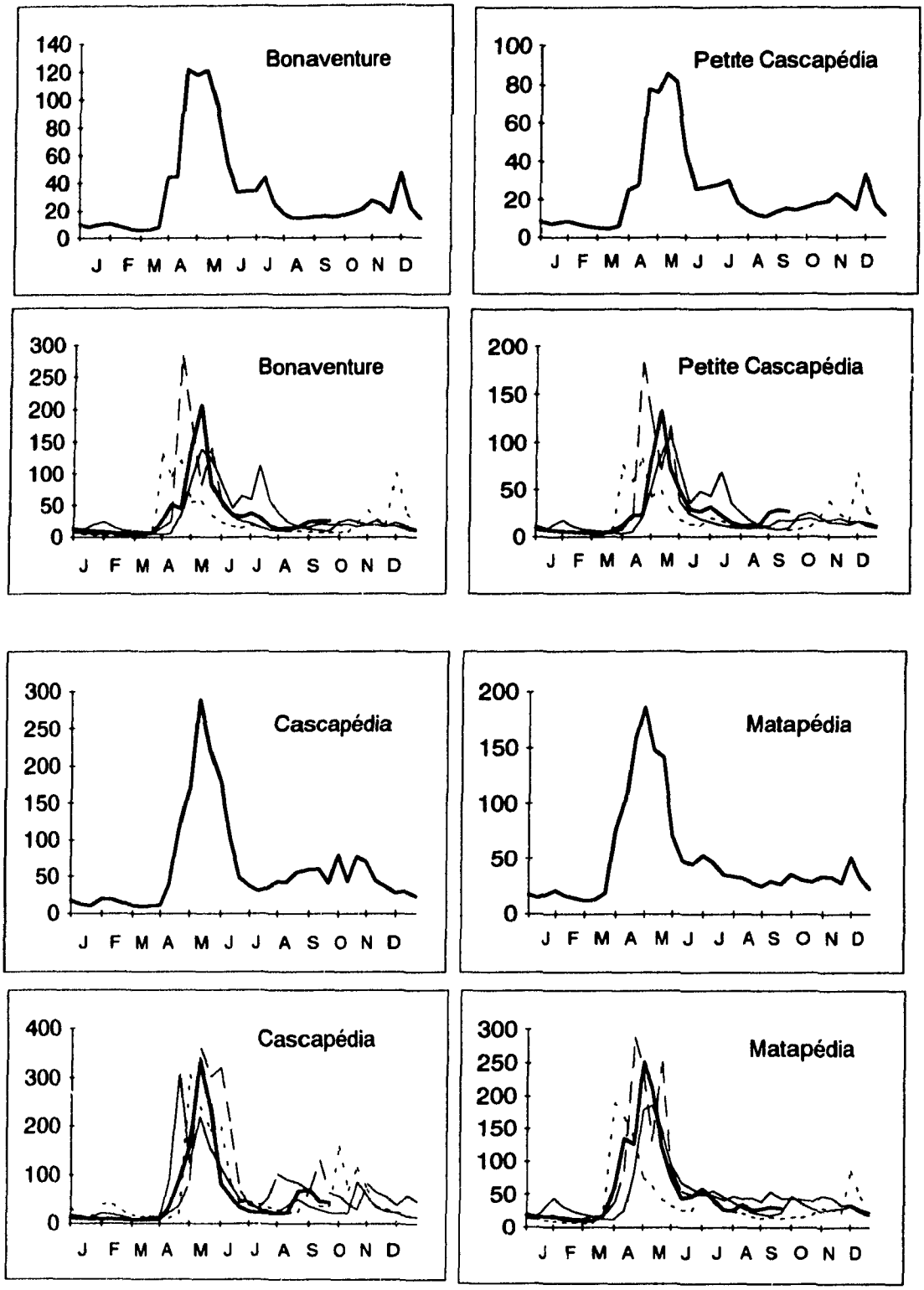
Bonaventure
Petite Cascapédia
Bonaventure
Petite Cascapédia
Cascapédia
Matapédia
Cascapédia
Matapédia
J F M A M J J A S O N D

Fig. 2

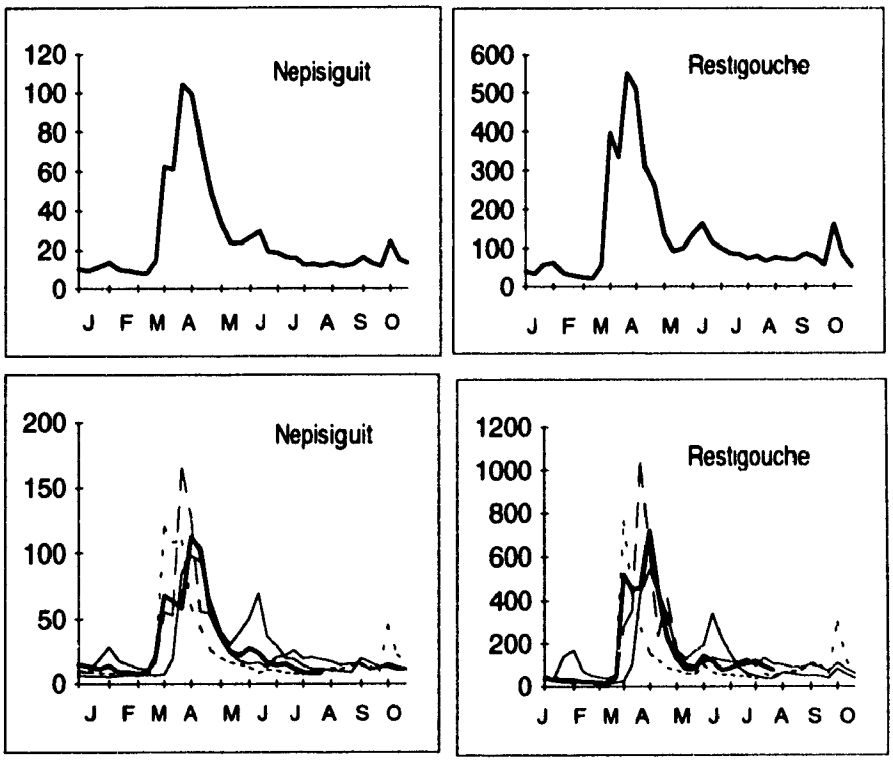
Nepisiguit
Restigouche
Nepisiguit
Restigouche
J F M A M J J A S O

Fig. 3

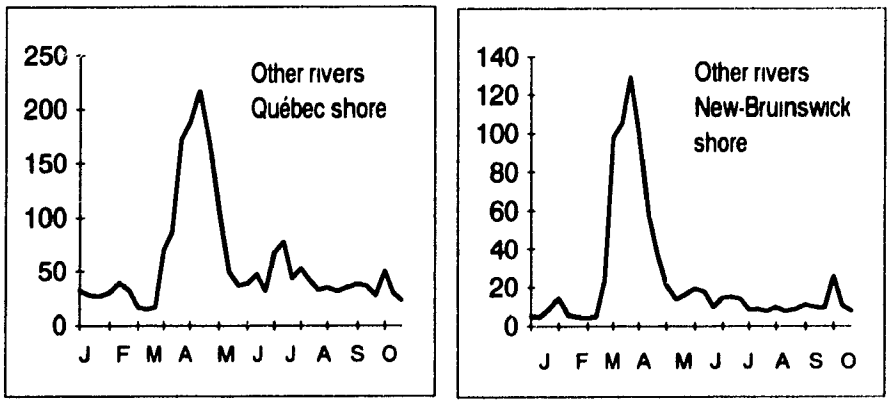
Other rivers
Québec shore
Other rivers
New-Brunswick
shore
J F M A M J J A S O

Fig. 4

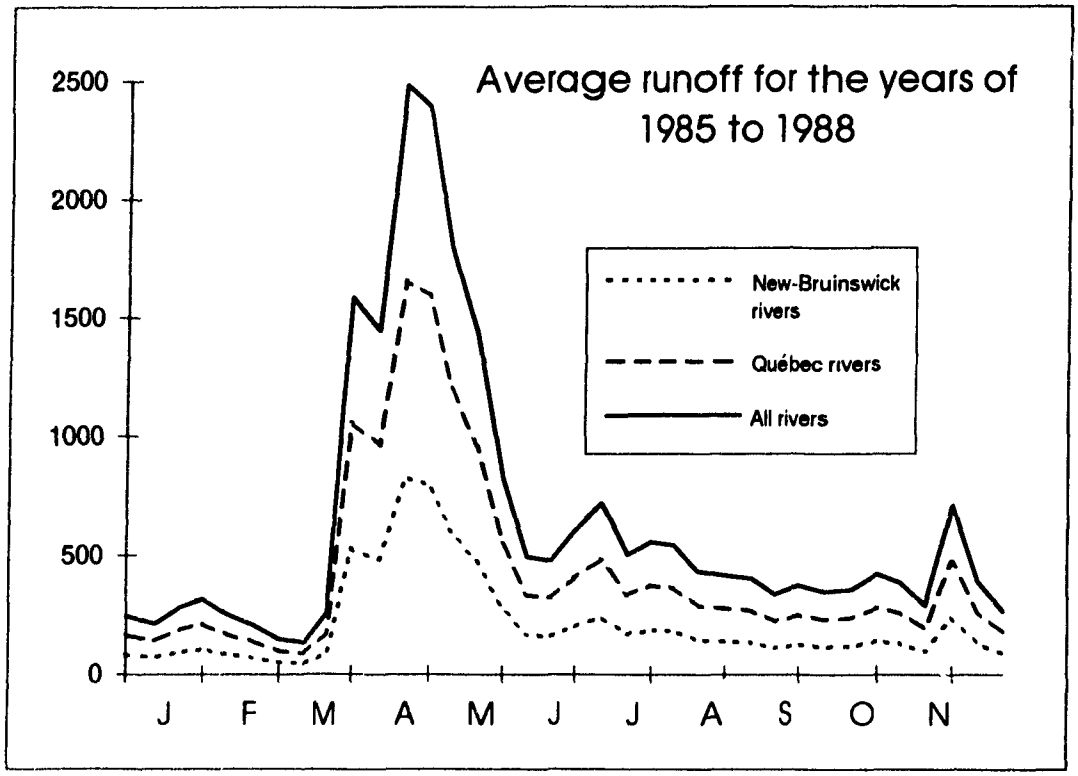
Average runoff for the years of 1985 to 1988
2500
2000
1500
1000
500
0
J
F
M
A
M
J
J
A
S
O
N
New-Bruinswick rivers
Québec rivers
All rivers

Fig.5

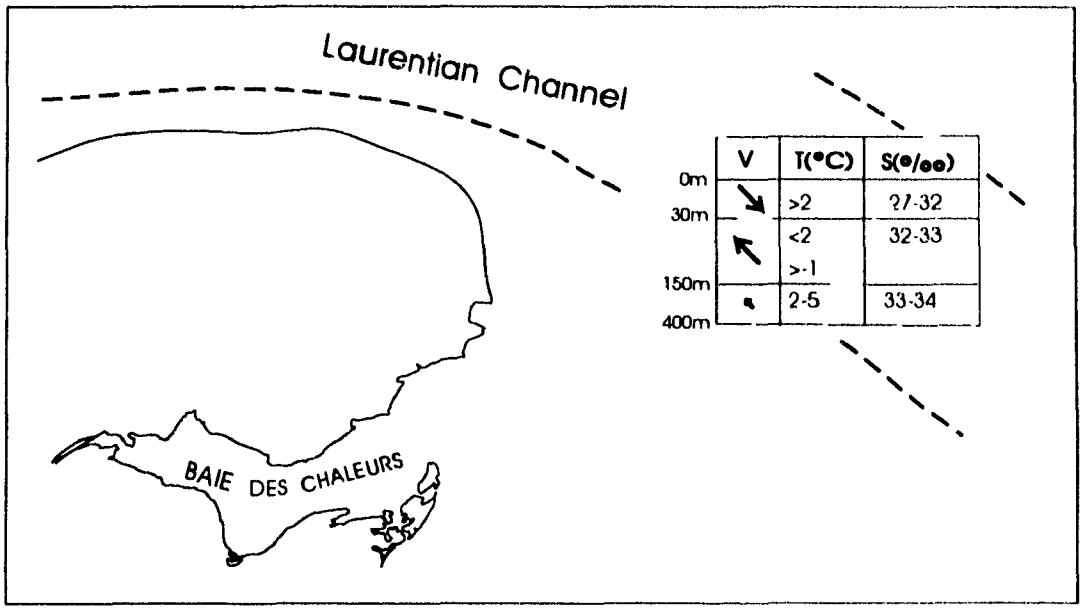
Laurentian Channel
BAIE DES CHALEURS
V
T(°C)
S(‰)
0m
30m
150m
400m
>2
27-32
<2
>-1
32-33
2-5
33-34

Fig.6

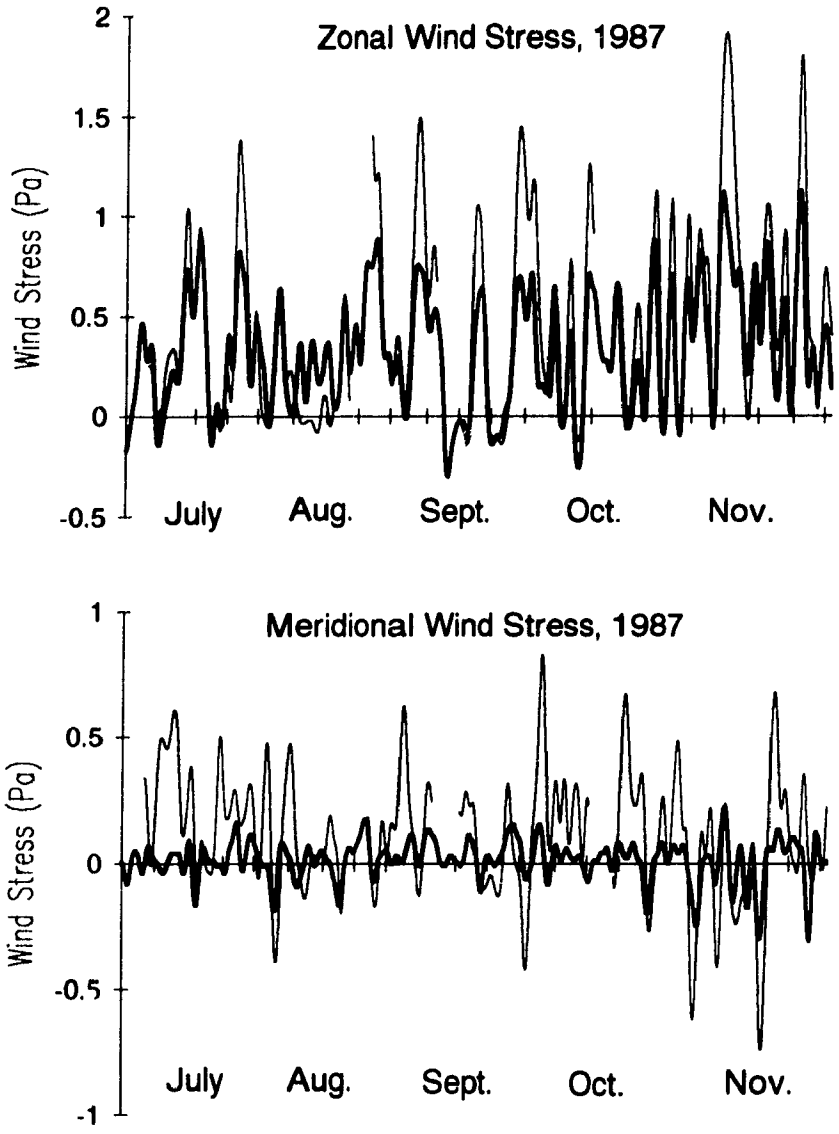
Zonal Wind Stress, 1987
Wind Stress (Pa)
2
1.5
1
0.5
0
-0.5
July
Aug.
Sept.
Oct.
Nov.
Meridional Wind Stress, 1987
Wind Stress (Pa)
1
0.5
0
-0.5
-1
July
Aug.
Sept.
Oct.
Nov.

Fig.7

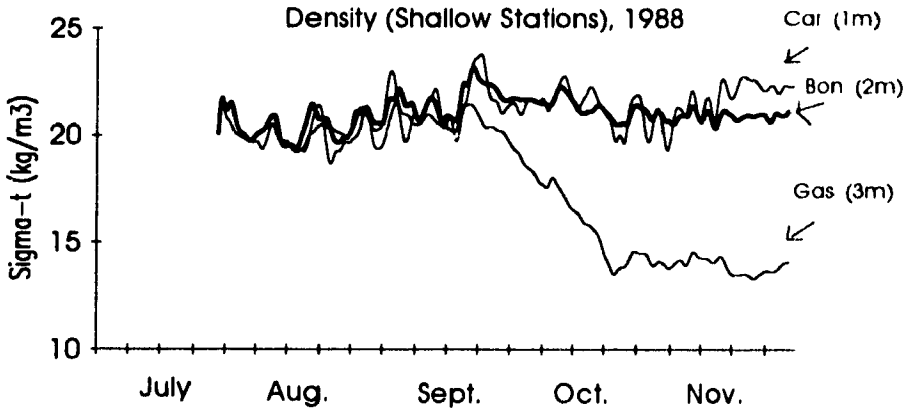
Density (Shallow Stations), 1988
Car (1m)
Bon (2m)
Gas (3m)
Sigma-t (kg/m3)
25
20
15
10
July
Aug.
Sept.
Oct.
Nov.

Fig. 8

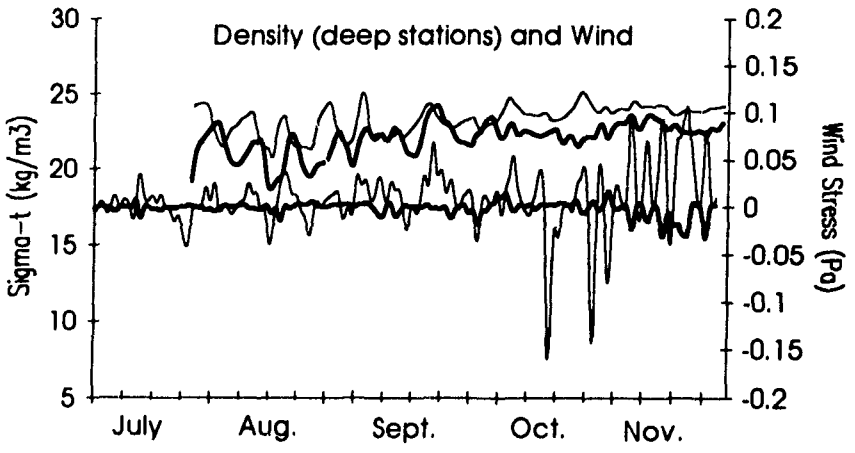
Density (deep stations) and Wind
Sigma-t (kg/m3)
Wind Stress (Pa)
30
25
20
15
10
5
0.2
0.15
0.1
0.05
0
-0.05
-0.1
-0.15
-0.2
July
Aug.
Sept.
Oct.
Nov.

Fig. 9

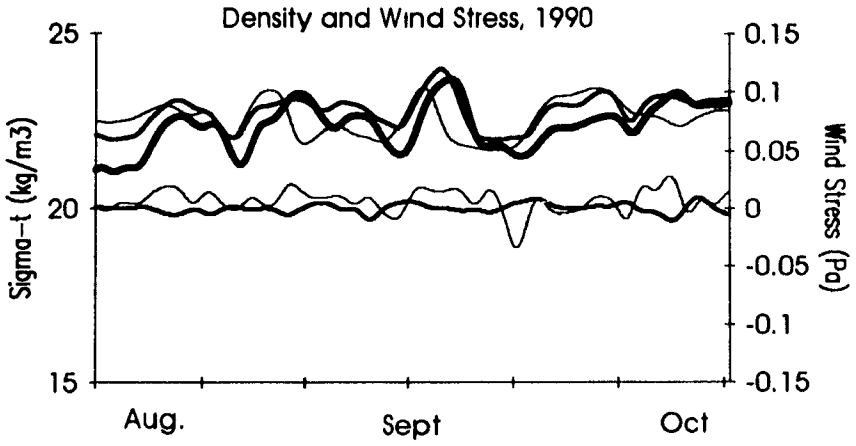
Density and Wind Stress, 1990
25
20
15
Sigma-t (kg/m3)
0.15
0.1
0.05
0
-0.05
-0.1
-0.15
Wind Stress (Pa)
Aug.
Sept
Oct

Fig. 10

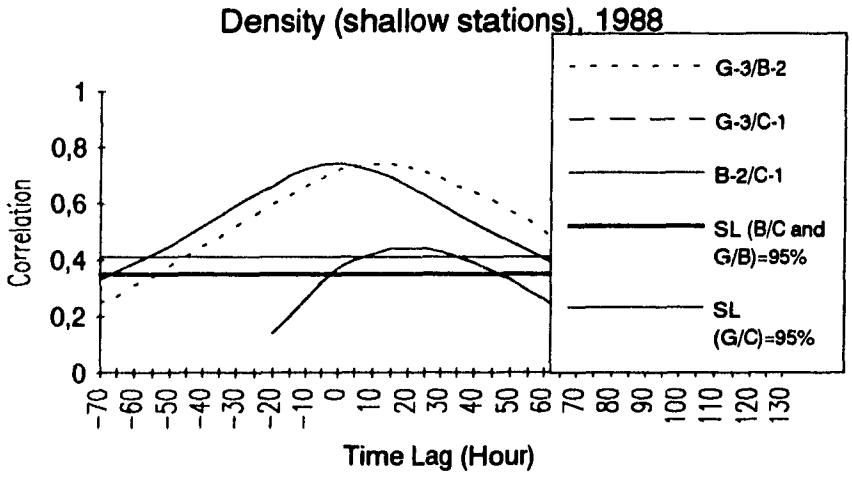
Density (shallow stations), 1988
G-3/B-2
G-3/C-1
B-2/C-1
SL (B/C and G/B)=95%
SL (G/C)=95%
Correlation
1
0,8
0,6
0,4
0,2
0
-70 -60 -50 -40 -30 -20 -10 0 10 20 30 40 50 60 70 80 90 100 110 120 130
Time Lag (Hour)

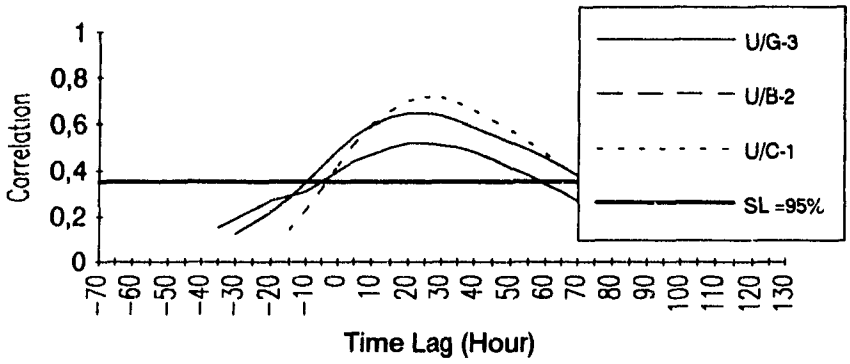
Zonal Wind Stress and Density (shallow stations), 1988
U/G-3
U/B-2
U/C-1
SL =95%
Correlation
1
0,8
0,6
0,4
0,2
0
-70 -60 -50 -40 -30 -20 -10 0 10 20 30 40 50 60 70 80 90 100 110 120 130
Time Lag (Hour)

b.

Fig. 11

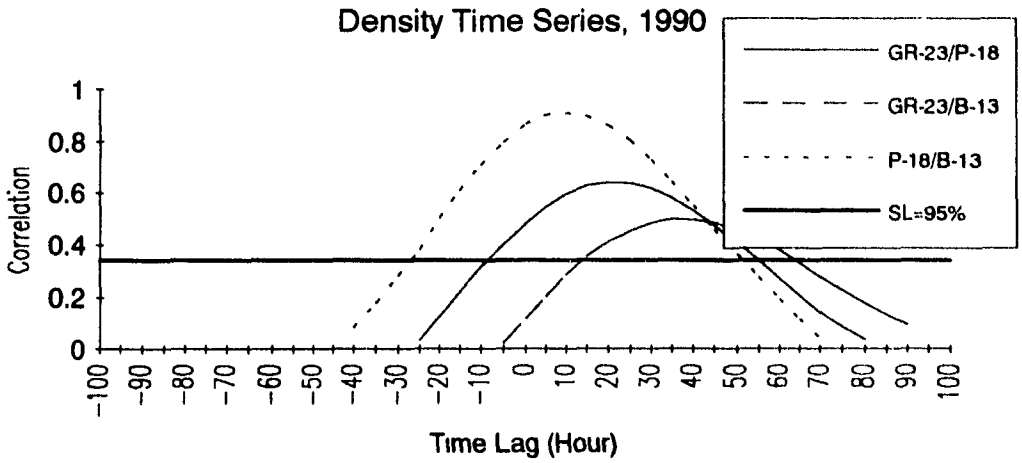
Density Time Series, 1990
GR-23/P-18
GR-23/B-13
P-18/B-13
SL=95%
Correlation
Time Lag (Hour)

f.

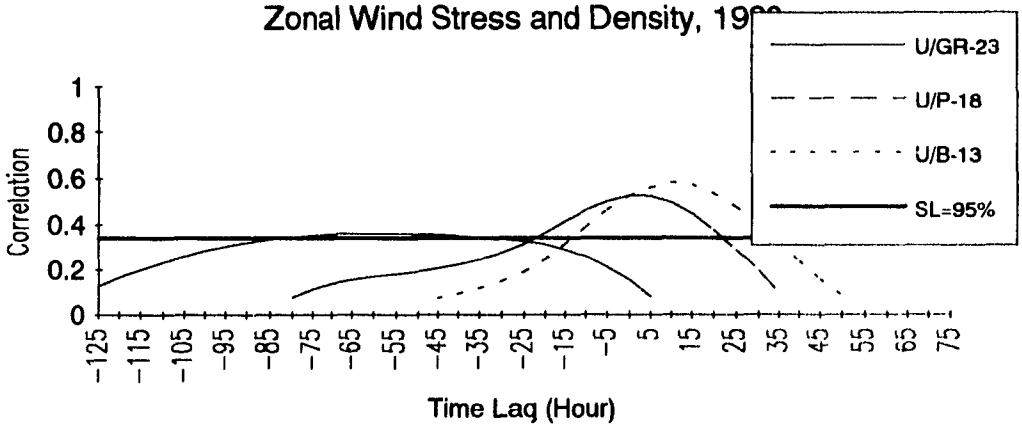
Zonal Wind Stress and Density, 19
U/GR-23
U/P-18
U/B-13
SL=95%
Correlation
Time Lag (Hour)

g.

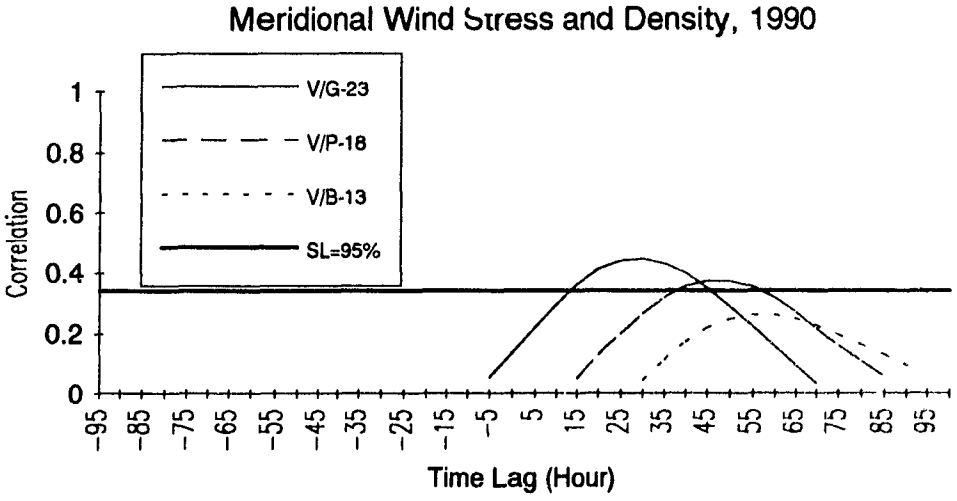
Meridional Wind Stress and Density, 1990
V/G-23
V/P-18
V/B-13
SL=95%
Correlation
Time Lag (Hour)

h.

Fig. 11

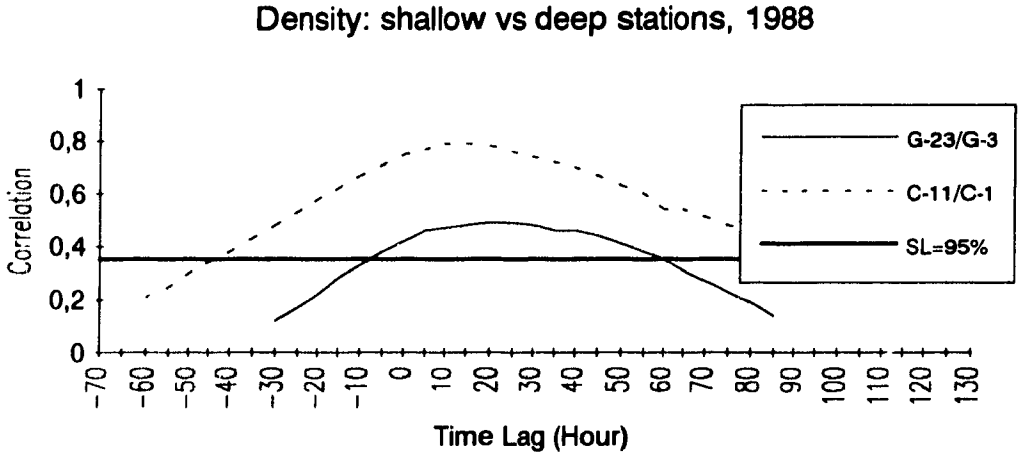
Density: shallow vs deep stations, 1988
Correlation
1
0,8
0,6
0,4
0,2
0
-70
-60
-50
-40
-30
-20
-10
0
10
20
30
40
50
60
70
80
90
100
110
120
130
Time Lag (Hour)
G-23/G-3
C-11/C-1
SL=95%

i.

Fig. 11

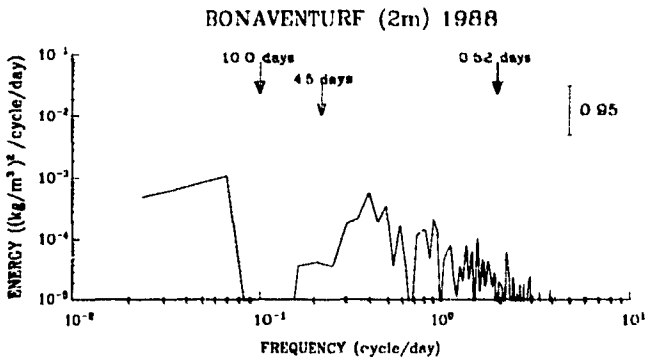
BONAVENTURE (2m) 1988
10 0 days
4 5 days
0 52 days
0 95
ENERGY ((kg/m³)² /cycle/day)
FREQUENCY (cycle/day)

a)

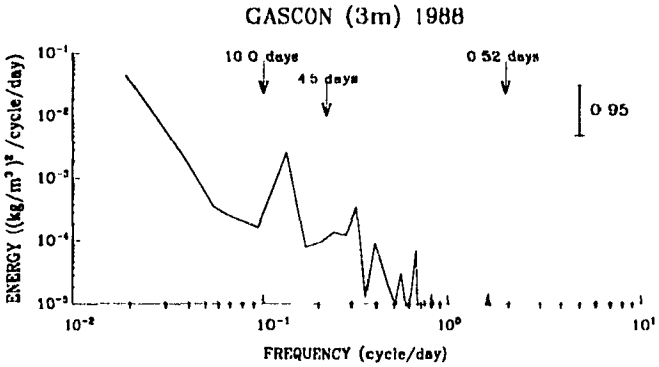
GASCON (3m) 1988
10 0 days
4 5 days
0 52 days
0 95
ENERGY ((kg/m³)² /cycle/day)
FREQUENCY (cycle/day)

b)

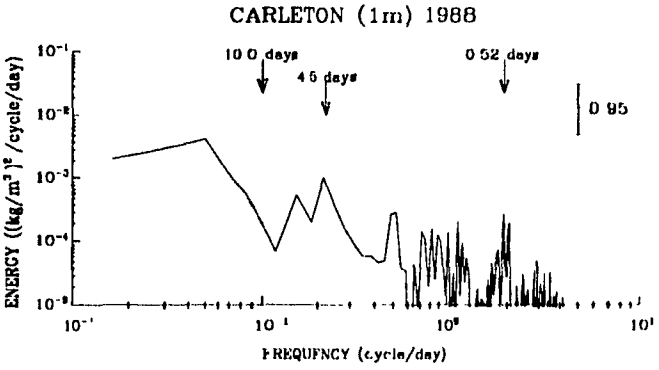
CARLETON (1m) 1988
10 0 days
4 5 days
0 52 days
0 95
ENERGY ((kg/m³)² /cycle/day)
FREQUENCY (cycle/day)

c)

Fig. 12

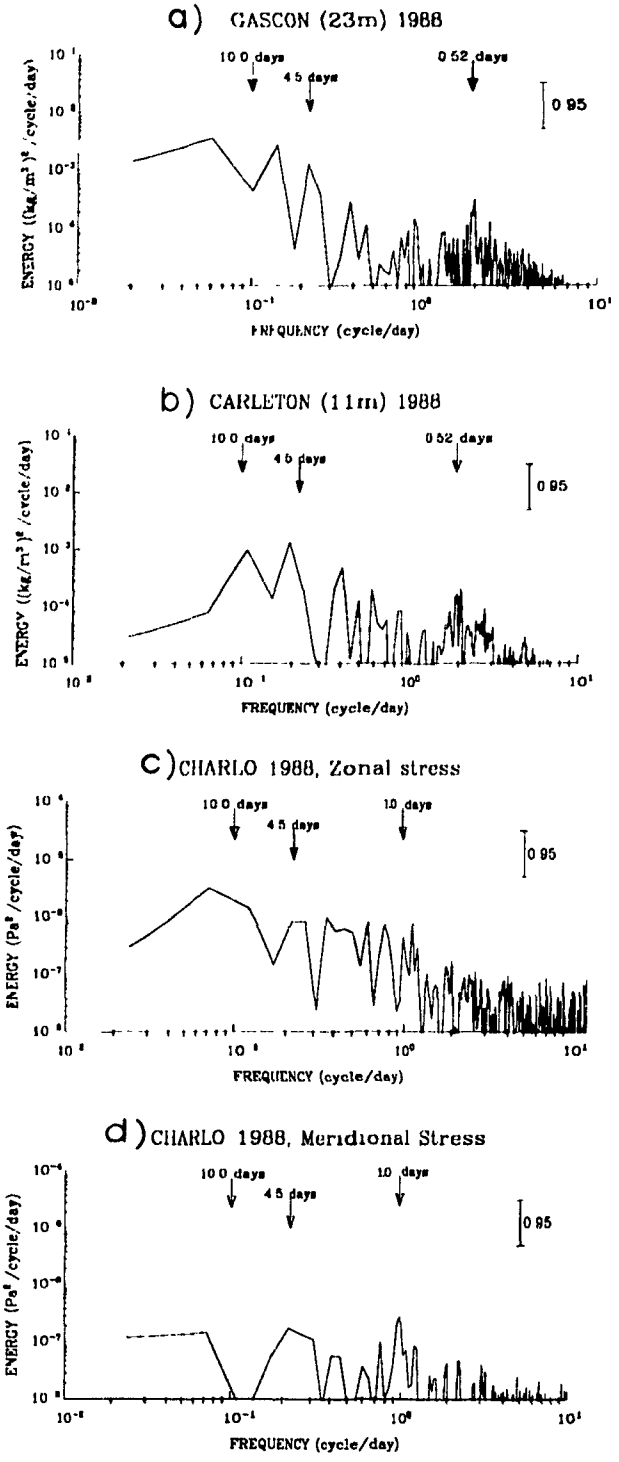
a) GASCON (23m) 1988
10 0 days
4 5 days
0 52 days
0 95
ENERGY ((kg/m³)² /cycle/day)
FREQUENCY (cycle/day)
b) CARLETON (11m) 1988
10 0 days
4 5 days
0 52 days
0 95
ENERGY ((kg/m³)² /cycle/day)
FREQUENCY (cycle/day)
c) CHARLO 1988, Zonal stress
10 0 days
4 5 days
10 days
0 95
ENERGY (Pa² /cycle/day)
FREQUENCY (cycle/day)
d) CHARLO 1988, Meridional Stress
10 0 days
4 5 days
10 days
0 95
ENERGY (Pa² /cycle/day)
FREQUENCY (cycle/day)

Fig. 13

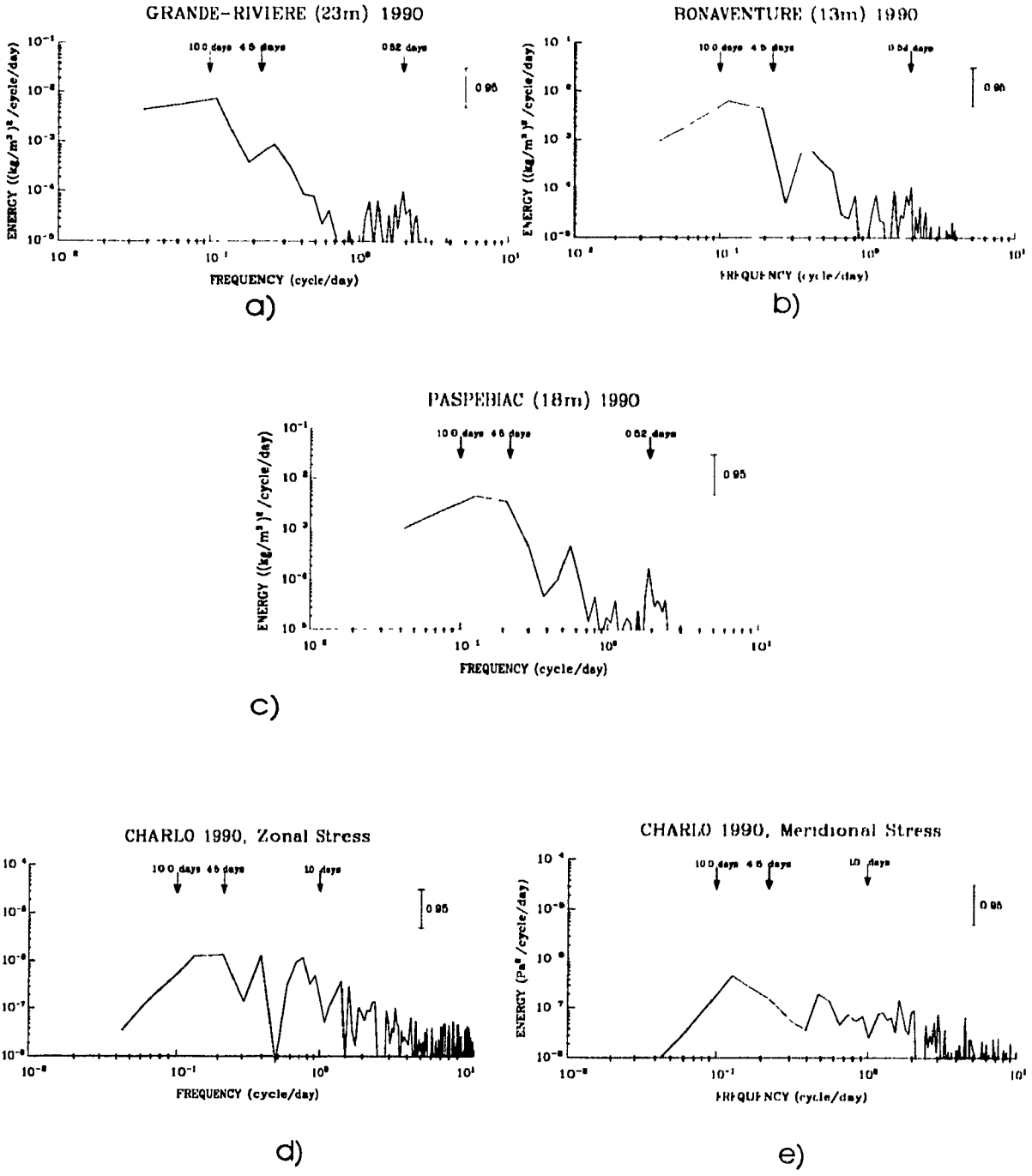
GRANDE-RIVIERE (23m) 1990
BONAVENTURE (13m) 1990
PASPEBIAC (18m) 1990
CHARLO 1990, Zonal Stress
CHARLO 1990, Meridional Stress
FREQUENCY (cycle/day)
a)
b)
c)
d)
e)

Fig. 14

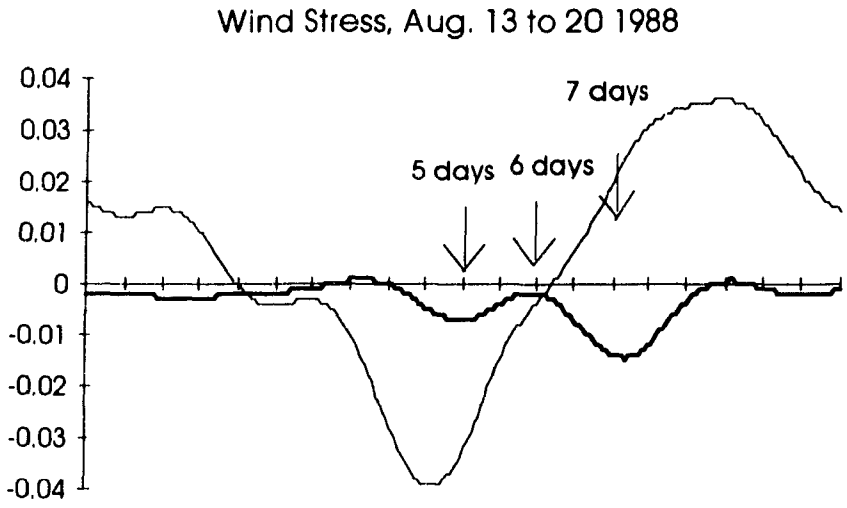
Wind Stress, Aug. 13 to 20 1988
0.04
0.03
0.02
0.01
0
-0.01
-0.02
-0.03
-0.04
7 days
5 days
6 days

Fig.15

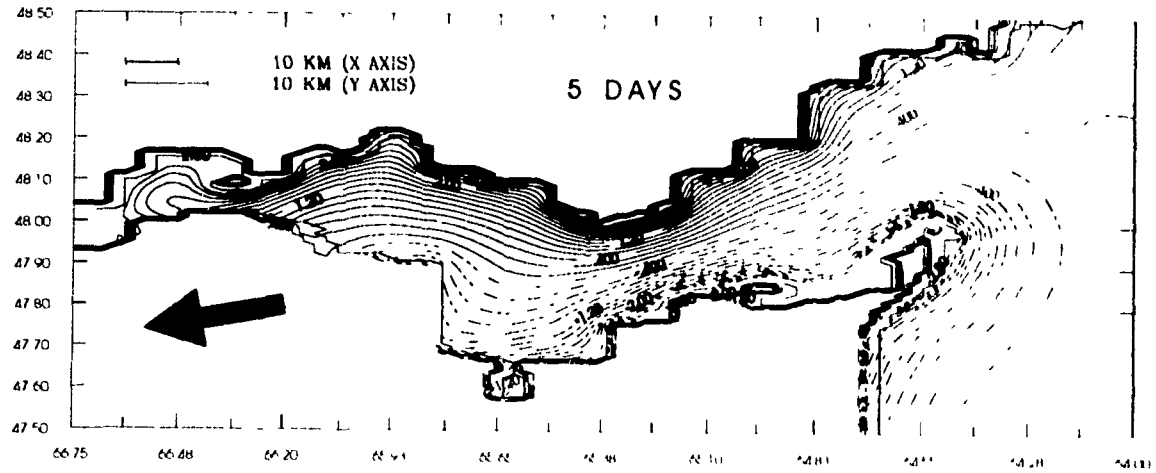

a)

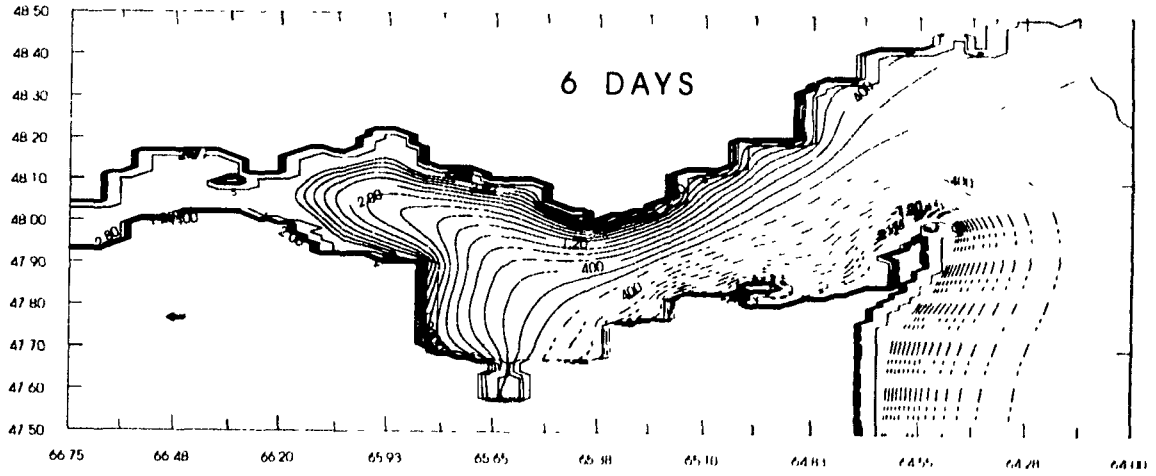

b)

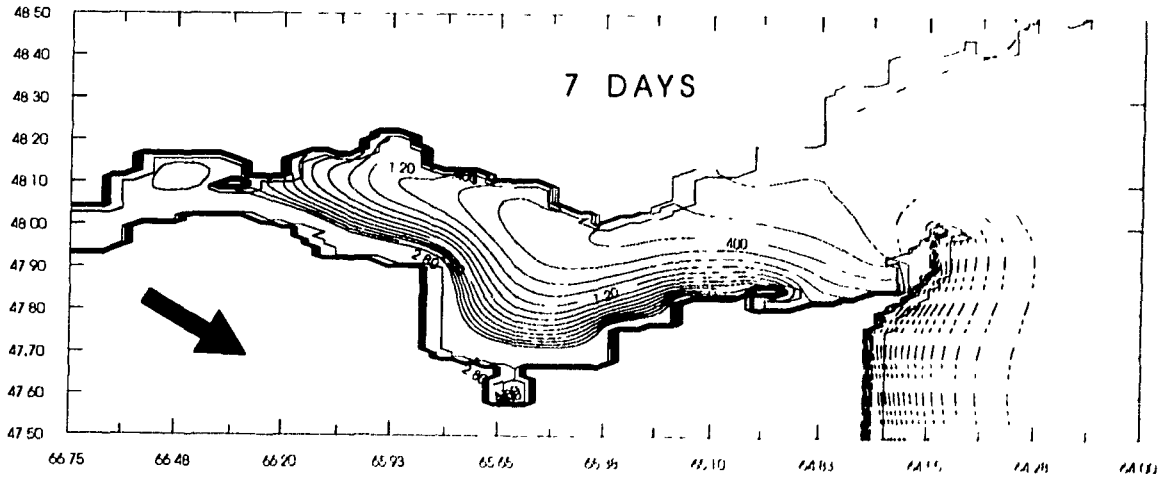

c)

Fig.16

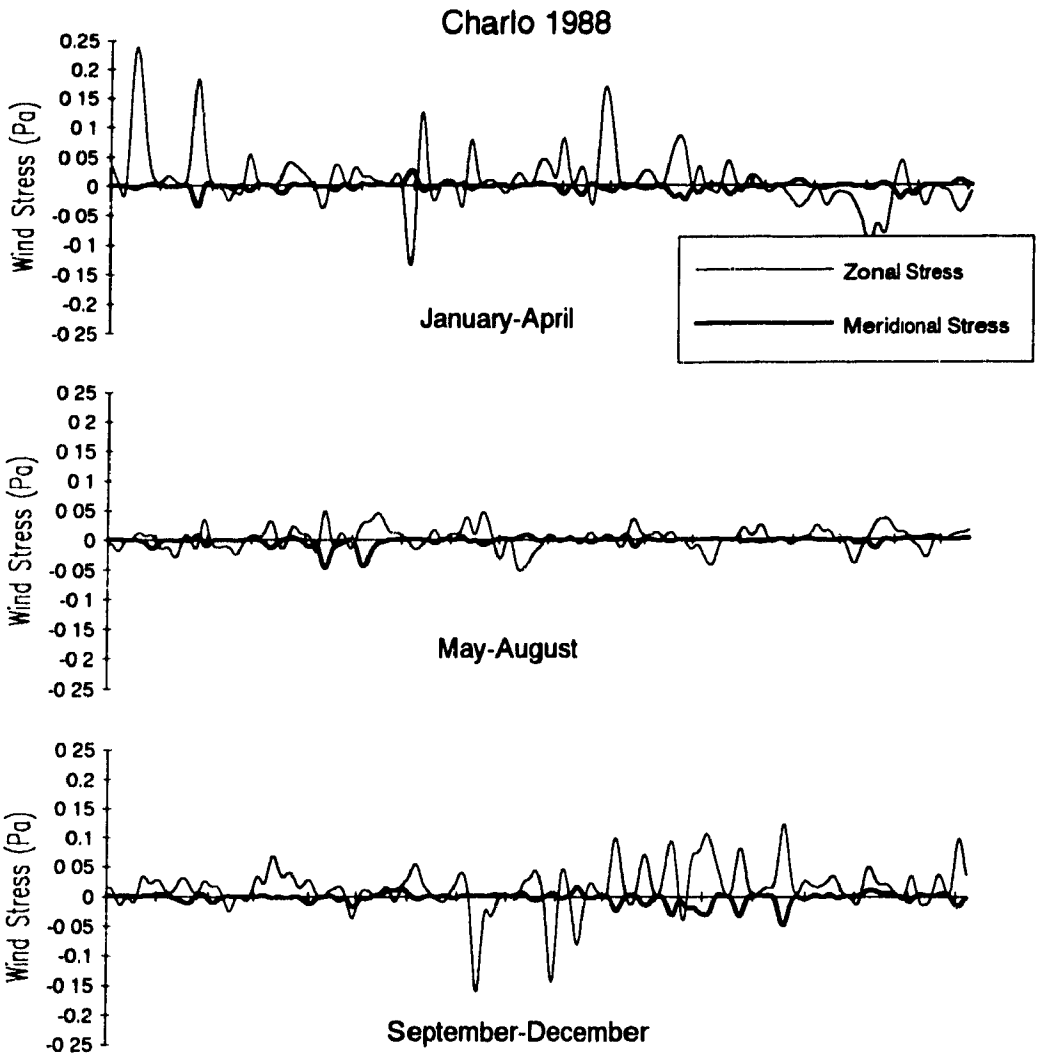
Charlo 1988
Wind Stress (Pa)
0.25
0.2
0 15
0 1
0 05
0
-0 05
-0 1
-0 15
-0.2
-0 25
January-April
Zonal Stress
Meridional Stress
Wind Stress (Pa)
0 25
0 2
0 15
0 1
0 05
0
-0 05
-0 1
-0 15
-0 2
-0 25
May-August
Wind Stress (Pa)
0 25
0.2
0 15
0.1
0 05
0
-0 05
-0.1
-0 15
-0.2
-0 25
September-December

Fig.17

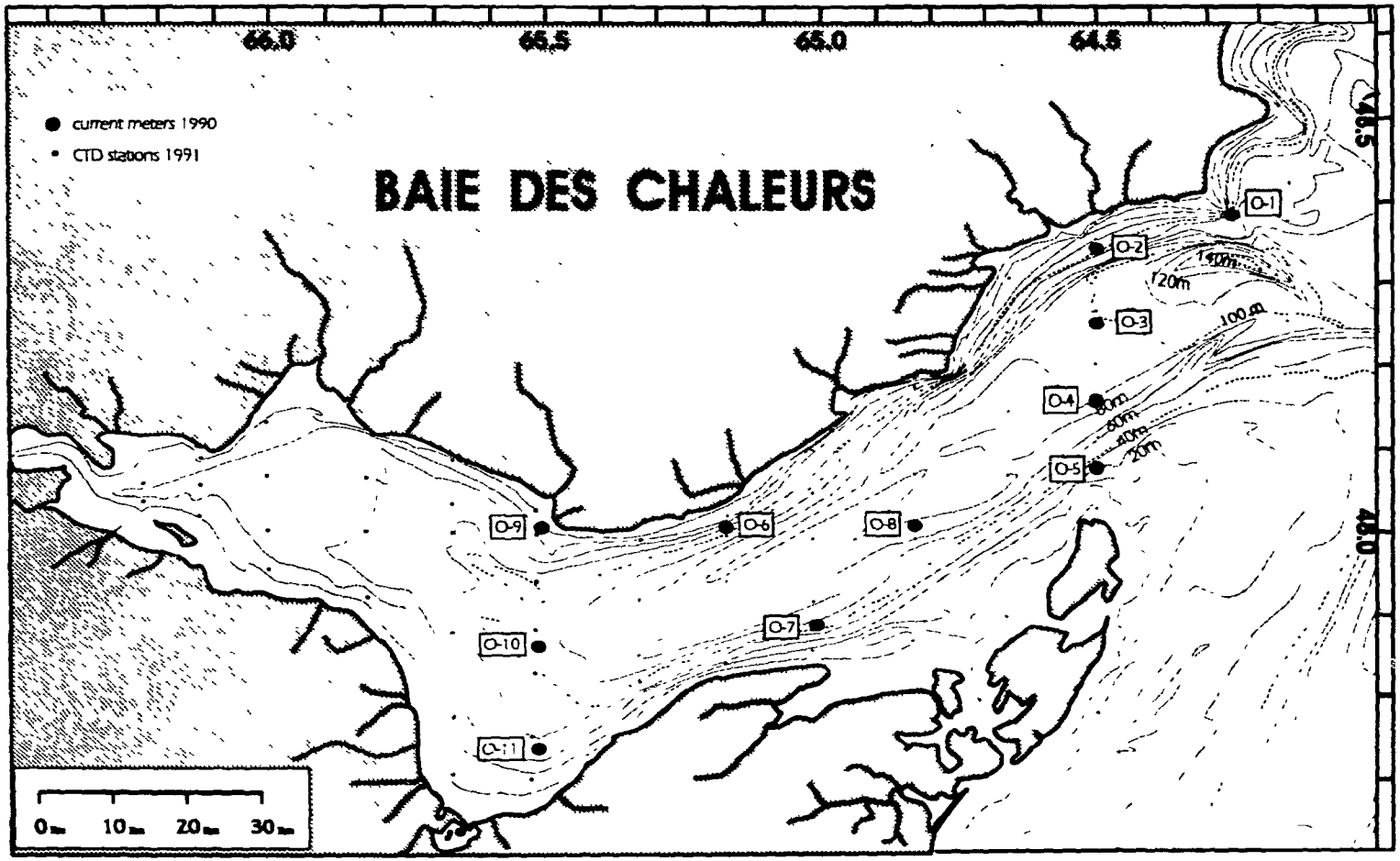
66.0
65.5
65.0
64.5
48.5
48.0
current meters 1990
CTD stations 1991
BAIE DES CHALEURS
O-1
O-2
O-3
O-4
O-5
O-6
O-7
O-8
O-9
O-10
O-11
120m
100m
80m
60m
40m
20m
0
10
20
30

Fig 18

Longitude=64.50 (B)

Temperature (°C) Salinity (°/₀₀) Sigma-t (kg/m^3)

Not available

Longitude=64.67 (C)

Temperature (°C) Salinity (°/₀₀) Sigma-t (kg/m^3)

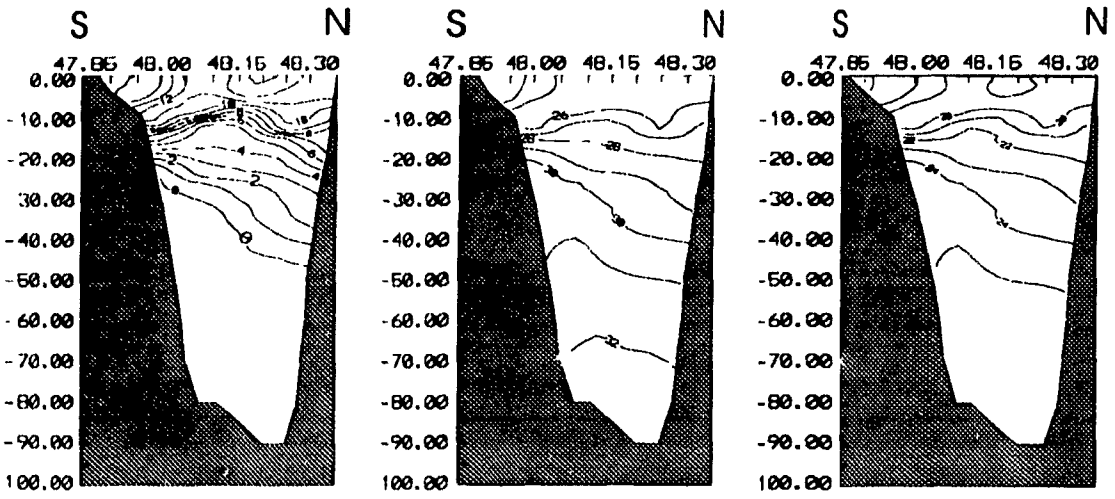

Baie des Chaleurs
RHO: 10, 11, 12 June 1991
Fig. 19

Longitude=64.83 (D)

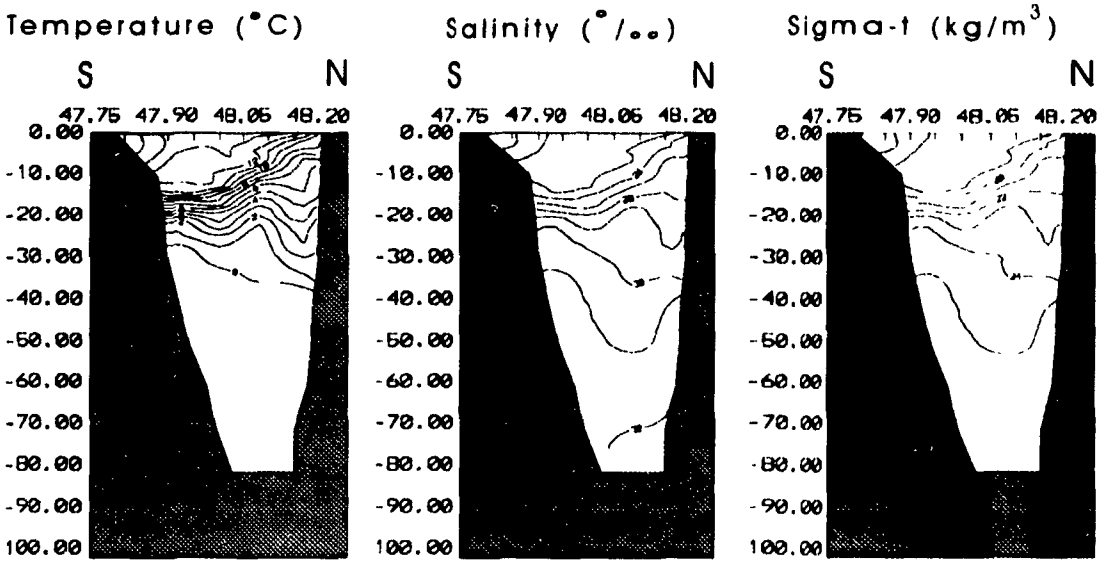

Longitude=65.00 (E)

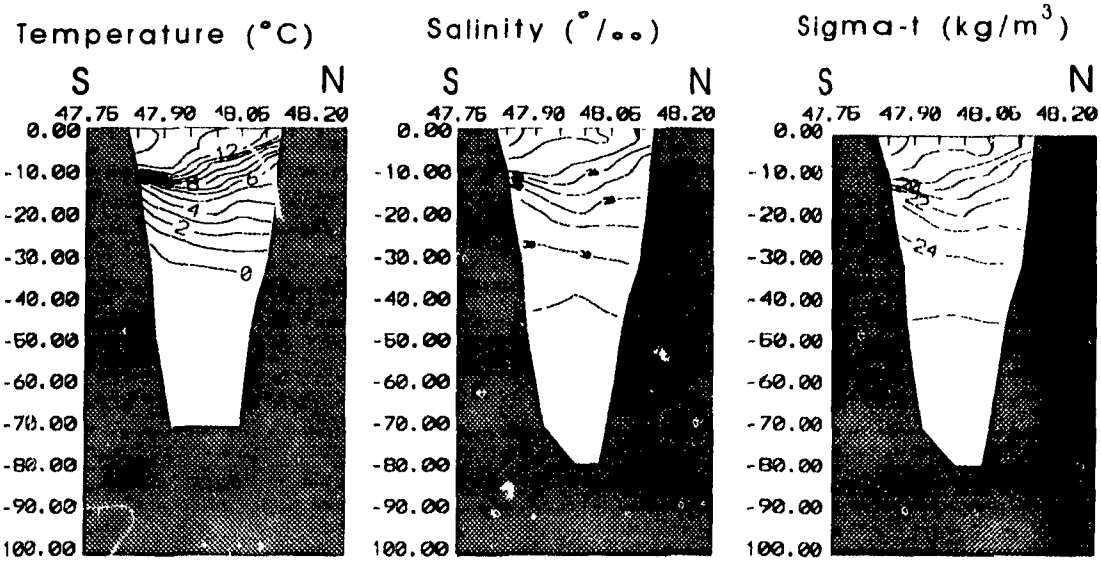

Baie des Chaleurs
RHO: 10, 11, 12 June 1991
Fig. 19

Longitude=65.17 (F)

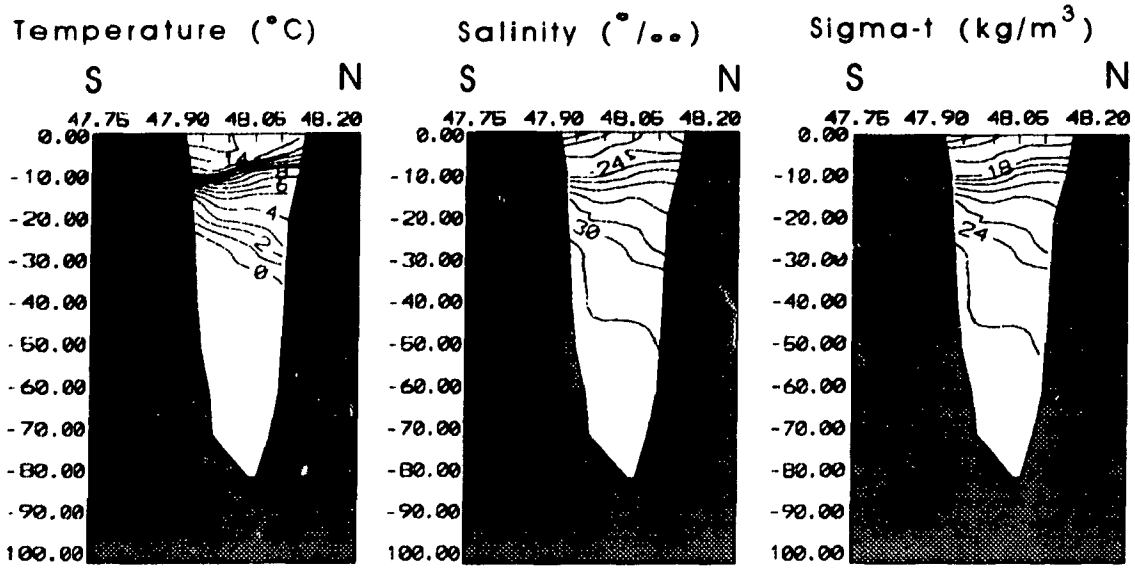

Longitude=65.33 (G)

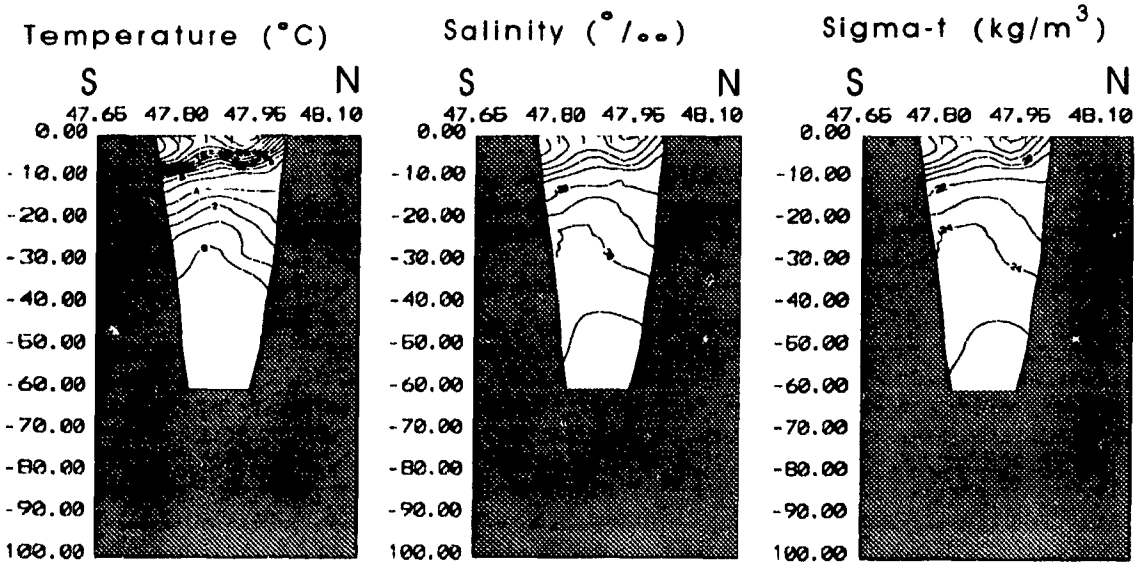

Baie des Chaleurs
RHO: 10, 11, 12 June 1991
Fig. 19

Longitude=65.50 (H)

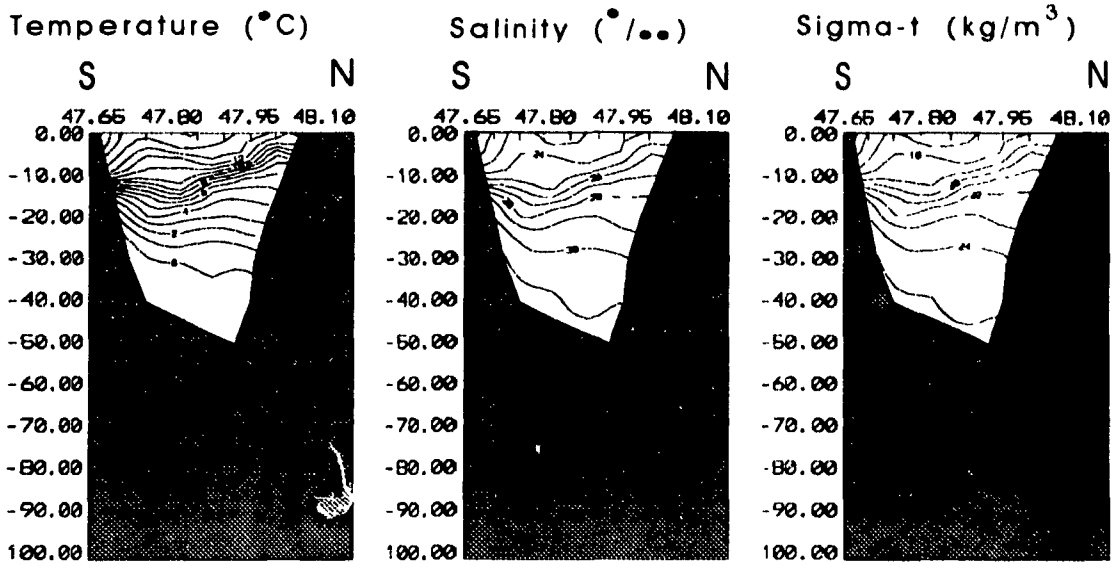

Longitude=65.67 (I)

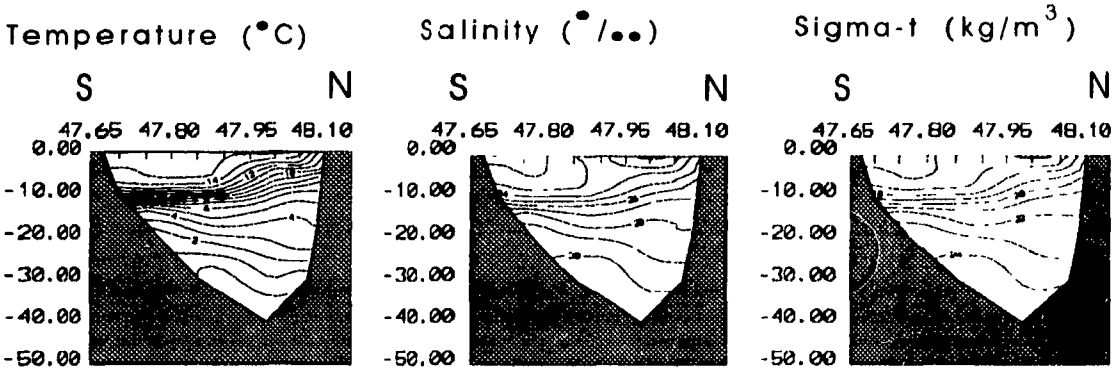

Longitude=65.83 (J)

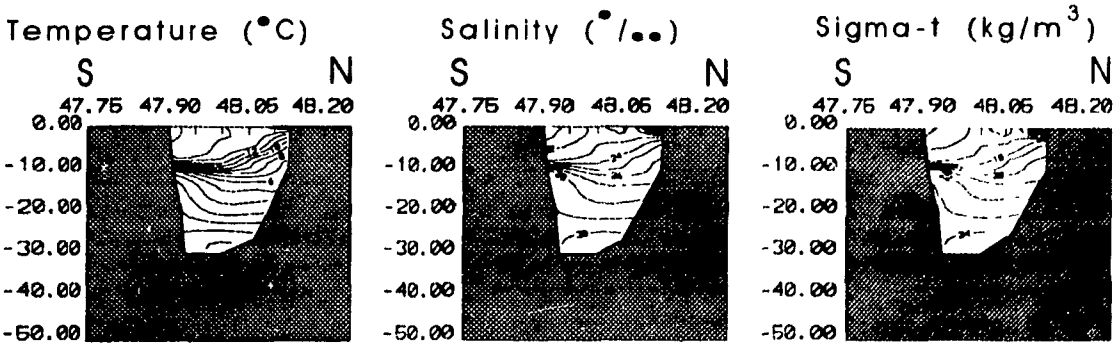

Baie des Chaleurs
RHO: 10, 11, 12 June 1991
Fig. 19

Longitude=66.00 (K)

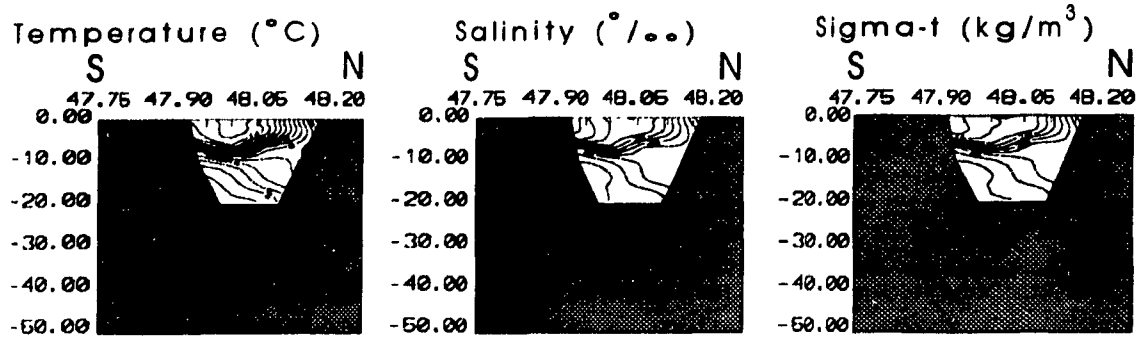

Longitude=66.17 (L)

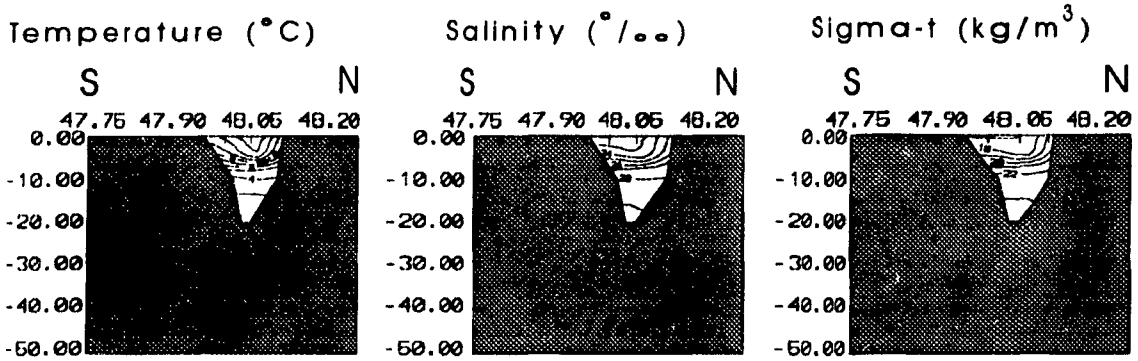

Longitude=66.28 (M)

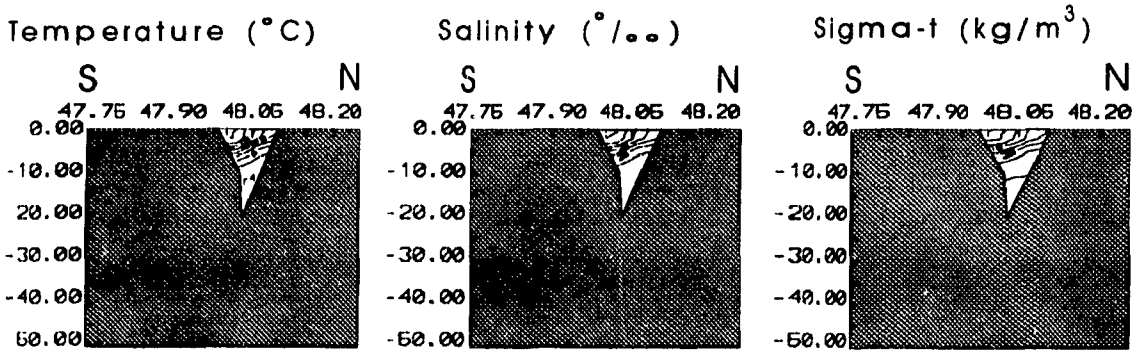

Baie des Chaleurs
RHO: 10, 11, 12 June 1991
Fig. 19

Longitude=64.50 (B)

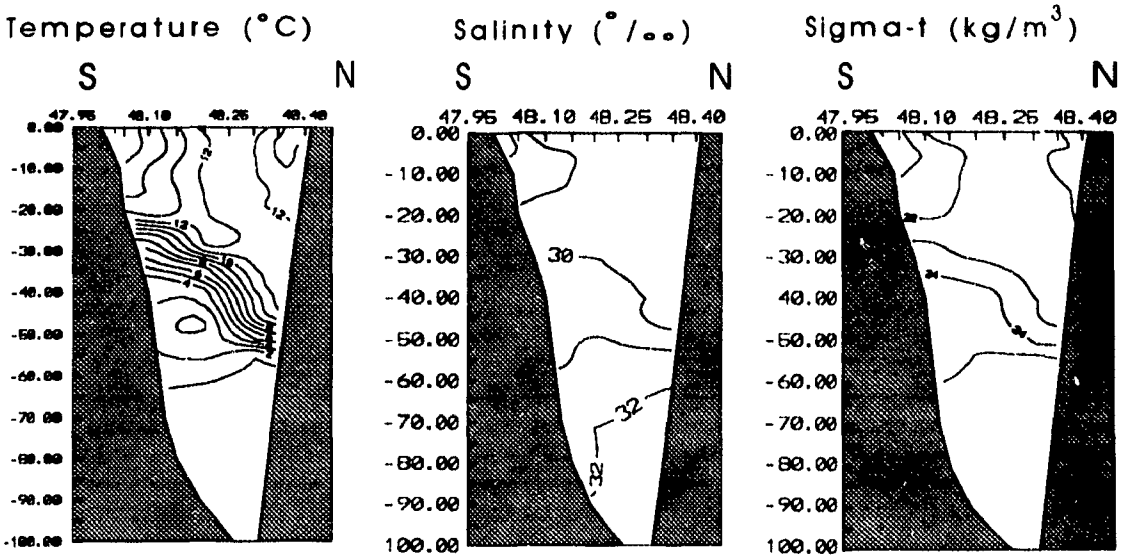

Longitude=64.67 (C)

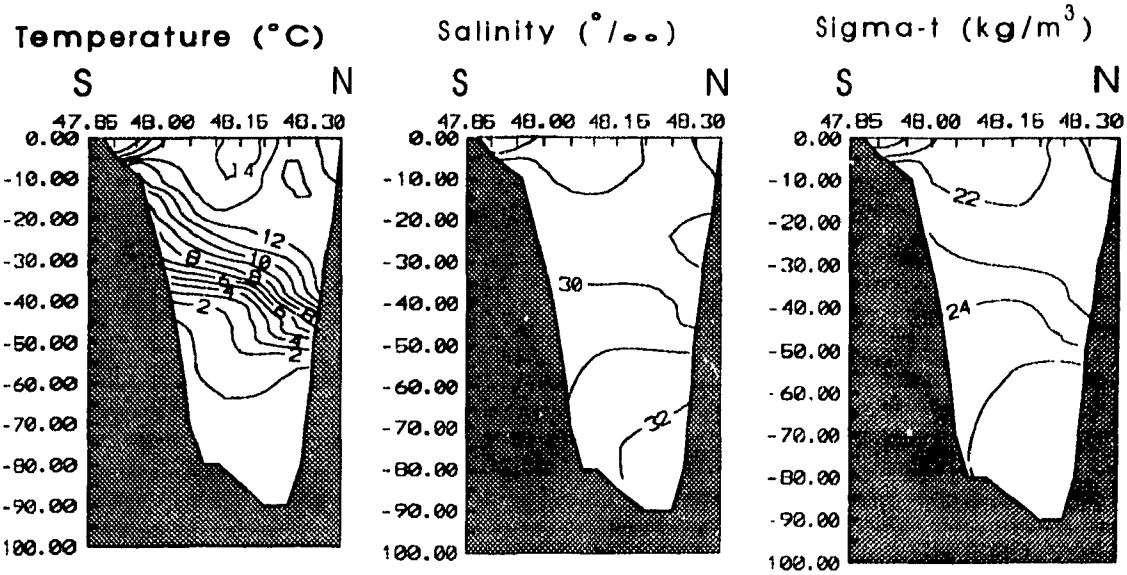

Baie des Chaleurs
RH1: 21, 22, 23 August 1991
Fig. 20

Longitude=64.83 (D)

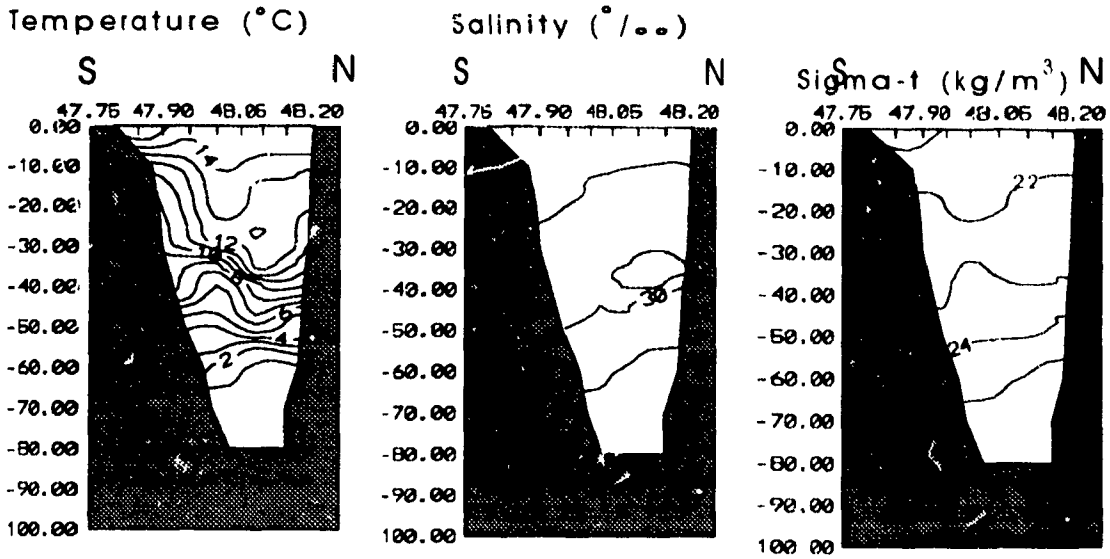

Longitude=65.00 (E)

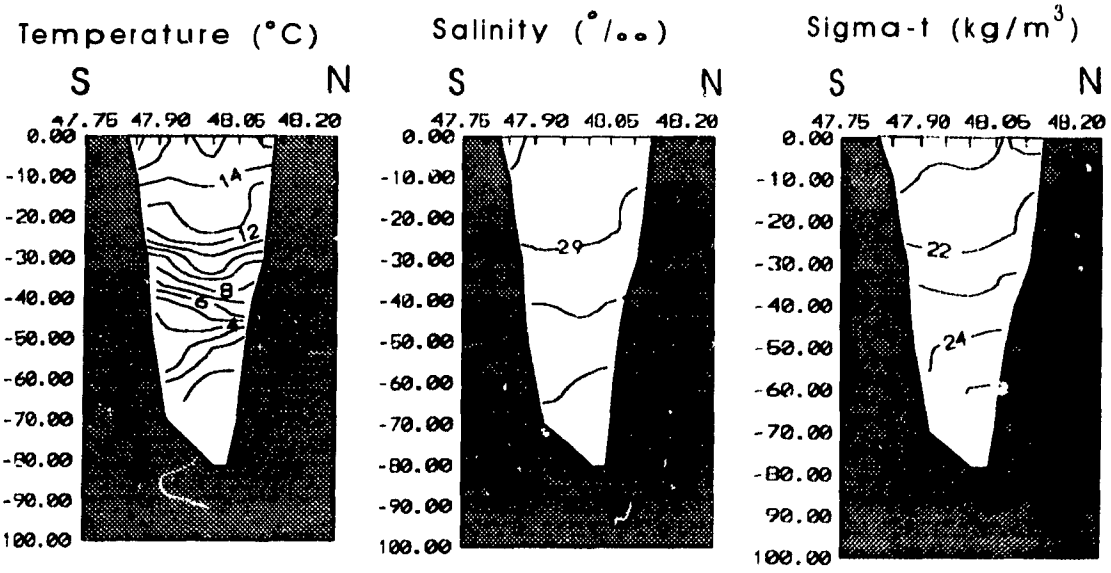

Baie des Chaleurs
RH1: 21, 22, 23 August 1991
Fig. 20

Longitude=65.17 (F)

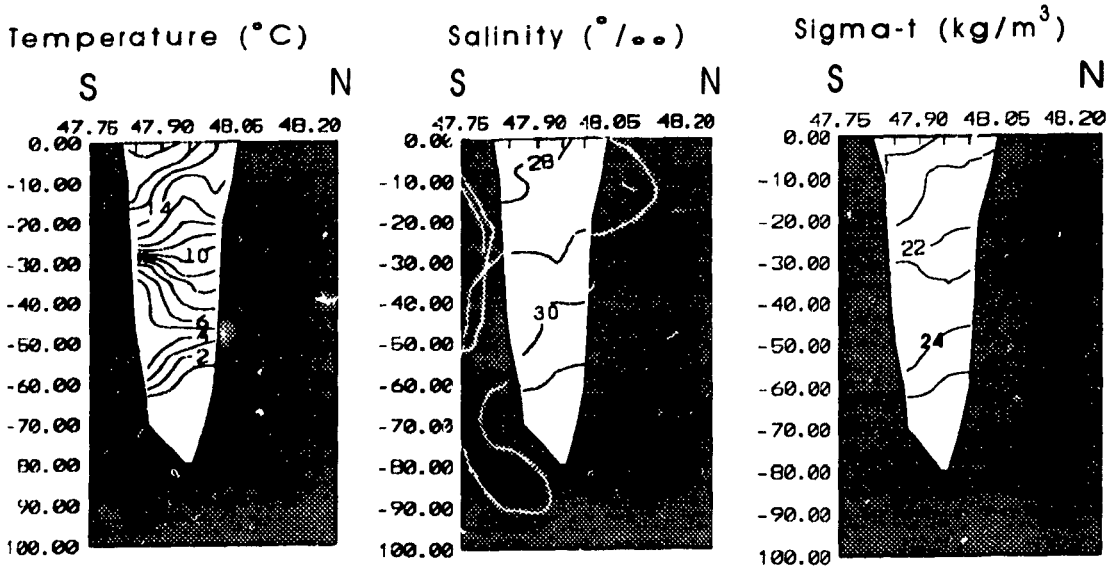

Longitude=65.33 (G)

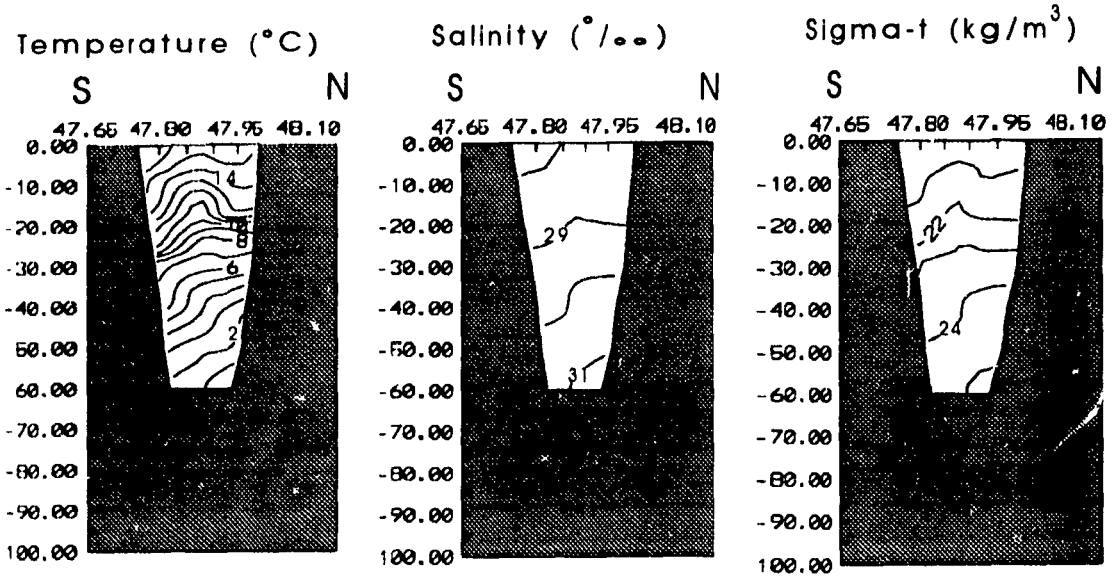

Baie des Chaleurs
RH1: 21, 22, 23 August 1991
Fig. 20

Longitude=65.50 (H)

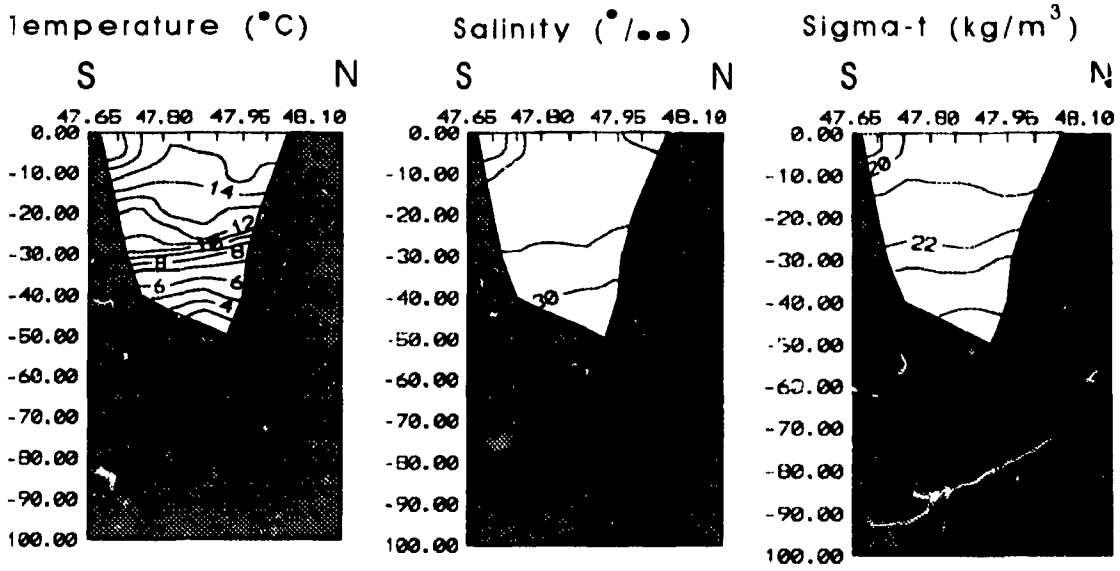

Longitude=65.67 (I)

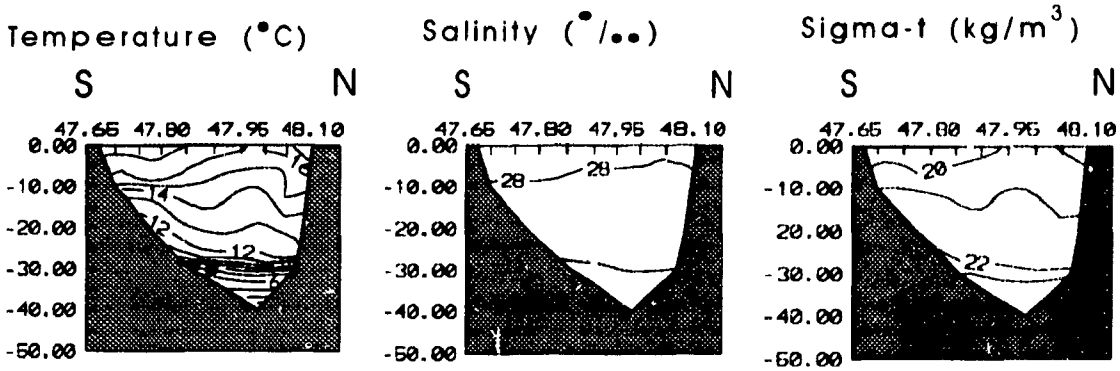

Longitude=65.83 (J)

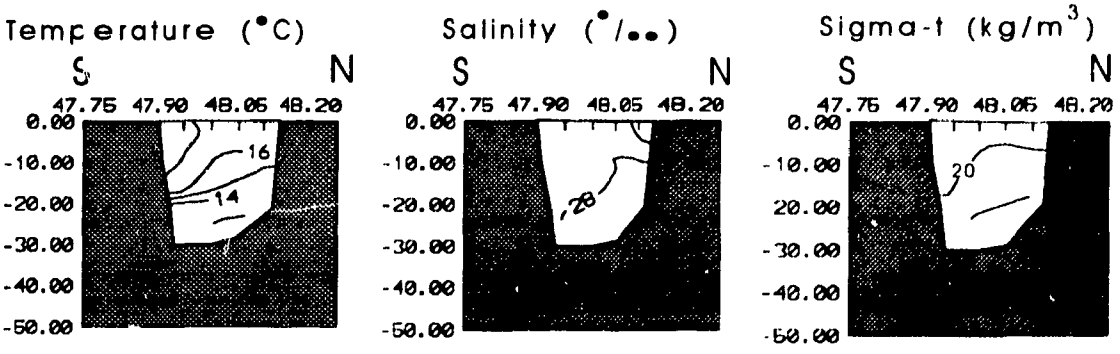

Baie des Chaleurs
RH1: 21, 22, 23 August 1991
Fig. 20

Longitude=66.00 (K)

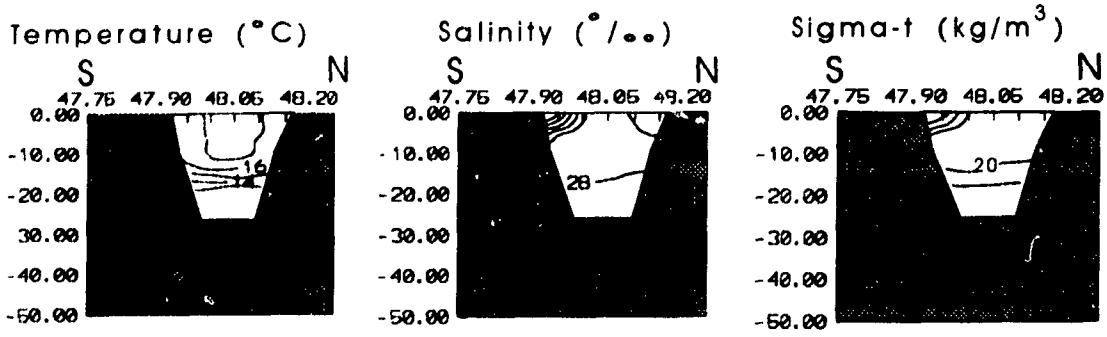

Longitude=66.17 (L)

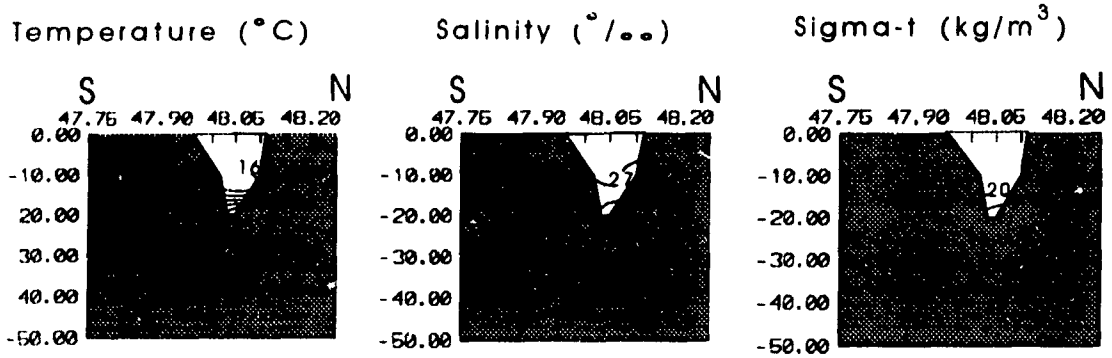

Longitude=66.28 (M)

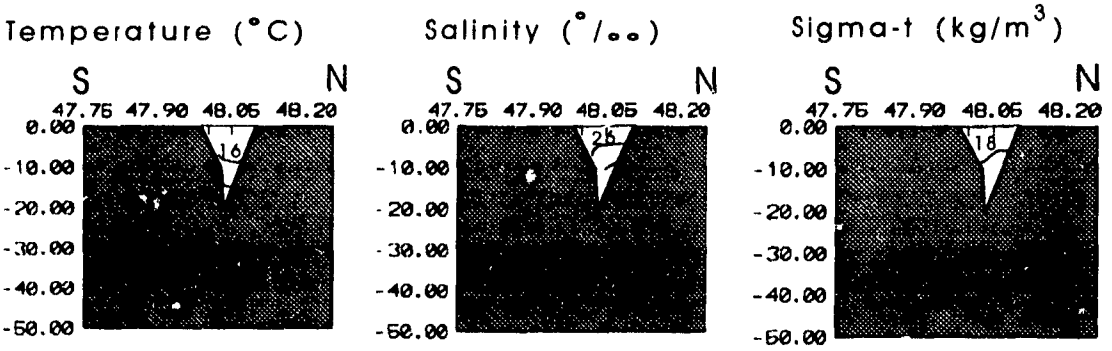

Baie des Chaleurs
RH1: 21, 22, 23 August 1991
Fig. 20

Longitude=64.50 (B)

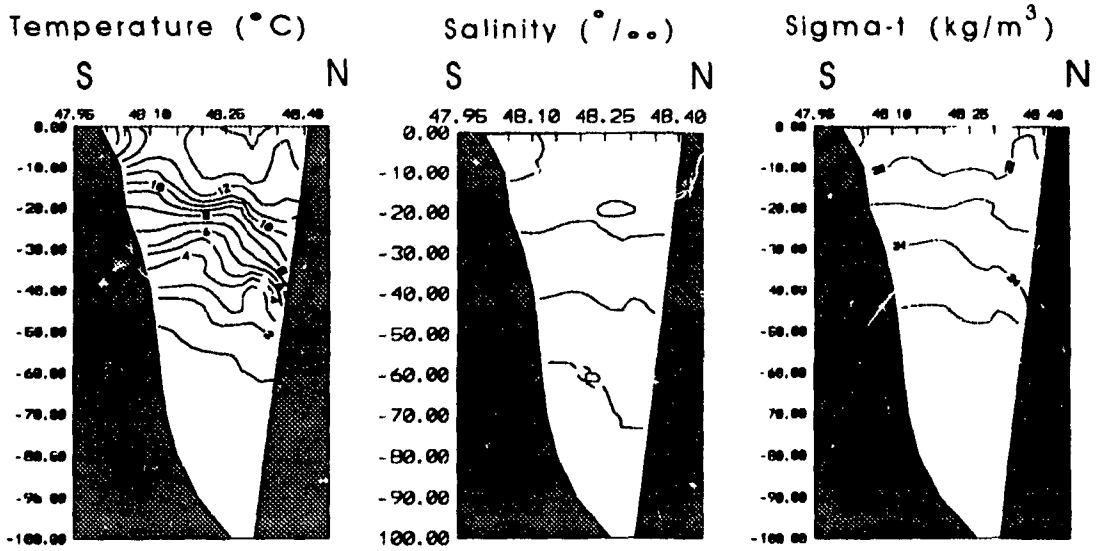

Longitude=64.67 (C)

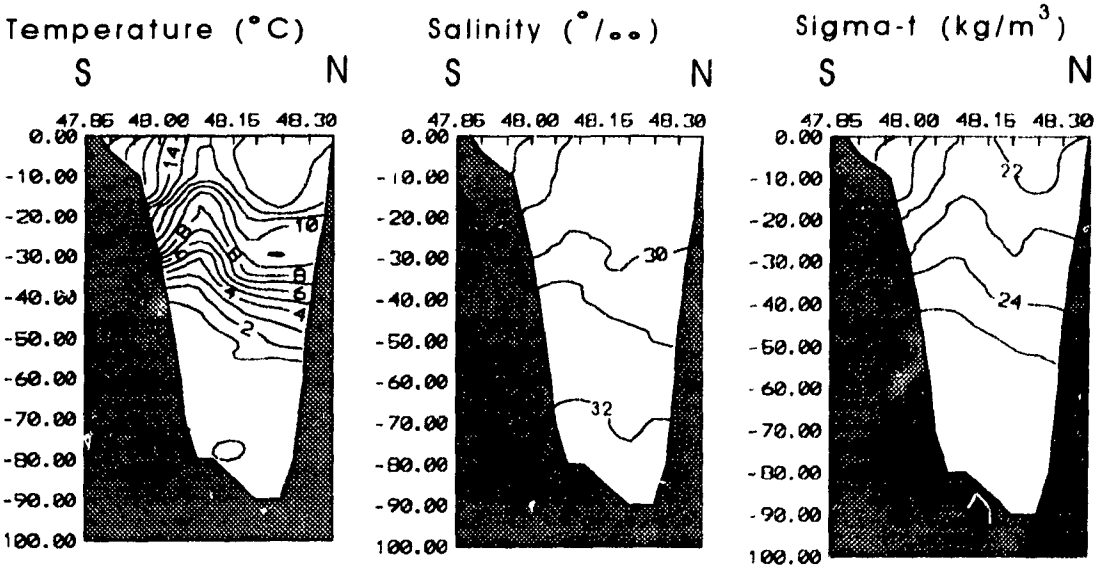

Baie des Chaleurs
RH2: 26, 27, 28 August 1991
Fig. 21

Longitude=64.83 (D)

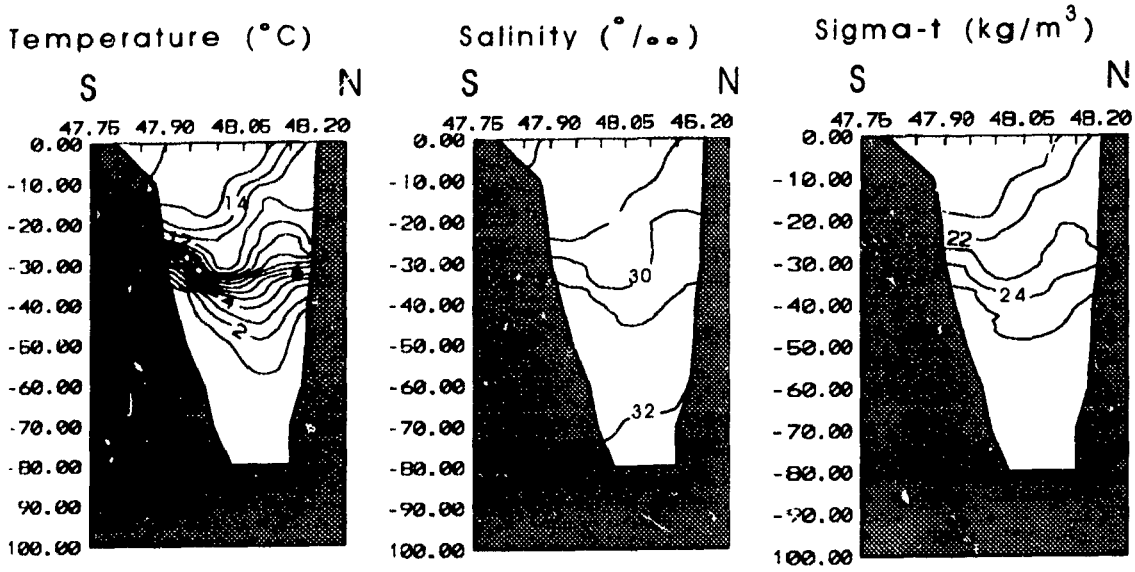

Longitude=65.00 (E)

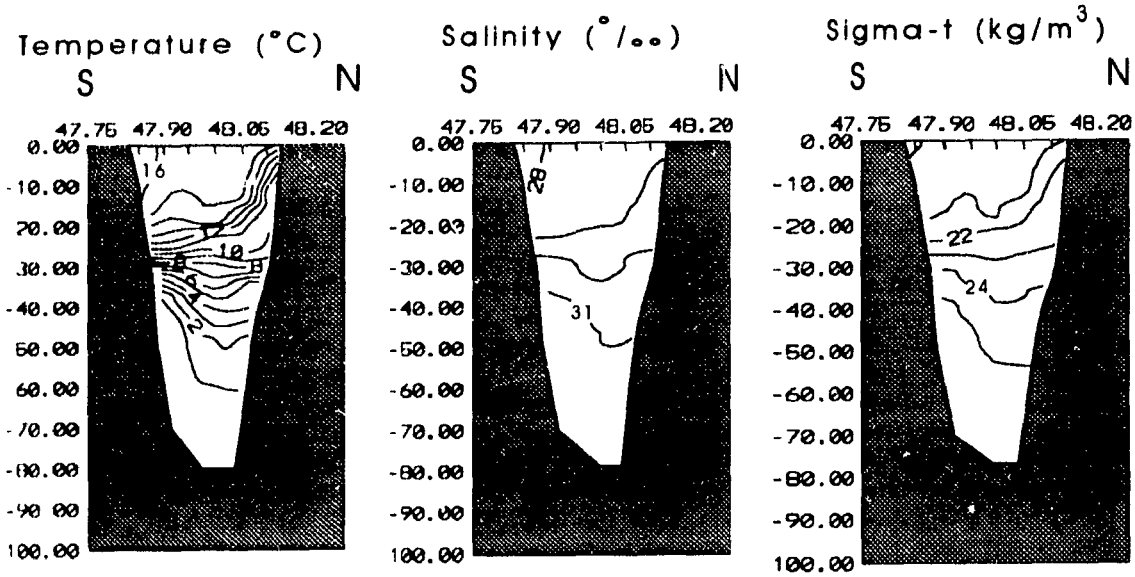

Baie des Chaleurs
RH2: 26, 27, 28 August 1991
Fig. 21

Longitude=65.17 (F)

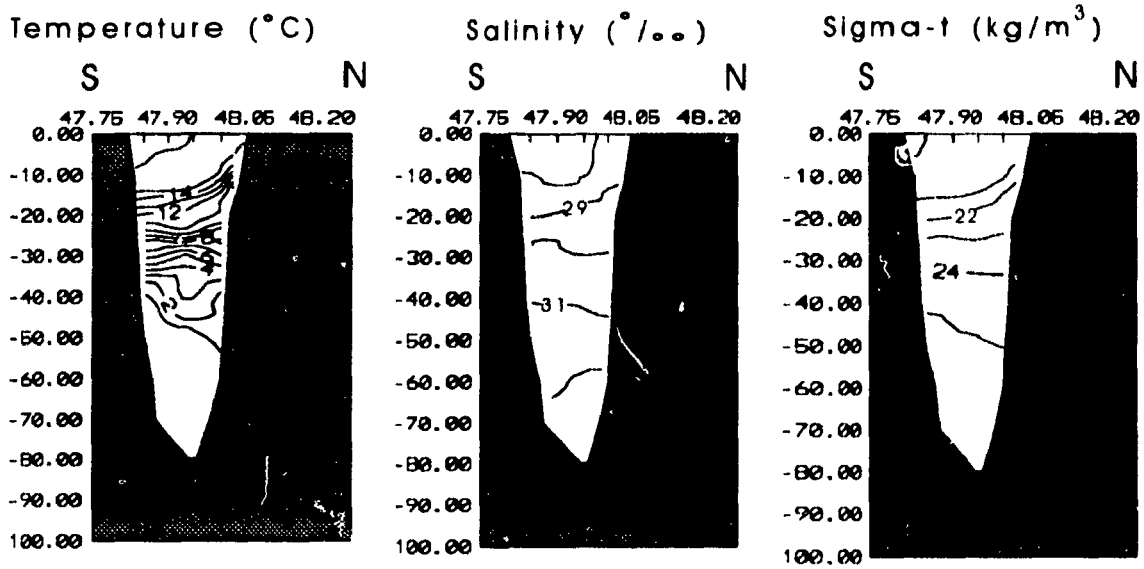

Longitude=65.33 (G)

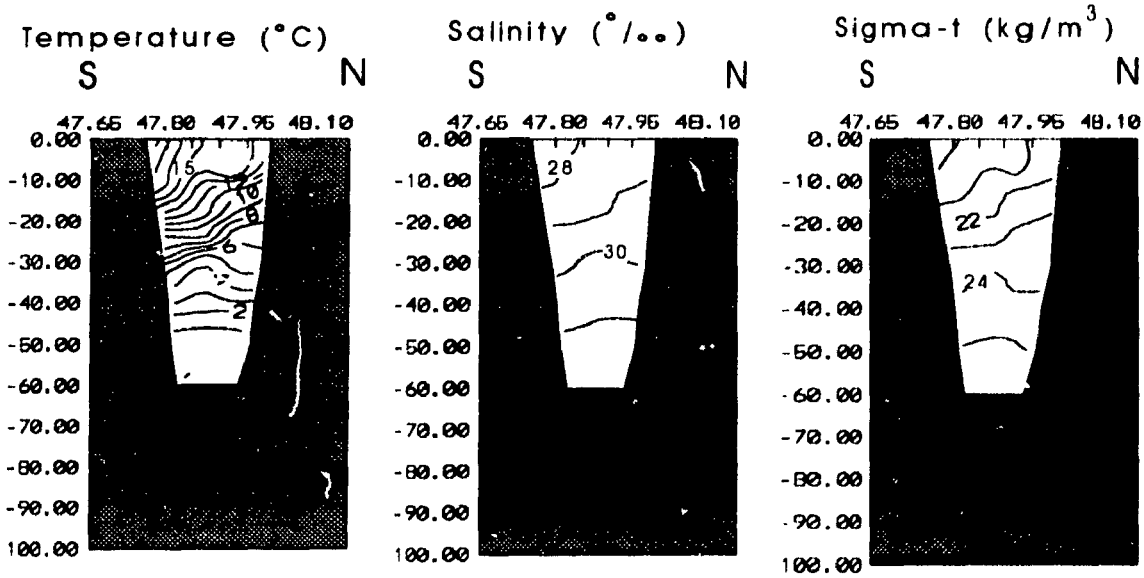

Baie des Chaleurs
RH2: 26, 27, 28 August 1991
Fig. 21

Longitude=65.50 (H)

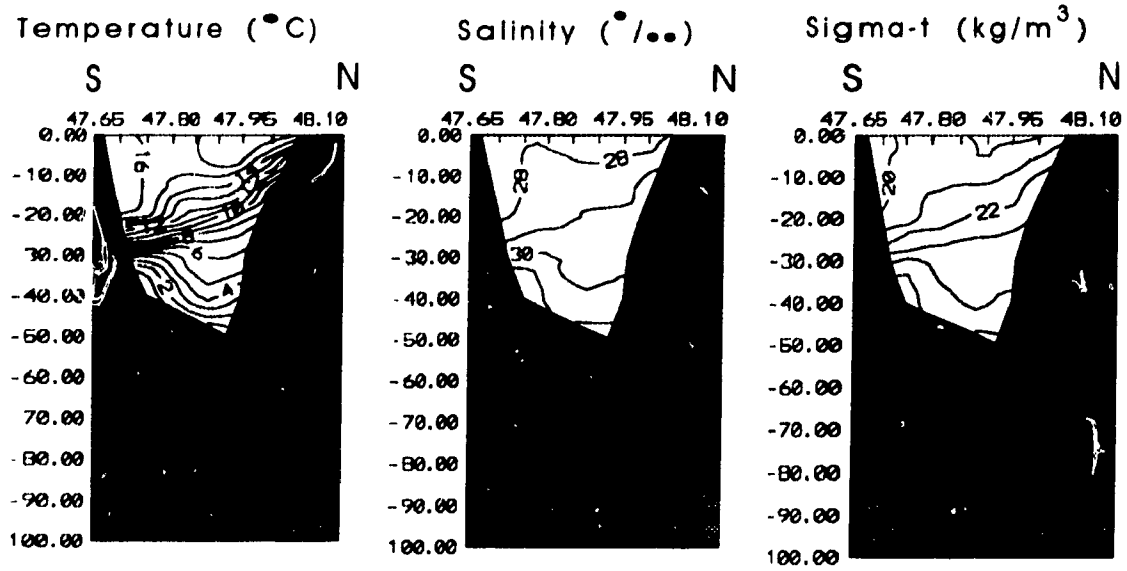

Longitude=65.67 (I)

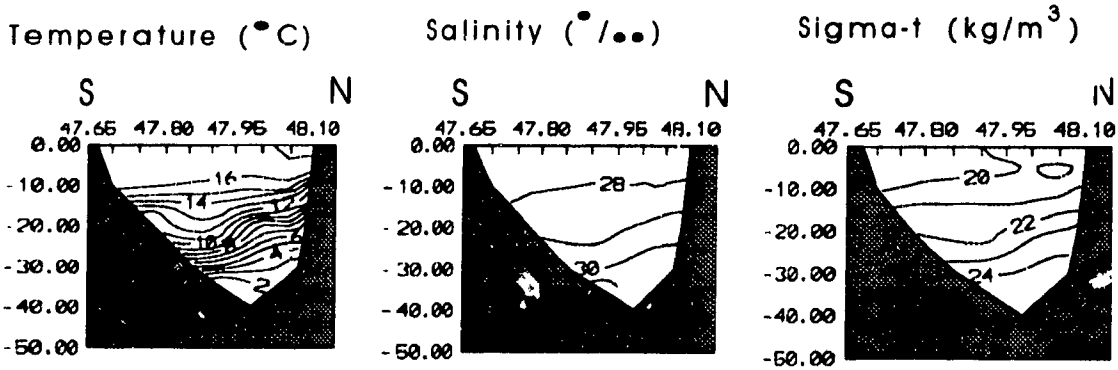

Longitude=65.83 (J)

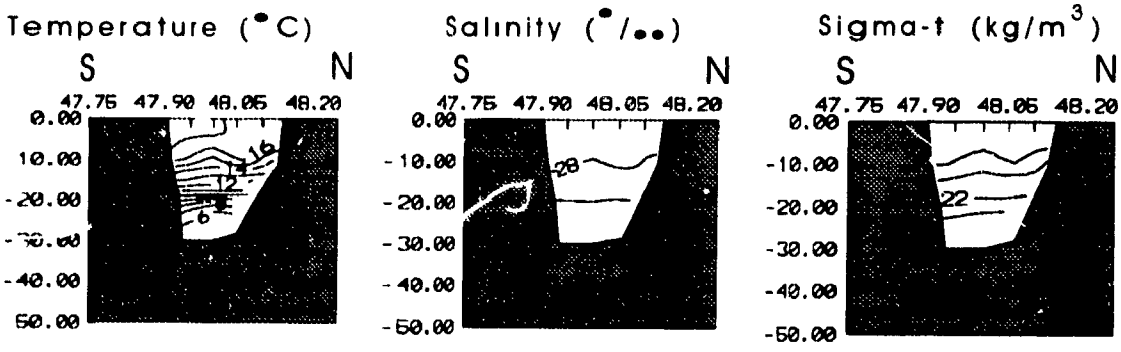

Baie des Chaleurs
RH2: 26, 27, 28 August 1991
Fig. 21

Longitude=66.00 (K)

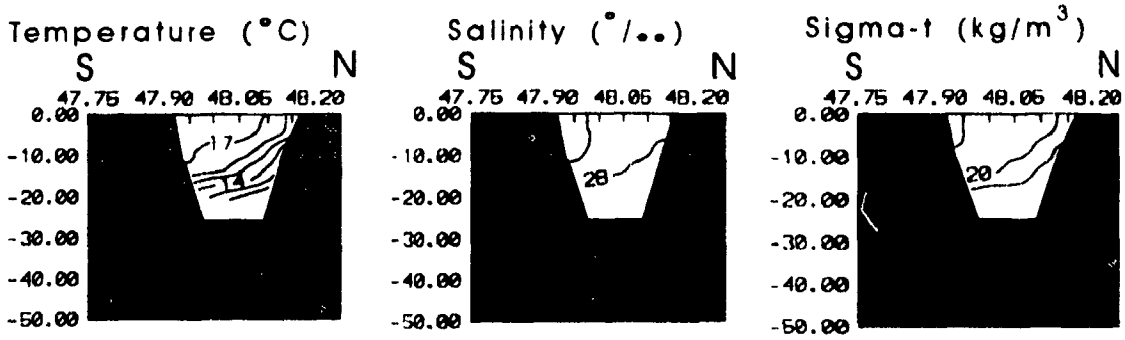

Longitude=66.17 (L)

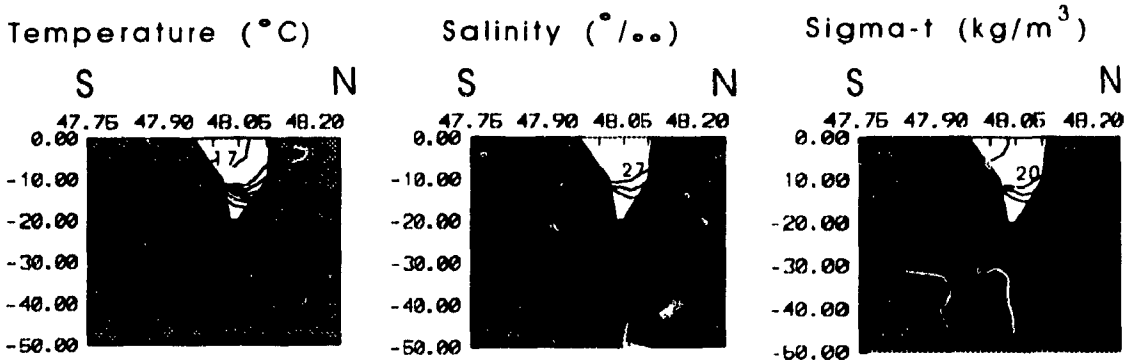

Longitude=66.28 (M)

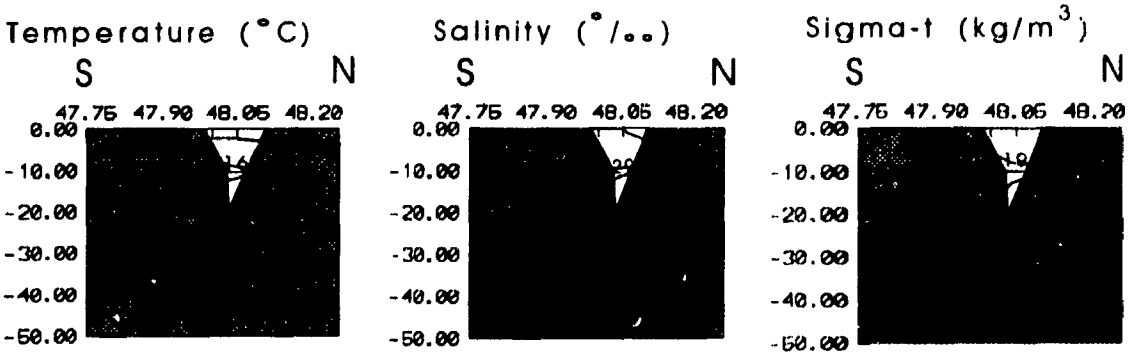

Baie des Chaleurs
RH2: 26, 27, 28 August 1991
Fig. 21

Longitude=64.50 (B)

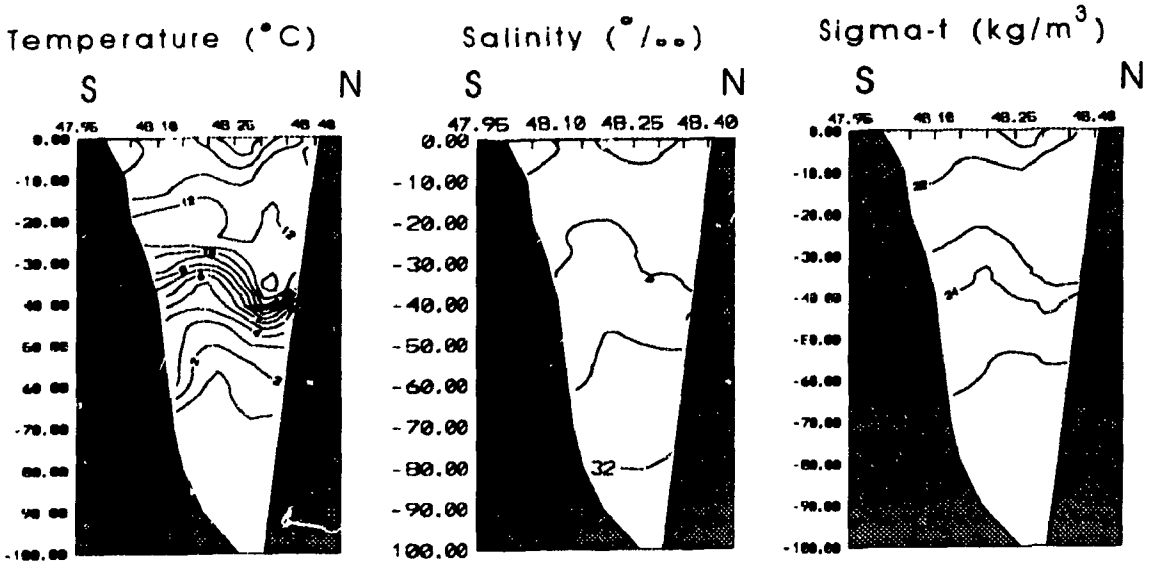

Longitude=64.67 (C)

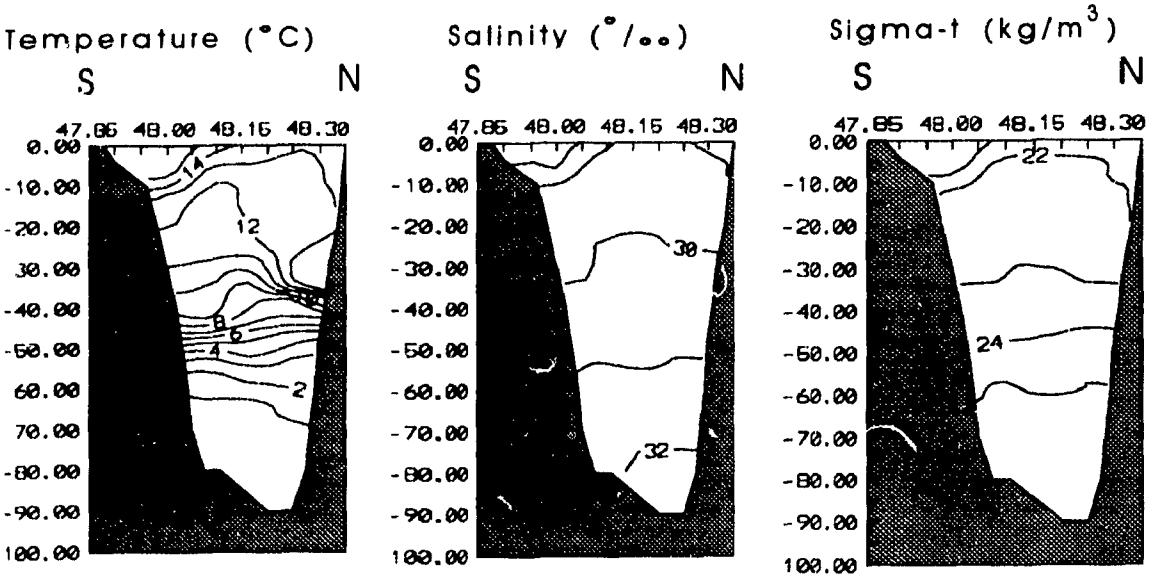

Baie des Chaleurs
RH5: 5, 6, 7 September 1991
Fig. 22

Longitude=64.83 (D)

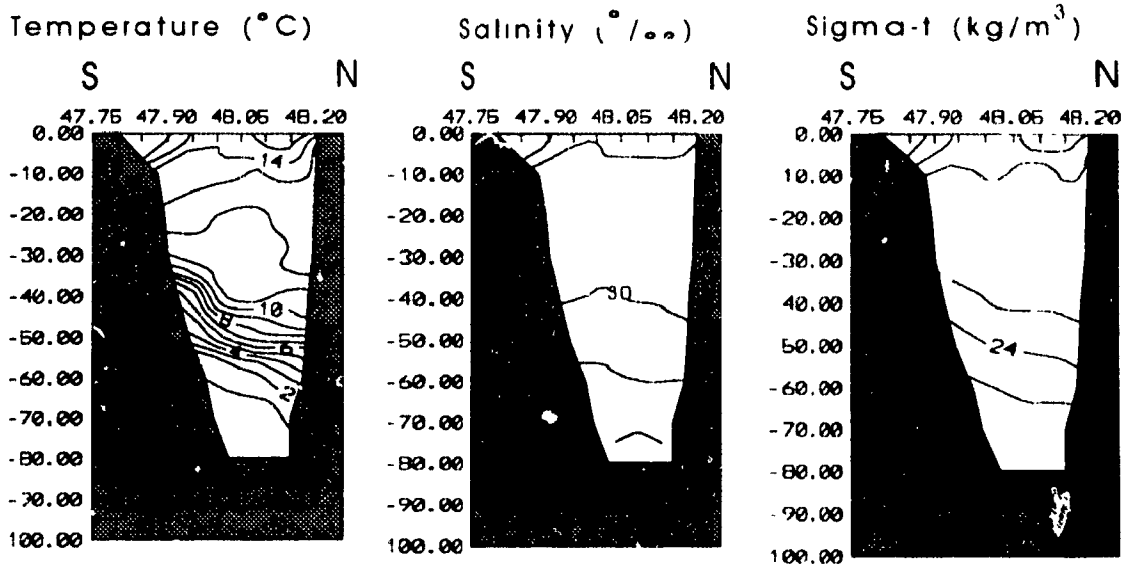

Longitude=65.00 (E)

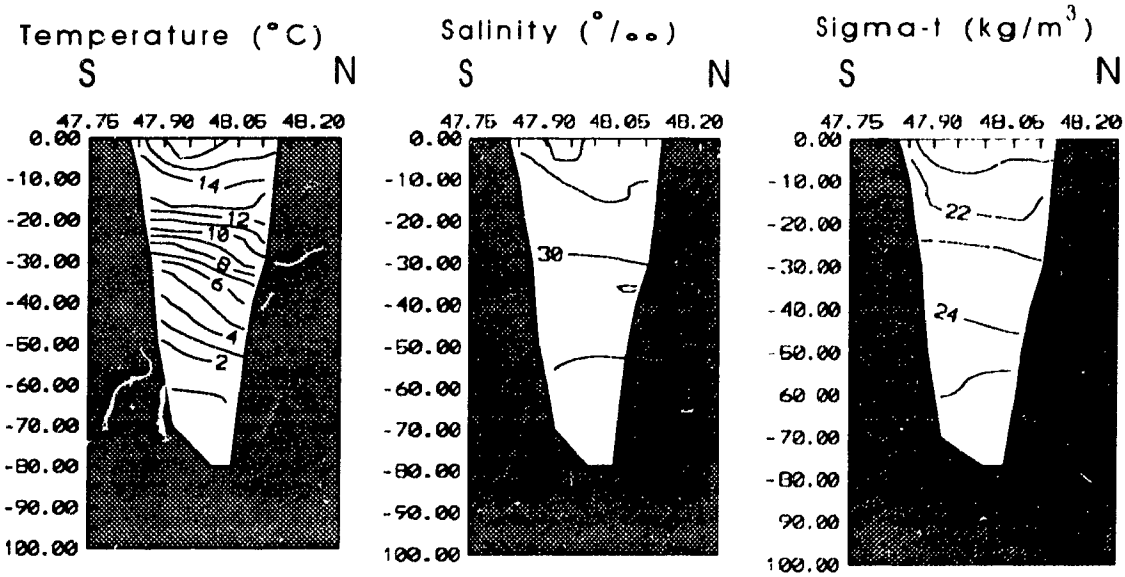

Baie des Chaleurs
RH5: 5, 6, 7 September
Fig. 22

Longitude=65.17 (F)

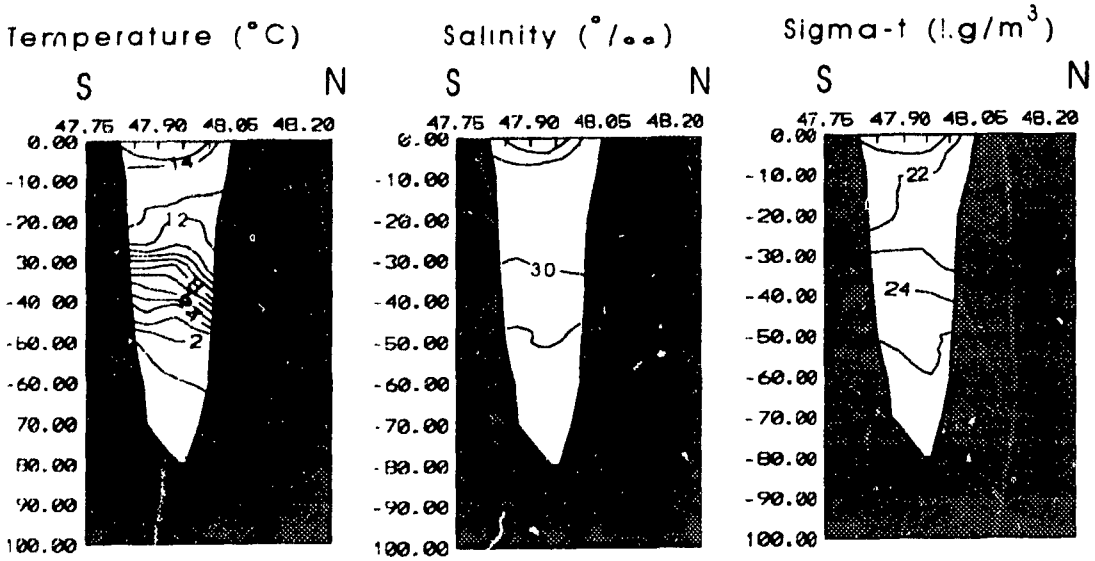

Longitude=65.33 (G)

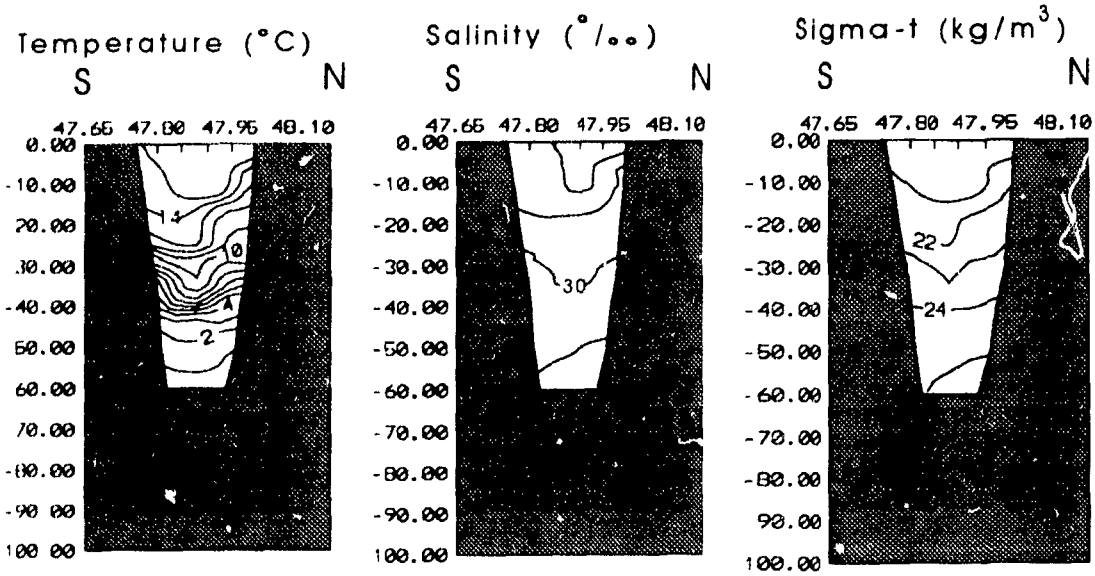

Baie des Chaleurs
RH5: 5, 6, 7 September 1991
Fig. 22

Longitude=65.50 (H)

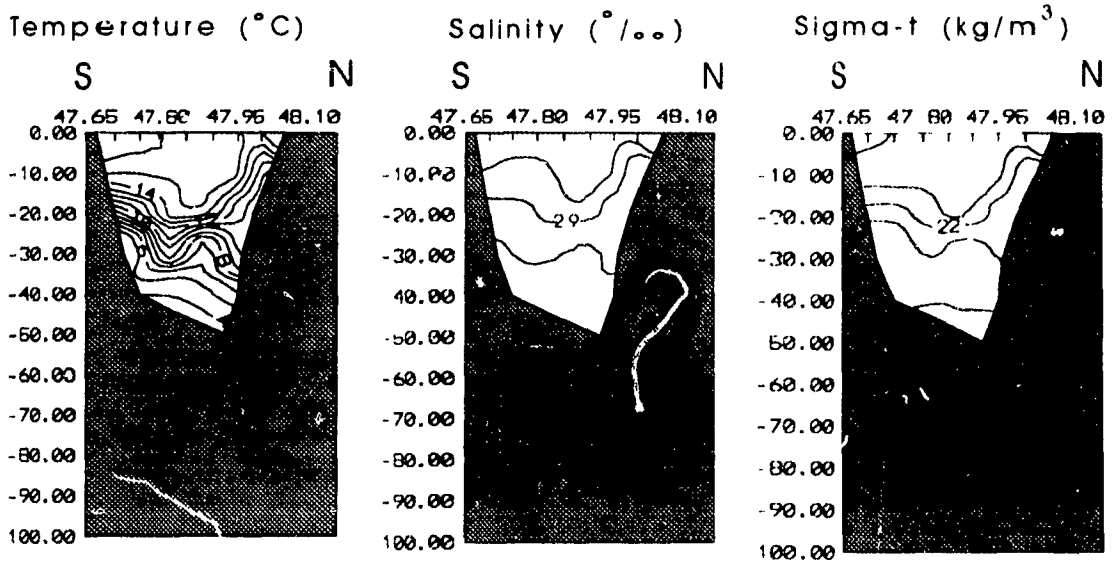

Longitude=65.67 (I)

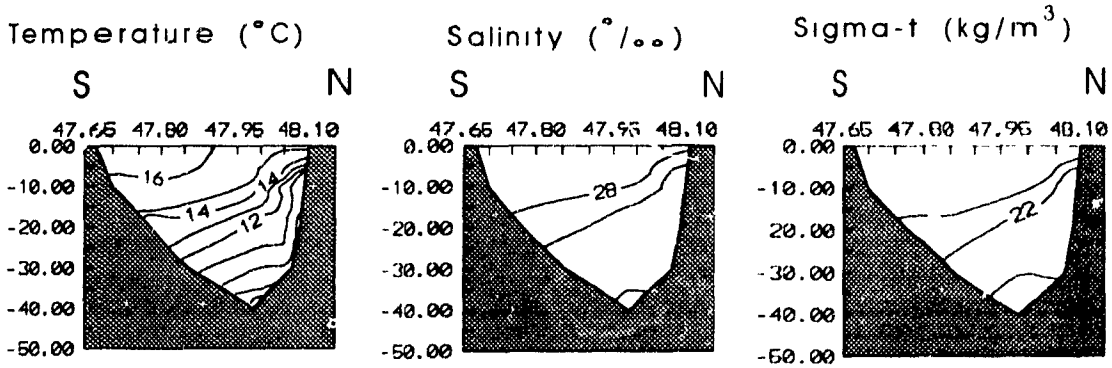

Longitude=65.83 (J)

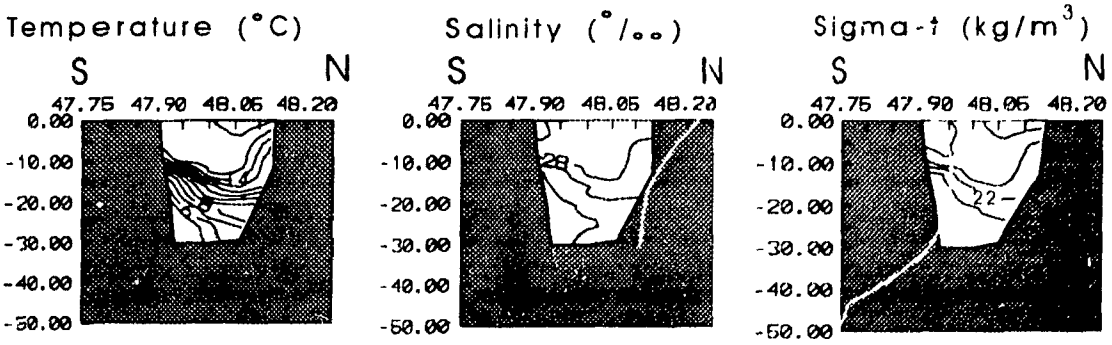

Baie des Chaleurs
RH5: 5, 6, 7 September 1991
Fig. 22

Longitude=66.00 (K)

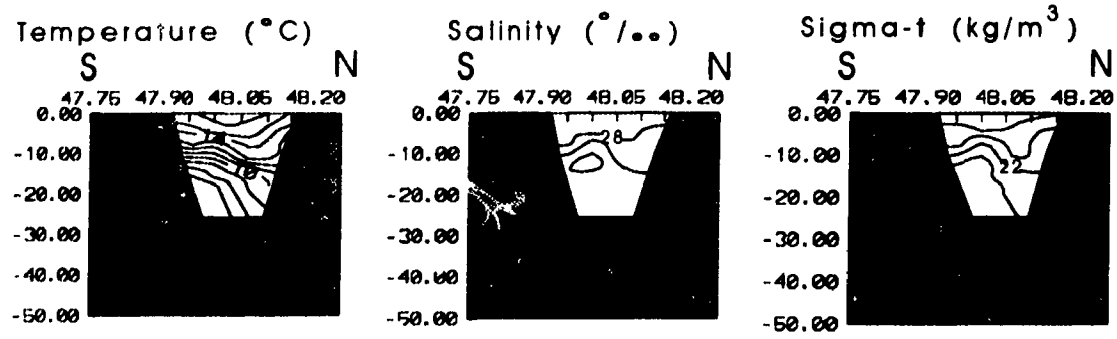

Longitude=66.17 (L)

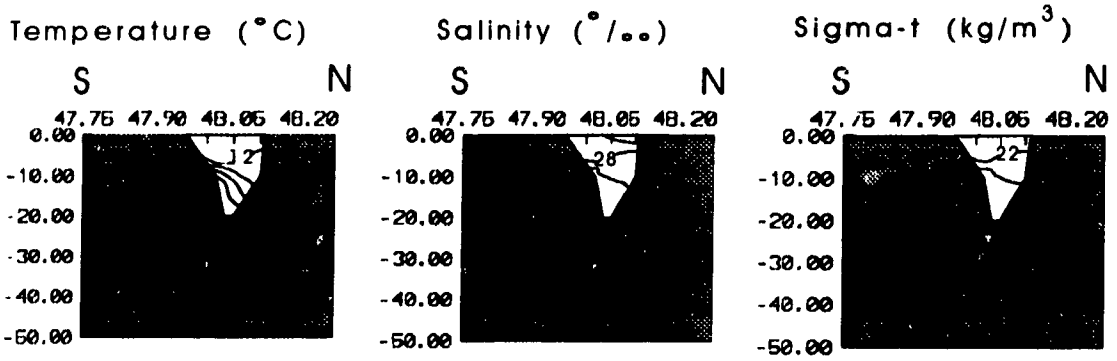

Longitude=66.28 (M)

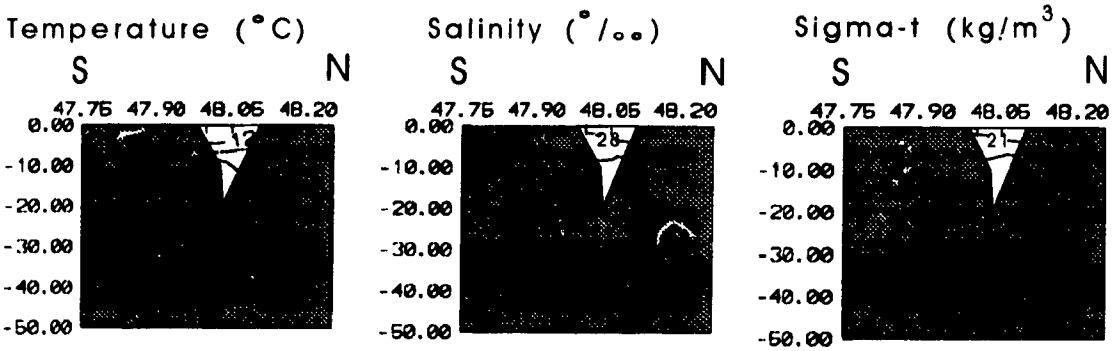

Baie des Chaleurs
RH5: 5, 6, 7 September 1991
Fig. 22

Longitude=64.50 (B)

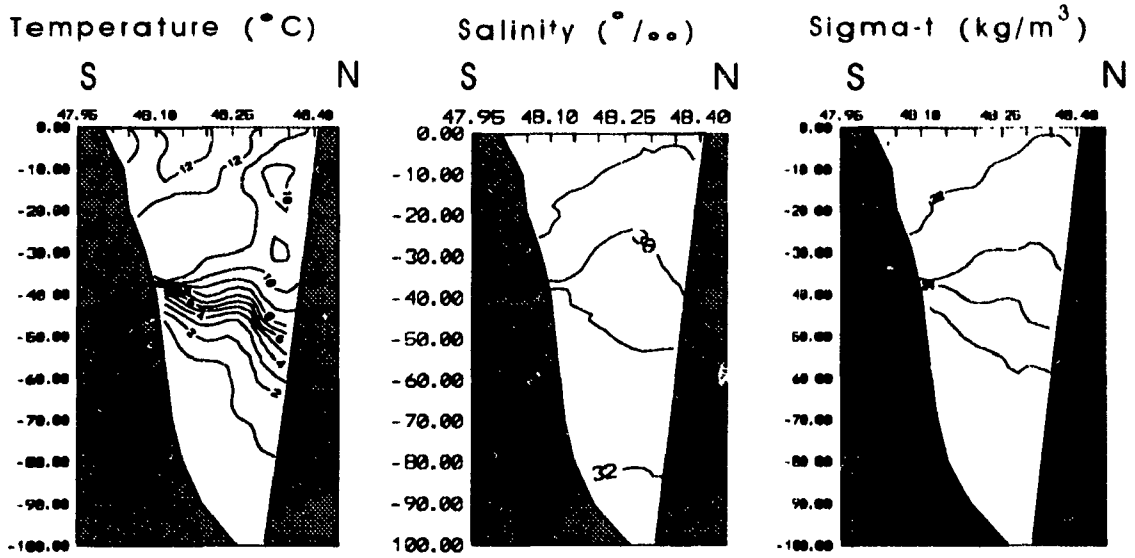

Longitude=64.67 (C)

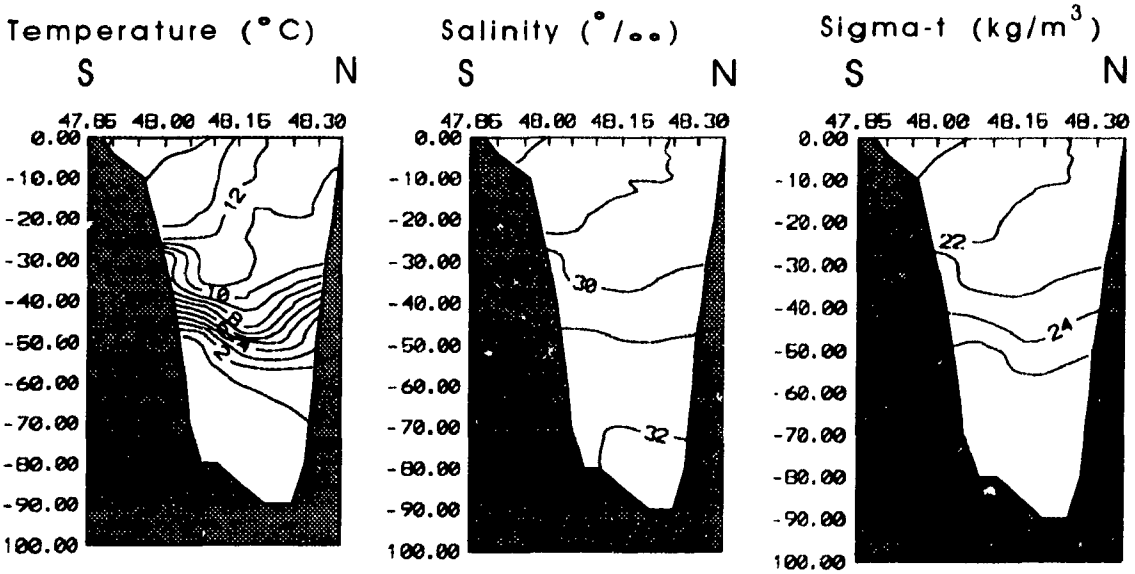

Baie des Chaleurs
RH6: 15, 16, 17 September 1991
Fig. 23

Longitude=64.83 (D)

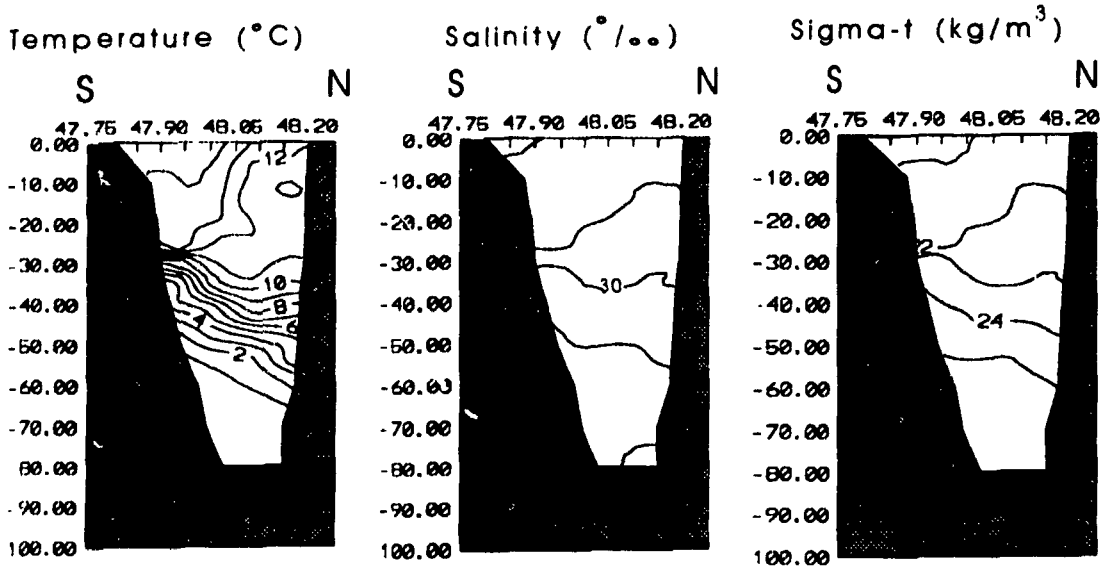

Longitude=65.00 (E)

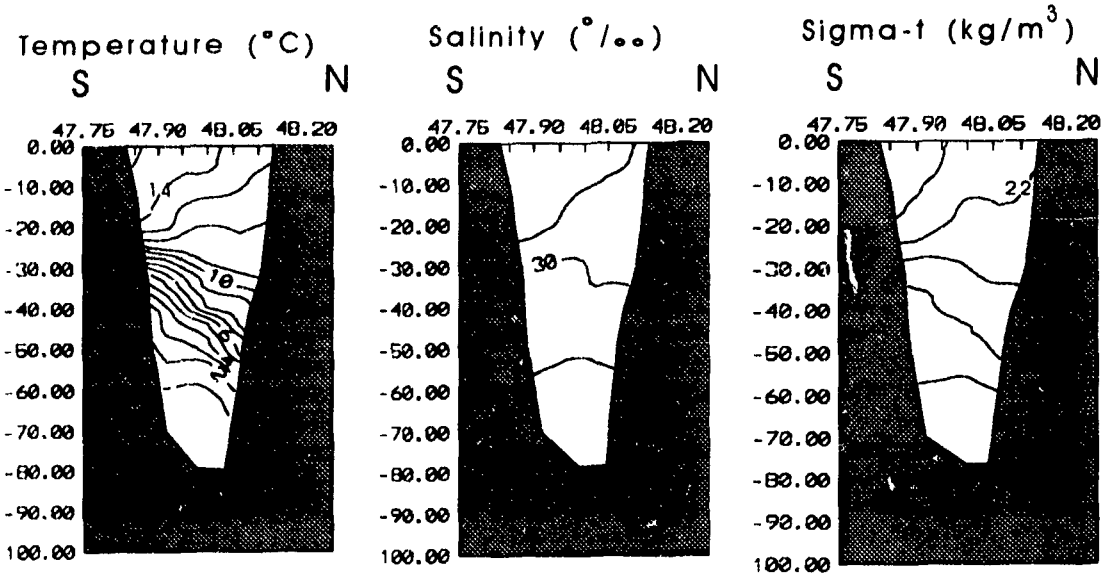

Baie des Chaleurs
RH6: 15, 16, 17 September 1991
Fig. 23

Longitude=65.17 (F)

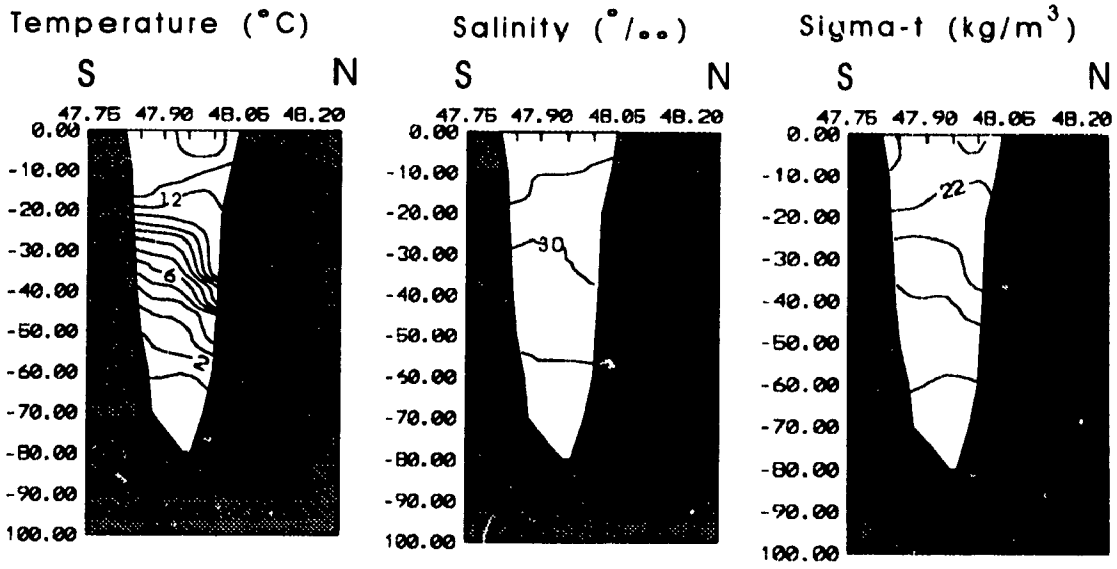

Longitude=65.33 (G)

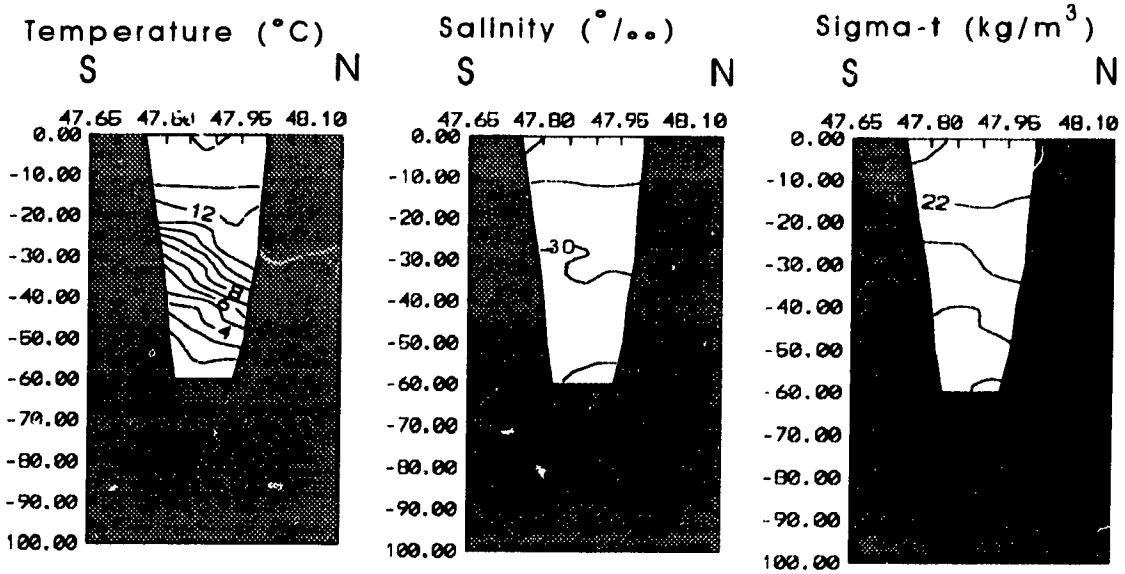

Baie des Chaleurs
RH6: 15, 16, 17 September 1991
Fig. 23

Longitude=65.50 (H)

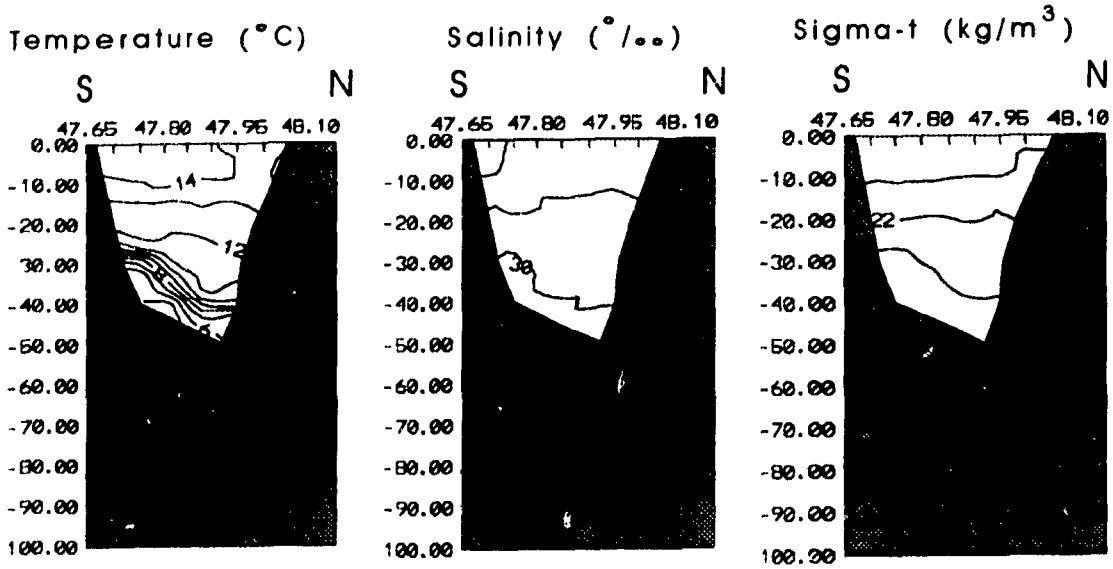

Longitude=65.67 (I)

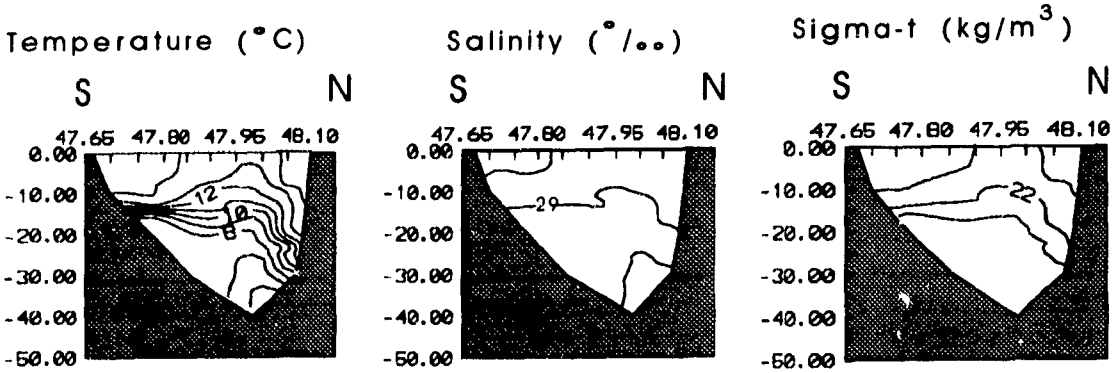

Longitude=65.83 (J)

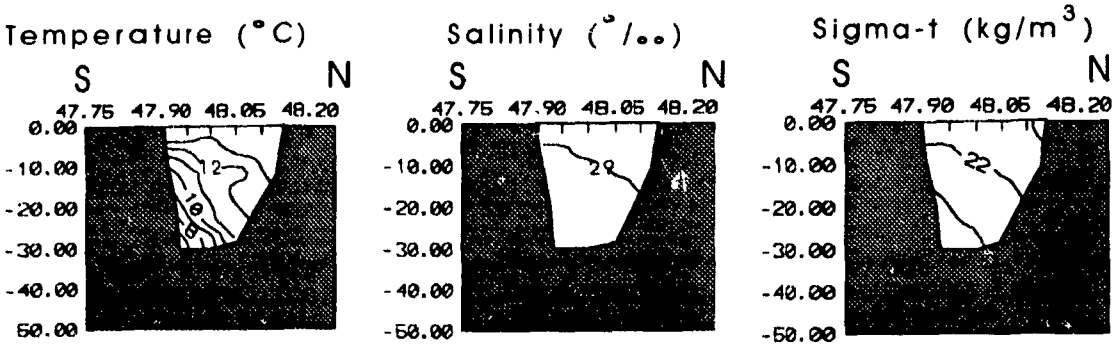

Baie des Chaleurs
RH6: 15, 16, 17 September 1991
Fig. 23

Longitude=66.00 (K)

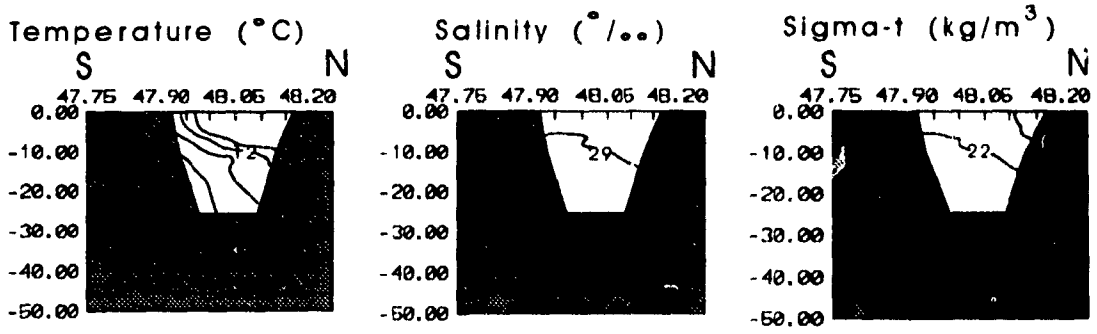

Longitude=66.17 (L)

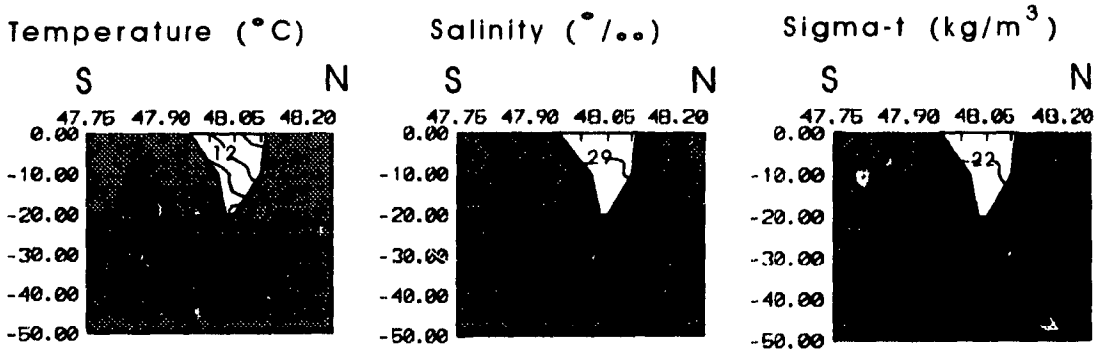

Longitude=66.28 (M)

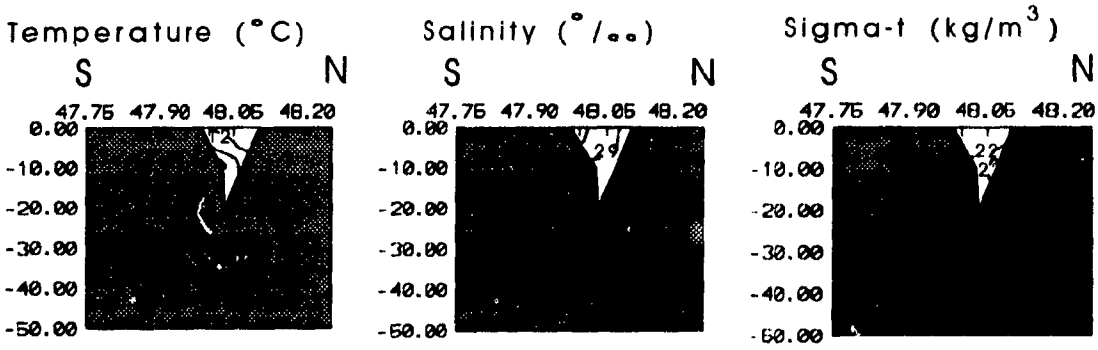

Baie des Chaleurs
RH6: 15, 16, 17 September 1991
Fig. 23

Longitude=64.50 (B)

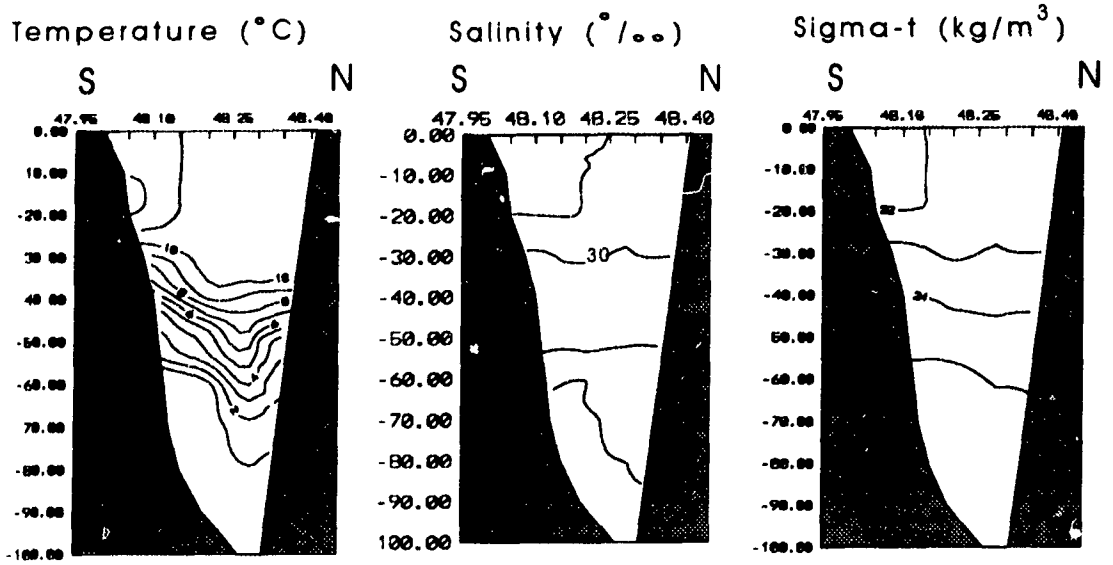

Longitude=64.67 (C)

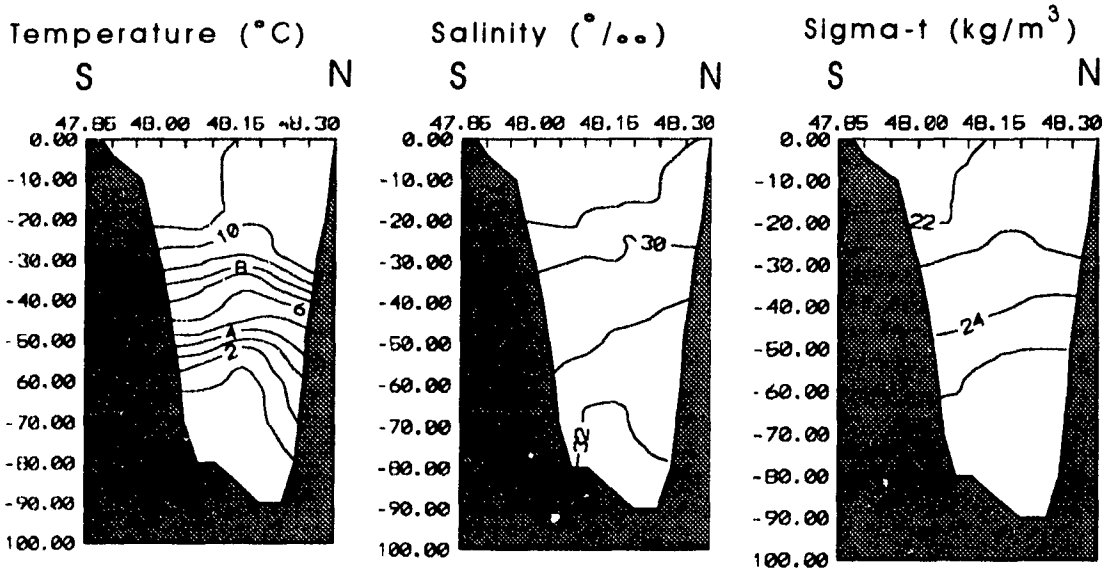

Baie des Chaleurs
RH8: 29, 30 September, 1 October 1991
Fig. 24

Longitude=64.83 (D)

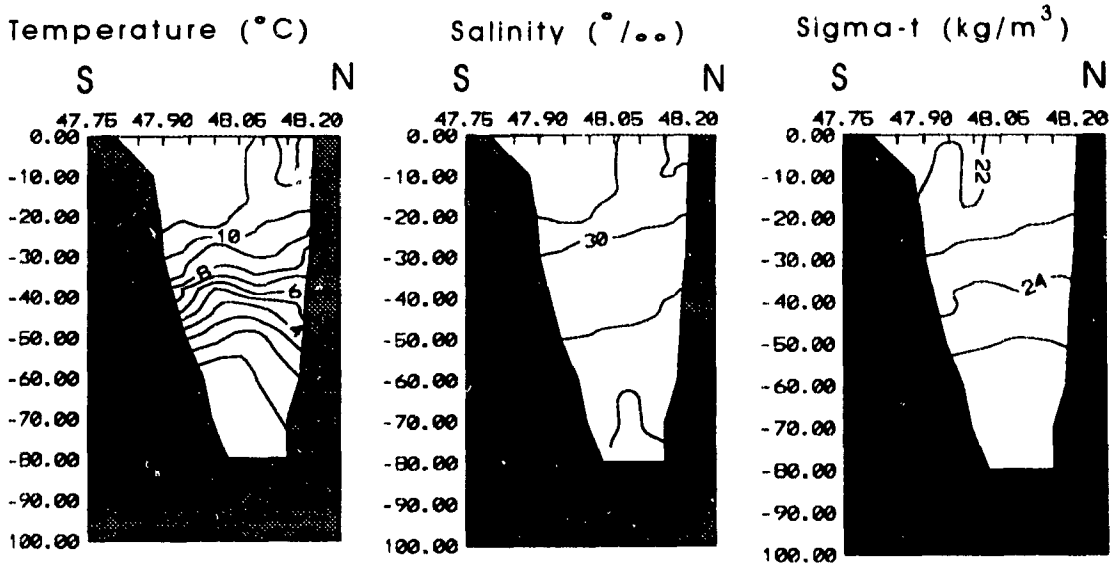

Longitude=65.00 (E)

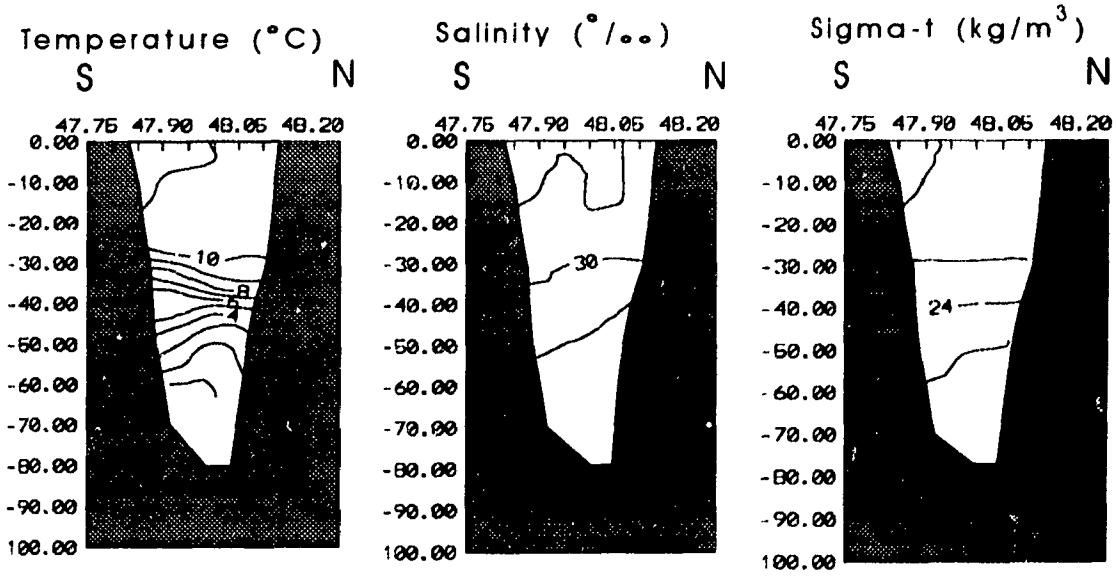

Baie des Chaleurs
RH8: 29, 30 September, 1 October 1991
Fig. 24

Longitude=65.17 (F)

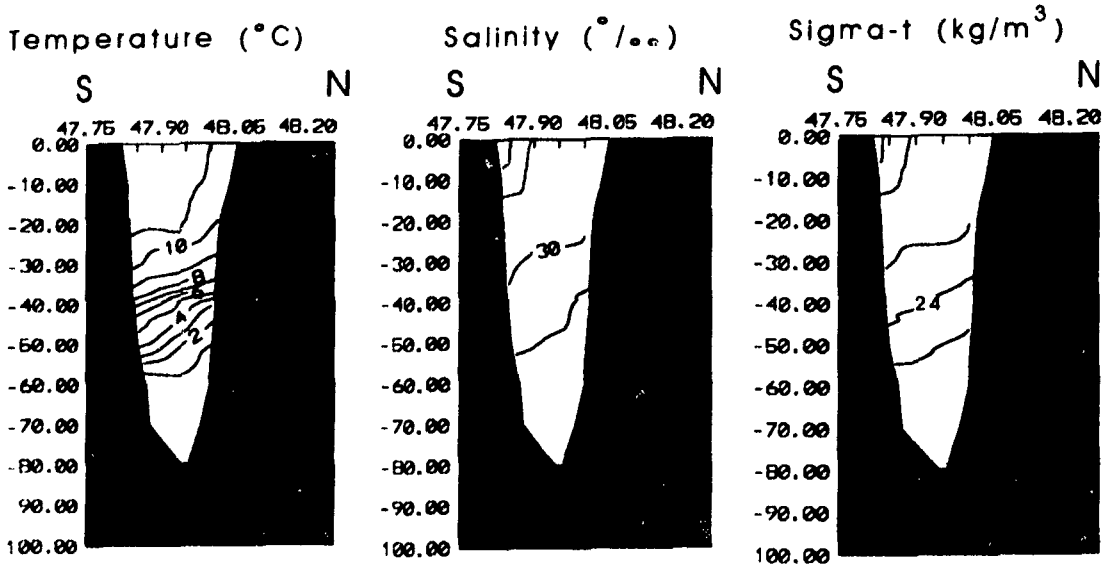

Longitude=65.33 (G)

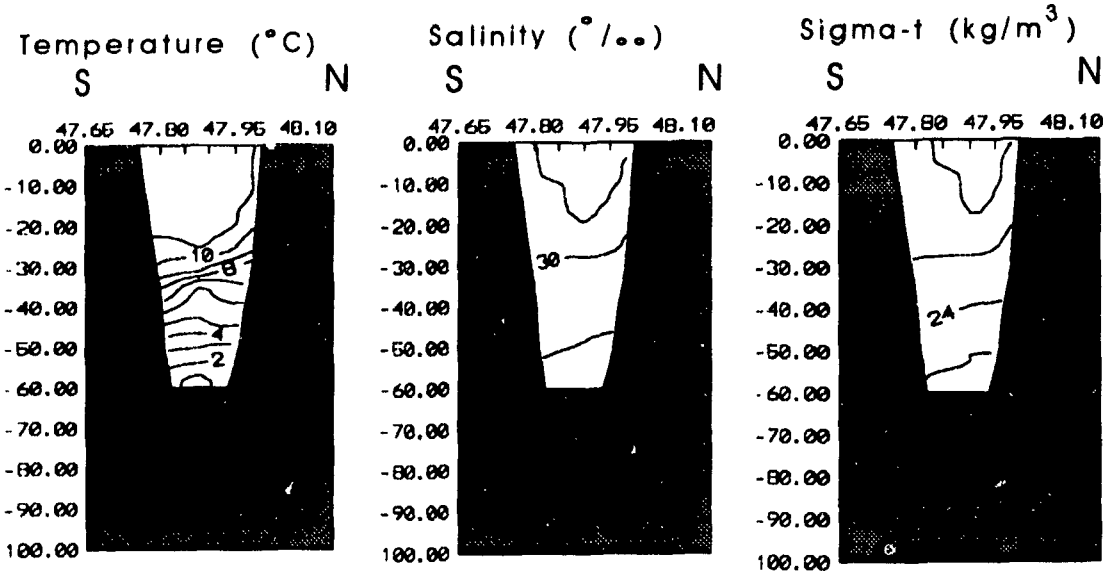

Baie des Chaleurs
RH8: 29, 30 September, 1 October 1991
Fig. 24

Longitude=65.50 (H)

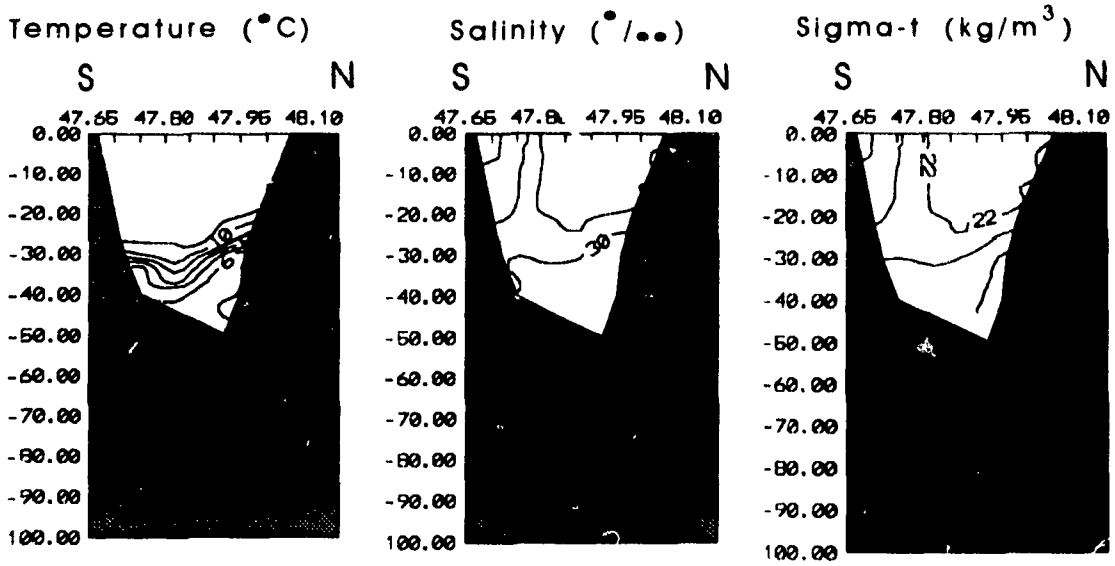

Longitude=65.67 (I)

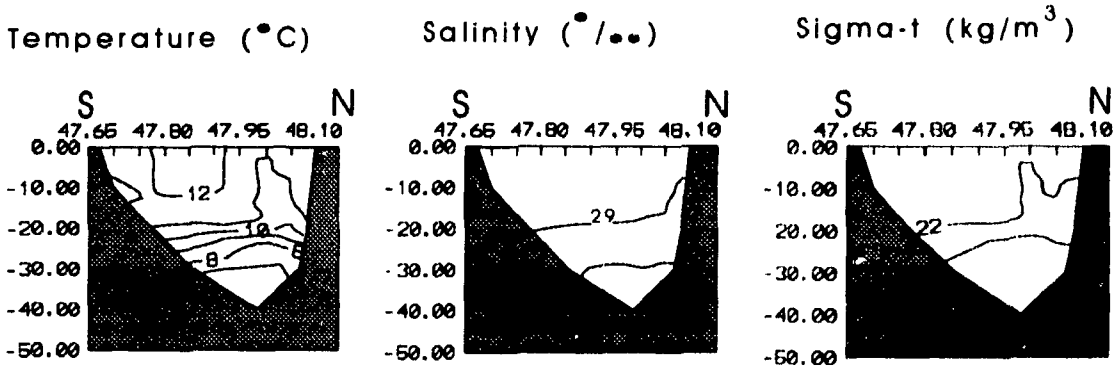

Longitude=65.83 (J)

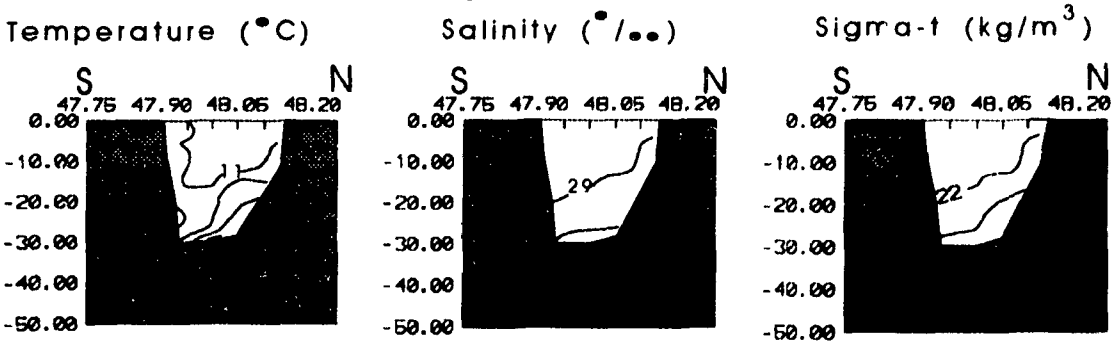

Baie des Chaleurs
RH8: 29, 30 September, 1 October 1991
Fig. 24

Longitude=66.00 (K)

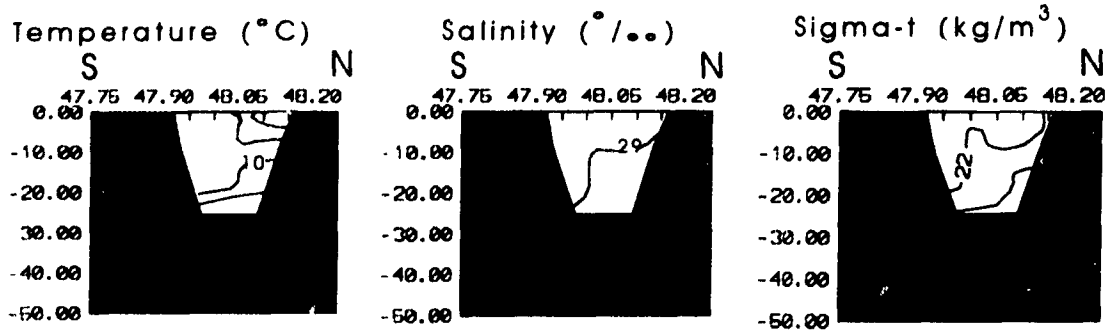

Longitude=66.17 (L)

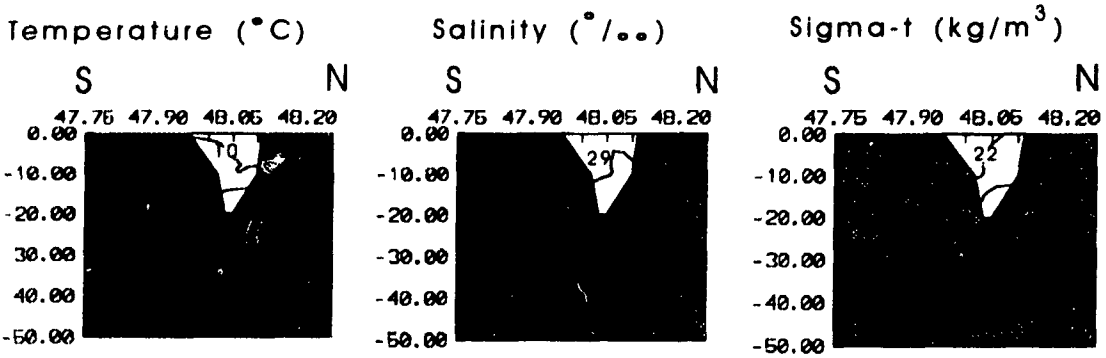

Longitude=66.28 (M)

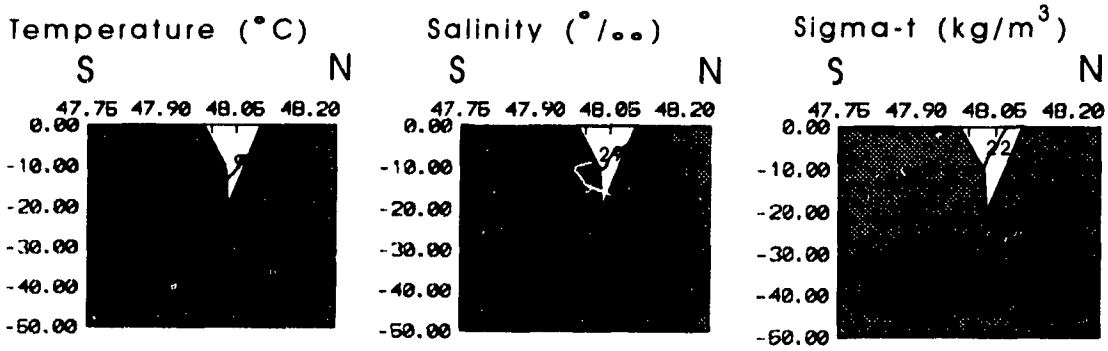

Baie des Chaleurs
RH8: 29, 30 September, 1 October 1991
Fig. 24

Longitude=64.50 (B)

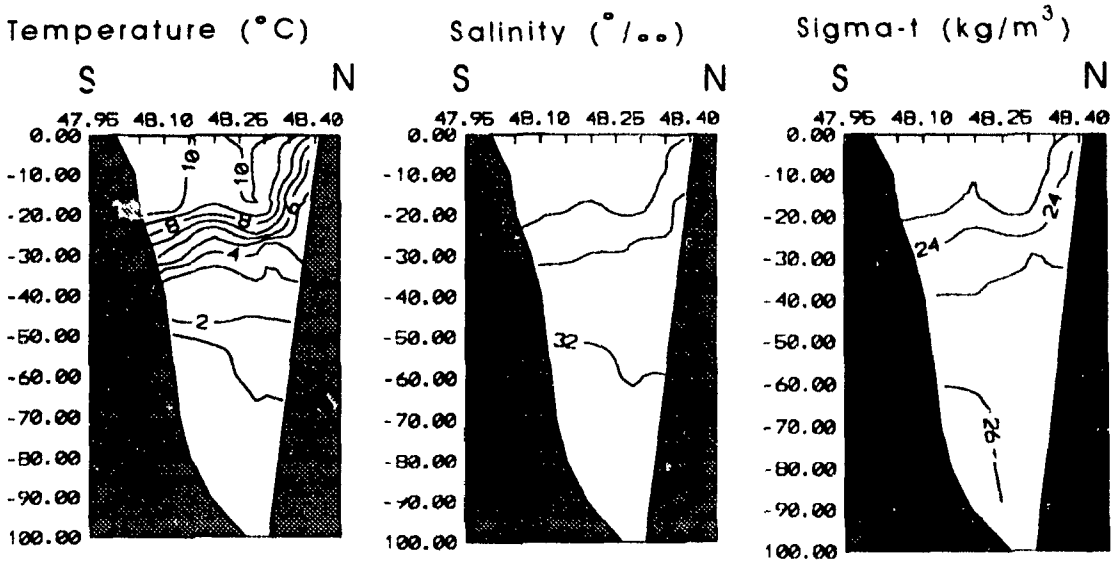

Longitude=64.67 (C)

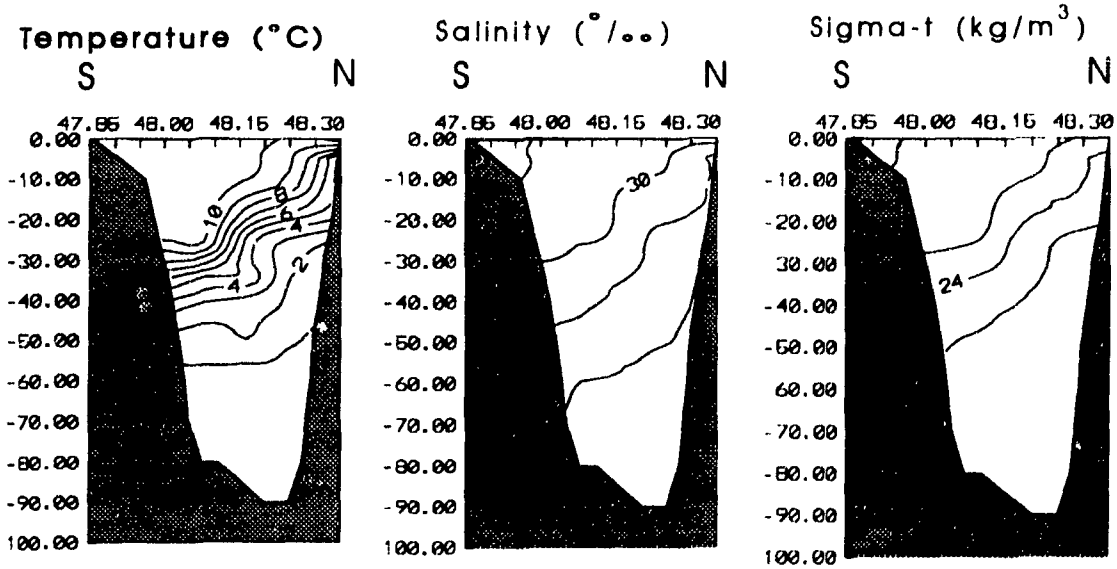

Baie des Chaleurs
RH9: 8, 9, 10 October 1991
Fig. 25

Longitude=64.83 (D)

Temperature (°C) Salinity (°/₀₀) Sigma-t (kg/m^3)

Not available

Longitude=65.00 (E)

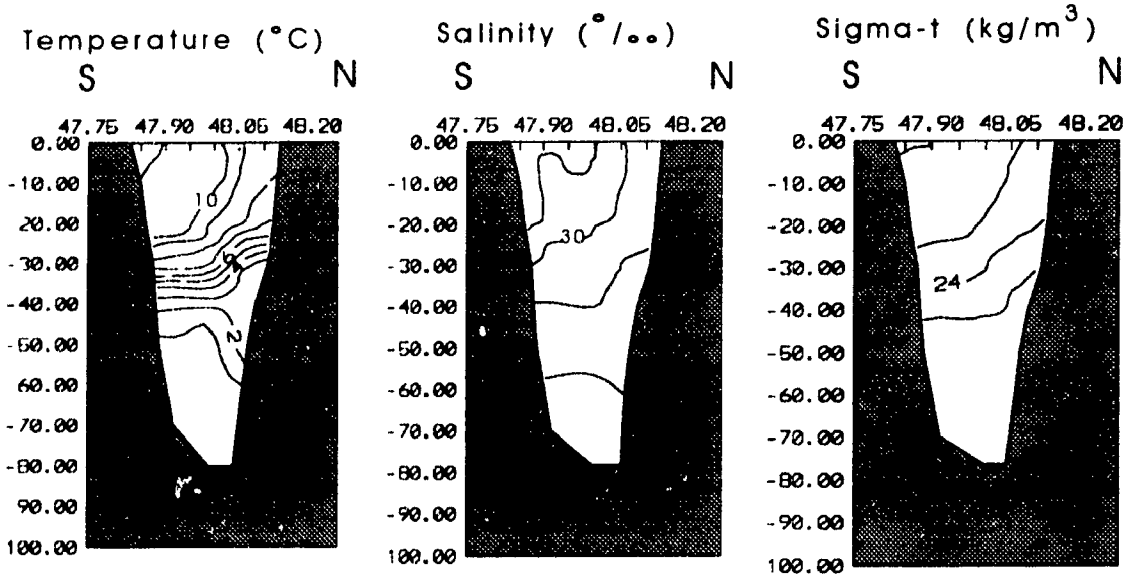

Baie des Chaleurs
RH9: 8, 9, 10 October 1991
Fig. 25

Longitude=65.17 (F)

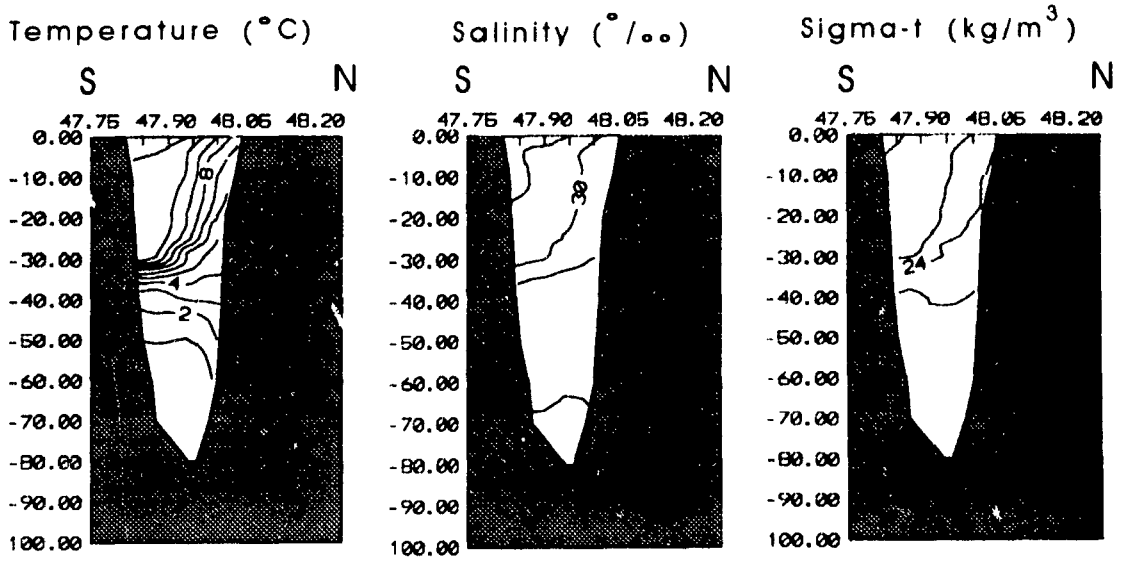

Longitude=65.33 (G)

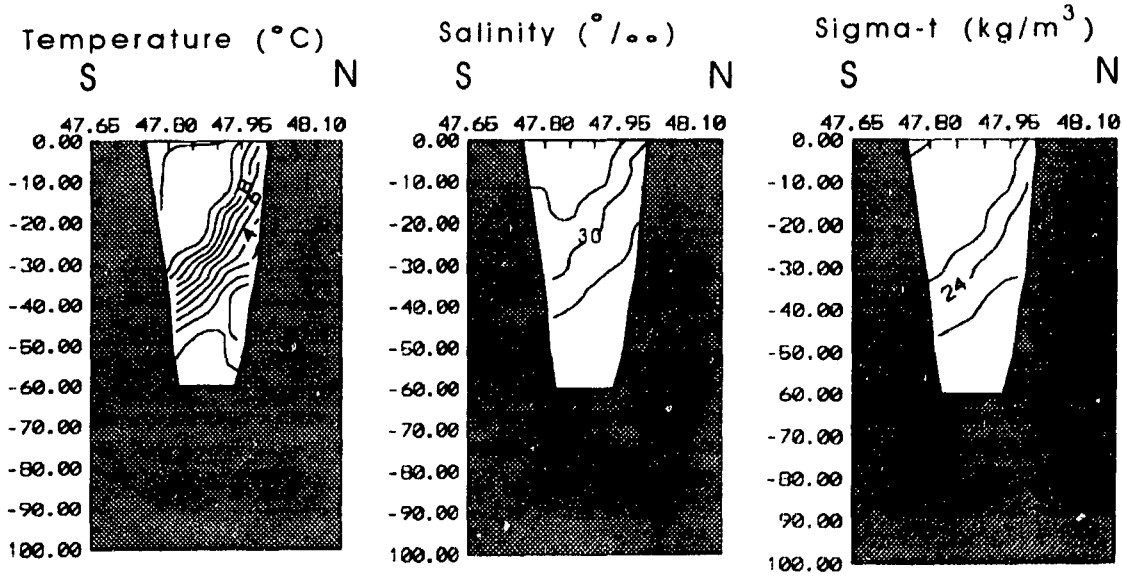

Baie des Chaleurs
RH9: 8, 9, 10 October 1991
Fig. 25

Longitude=65.50 (H)

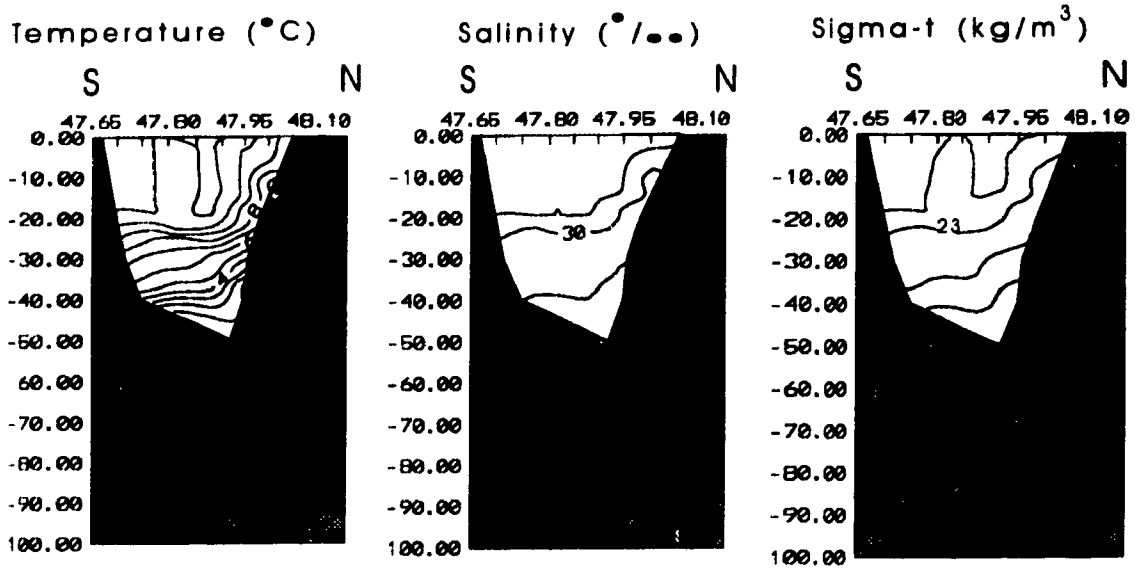

Longitude=65.67 (I)

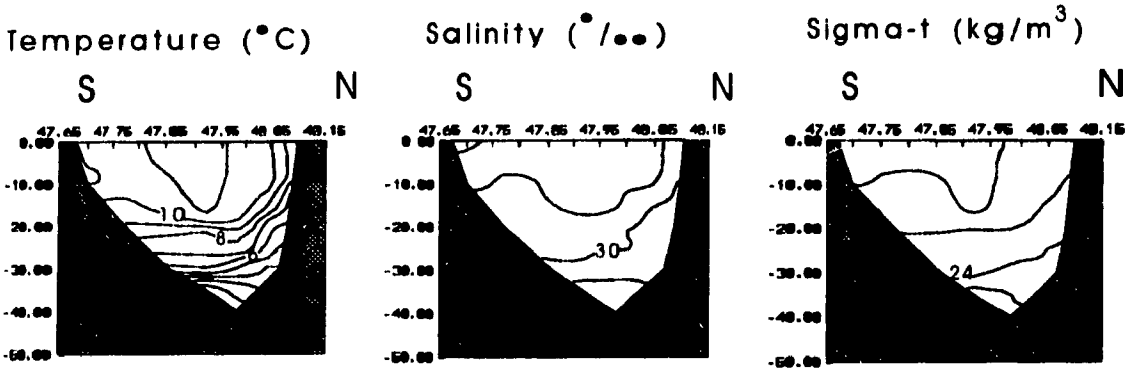

Longitude=65.83 (J)

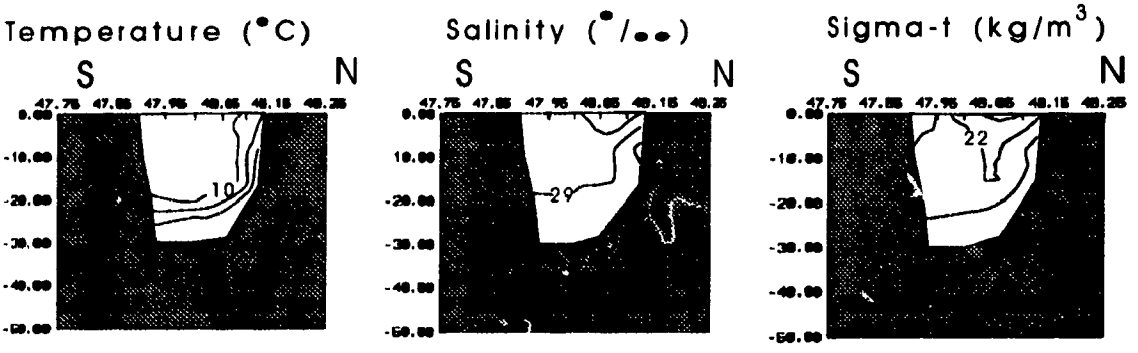

Baie des Chaleurs
RH9: 8, 9, 10 October 1991
Fig. 25

Longitude=66.00 (K)

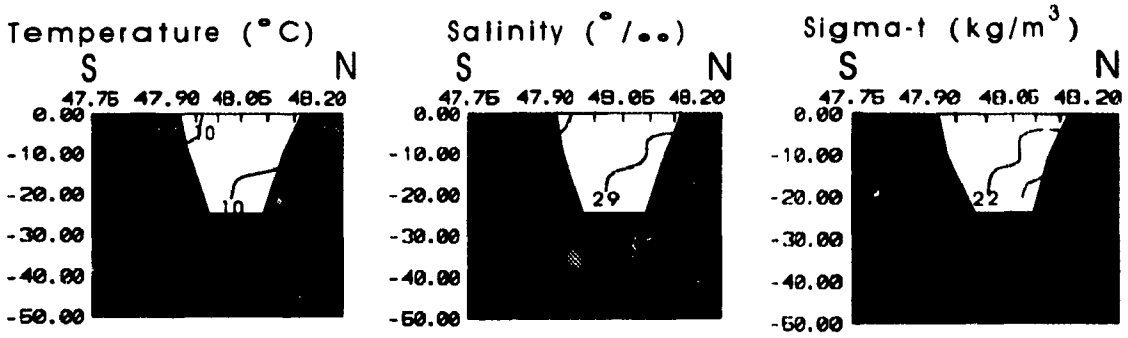

Longitude=66.17 (L)

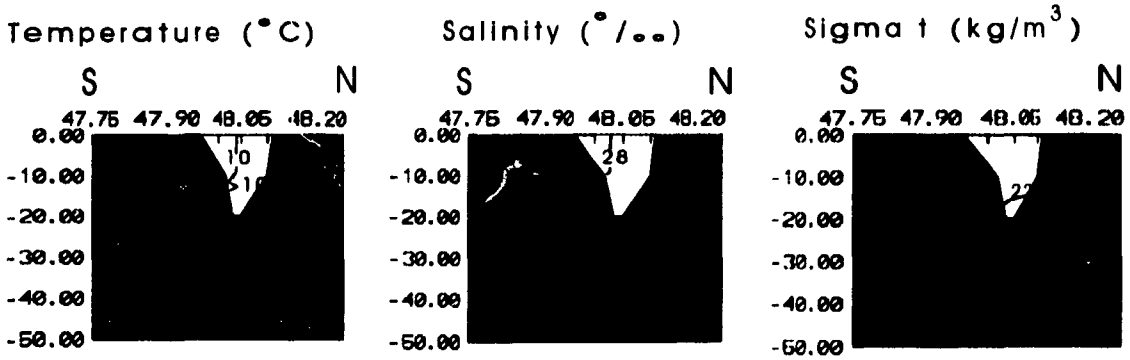

Longitude=66.28 (M)

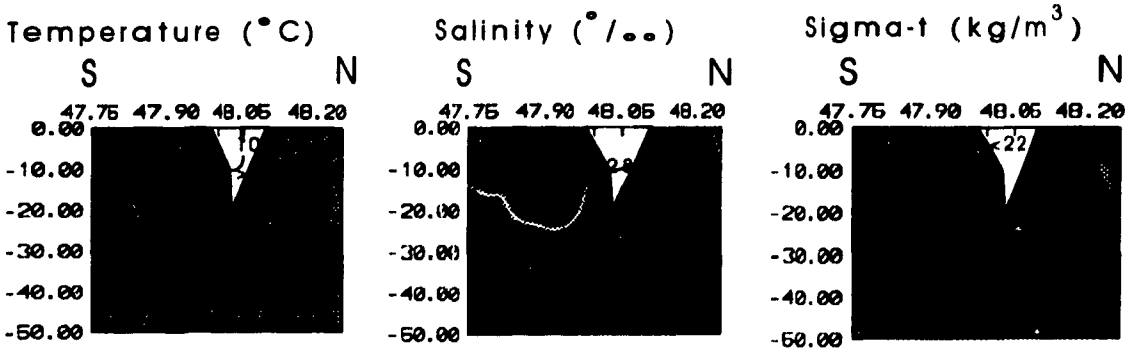

Baie des Chaleurs
RH9: 8, 9, 10 October 1991
Fig. 25

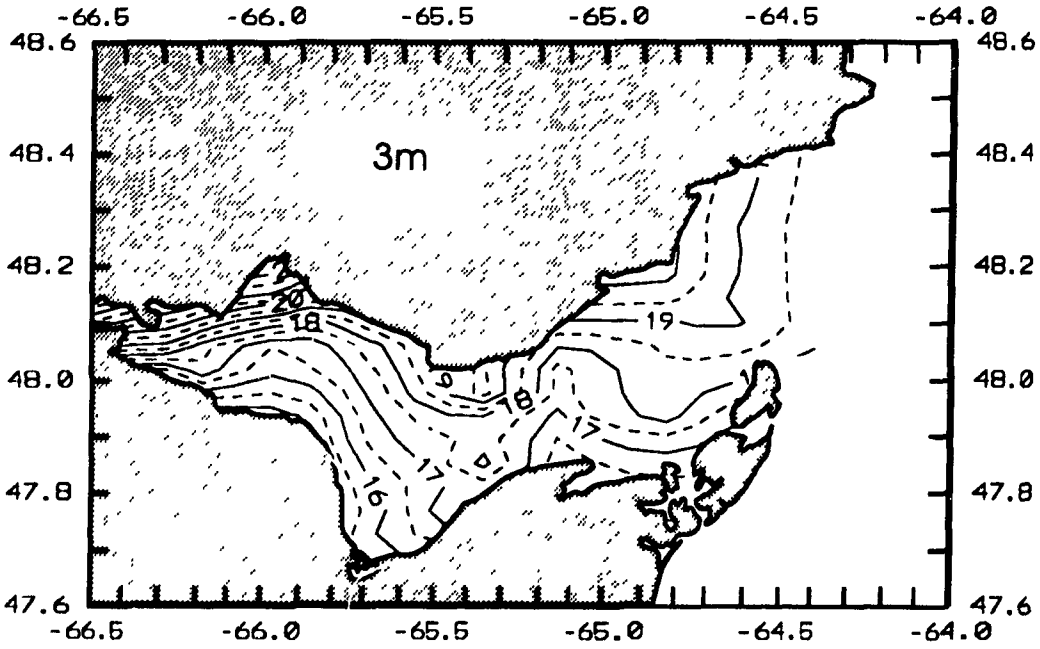

RHO: 10, 11, 12 June 1991

FIG. 26

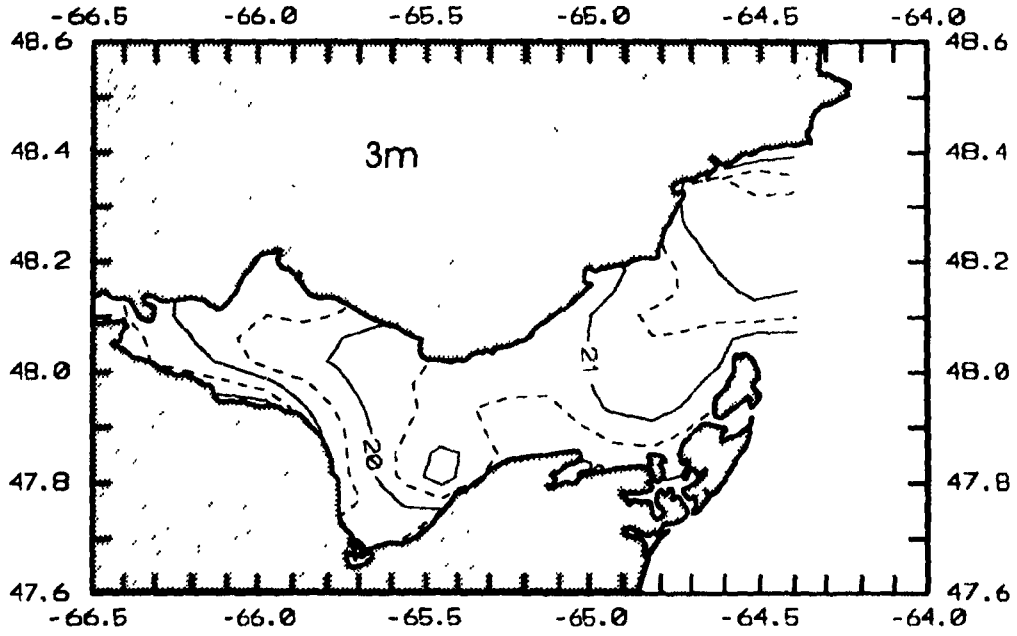

RH1: 21, 22, 23 August 1991

FIG. 27

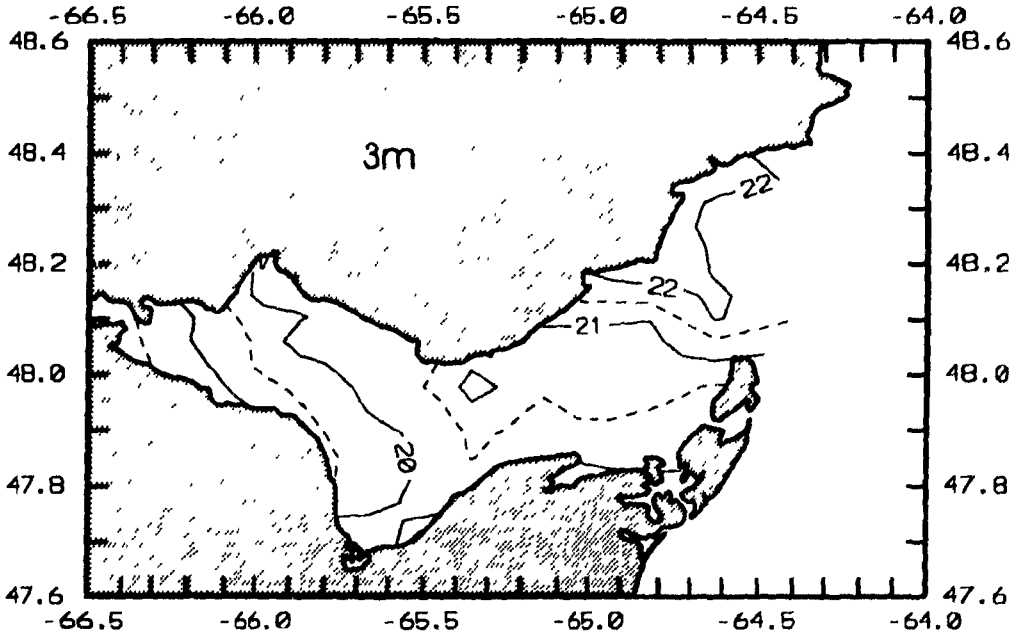

RH2: 26, 27, 28 August 1991

FIG. 28

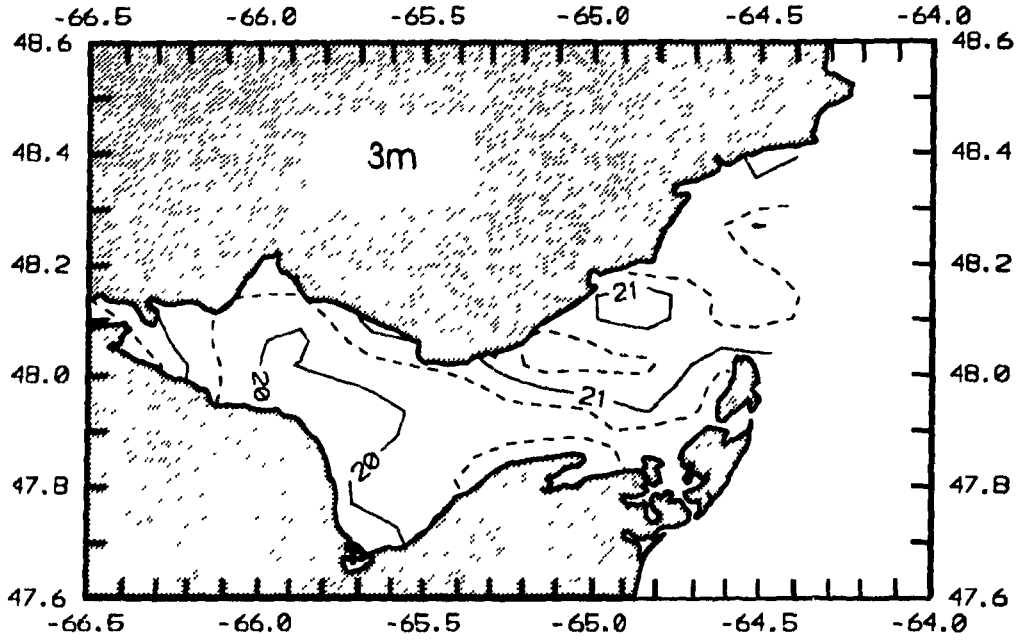

RH5: 5, 6, 7 September 1991

FIG. 29

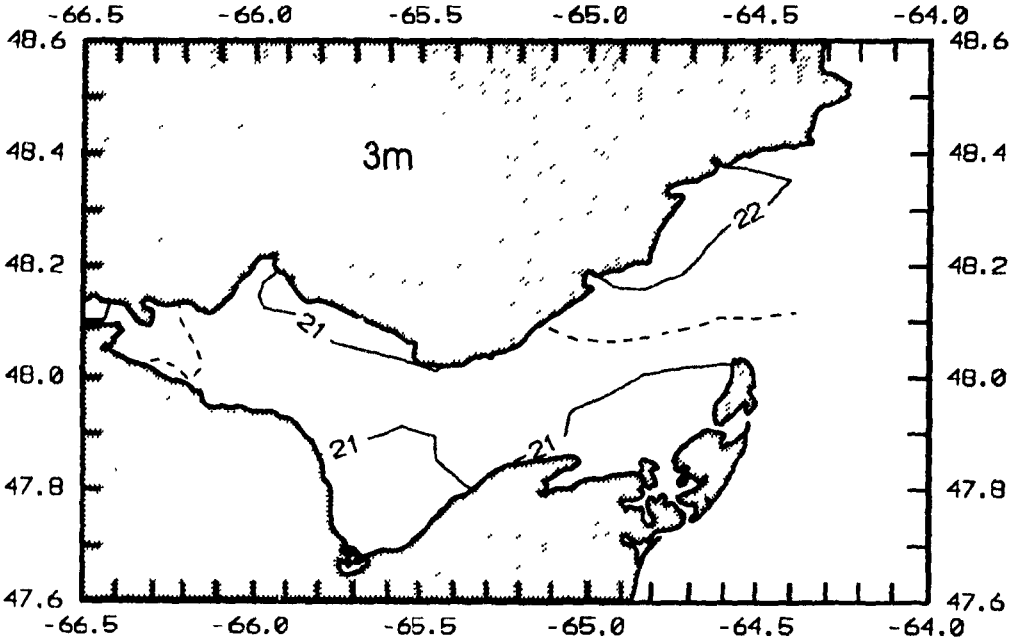

RH6: 15, 16, 17 September 1991

FIG. 30

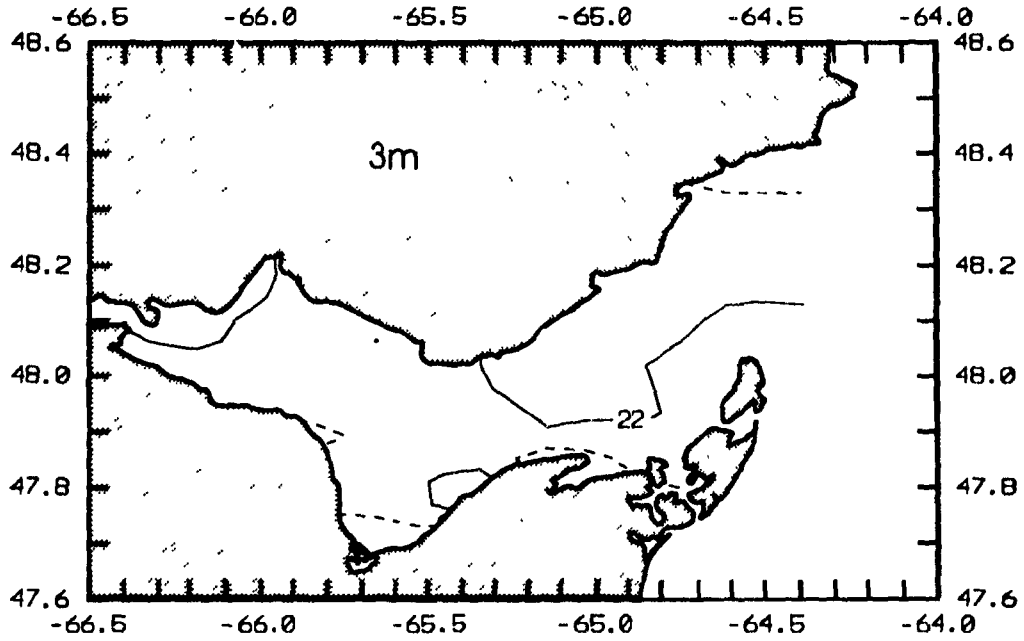

RH8: 29, 30 September, 1 October 1991

FIG. 31

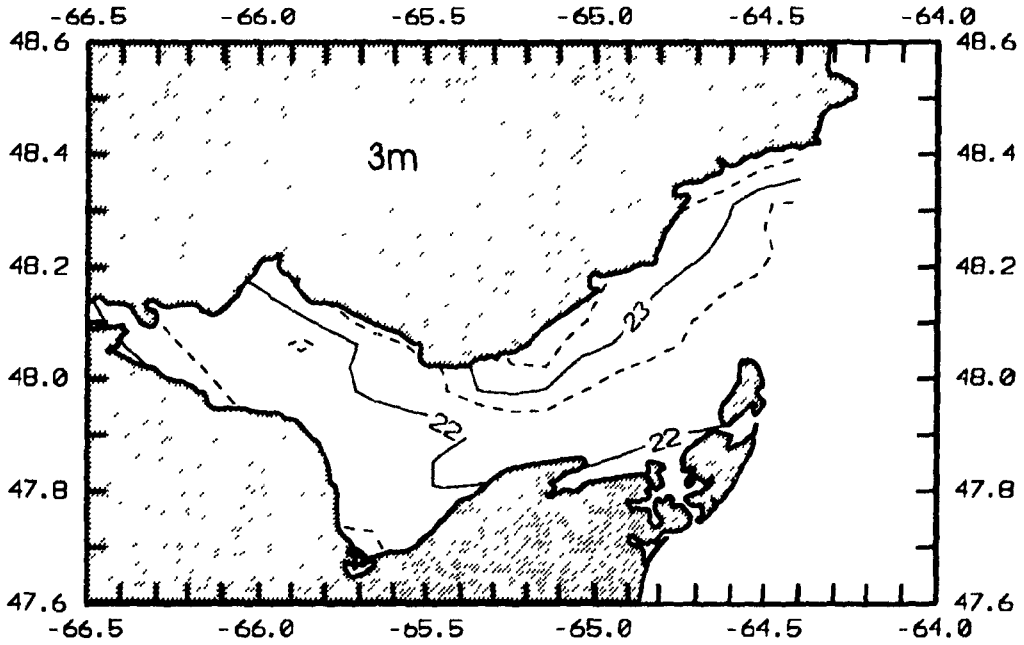

RH9: 8, 9, 10 October 1991

FIG. 32

Fig. 33

RHO: 10, 11, 12 June 1991

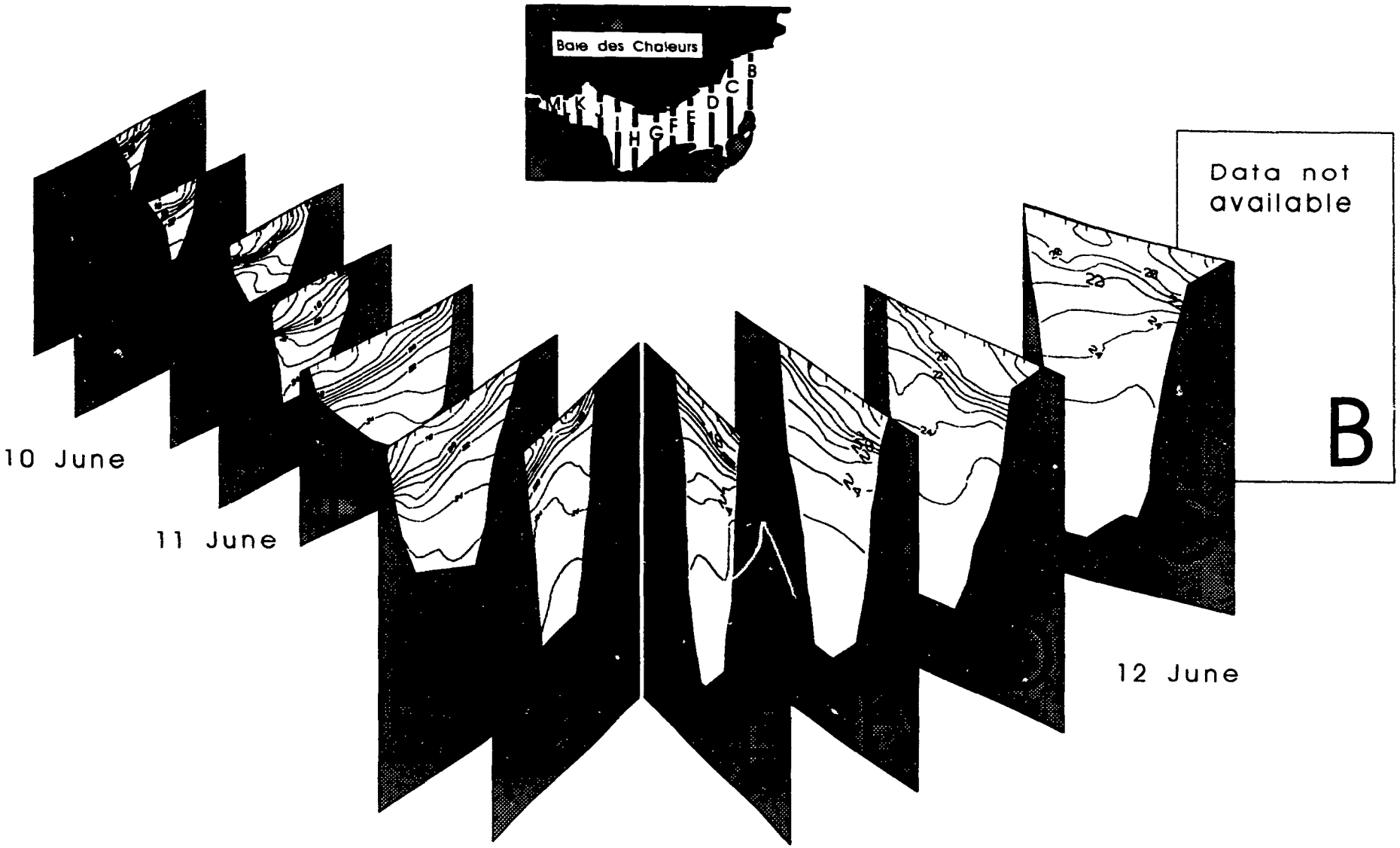

Fig. 34
RH1: 21, 22, 23 August 1991

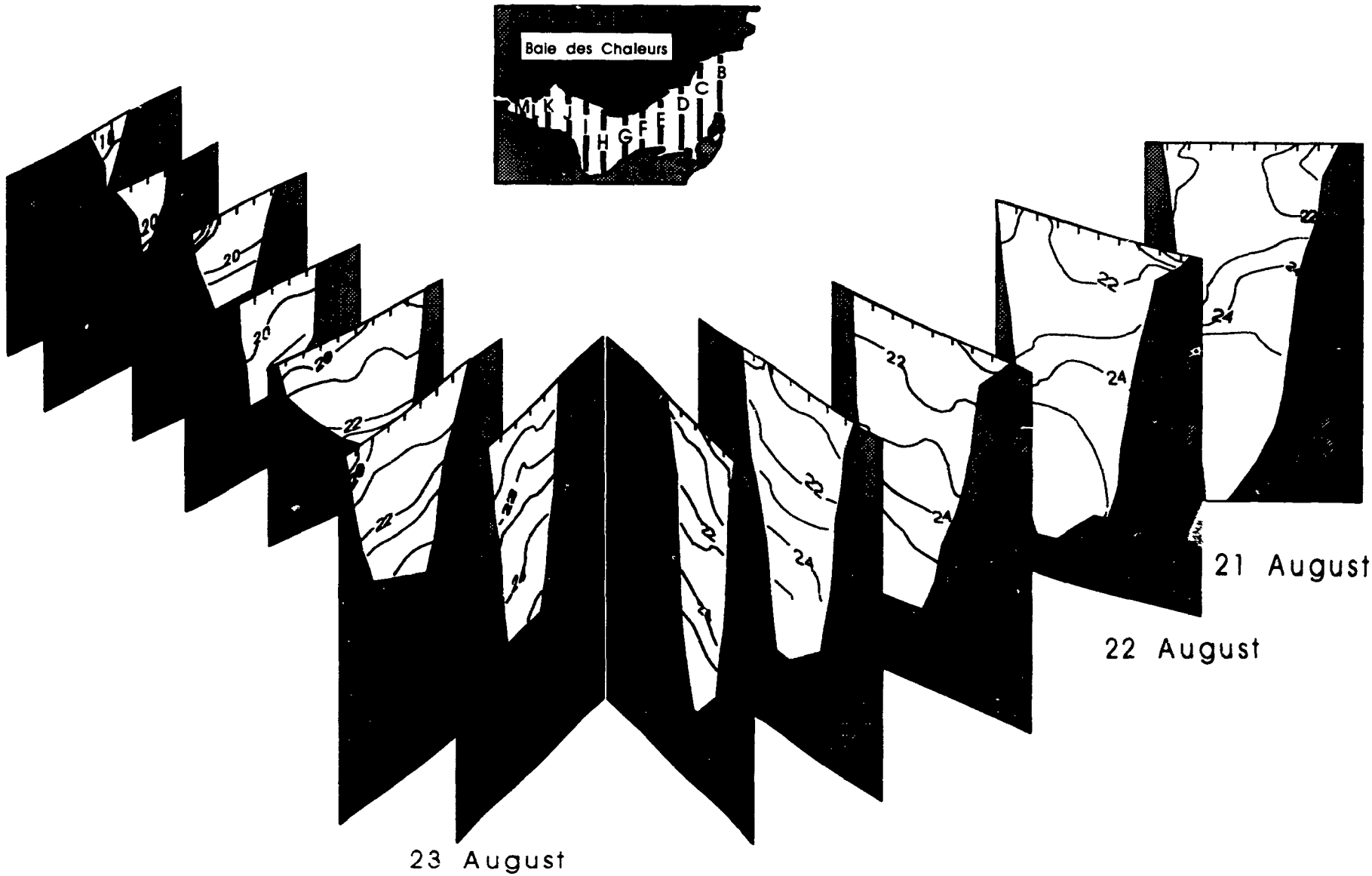

Fig. 35
RH2: 26, 27, 28 August 1991

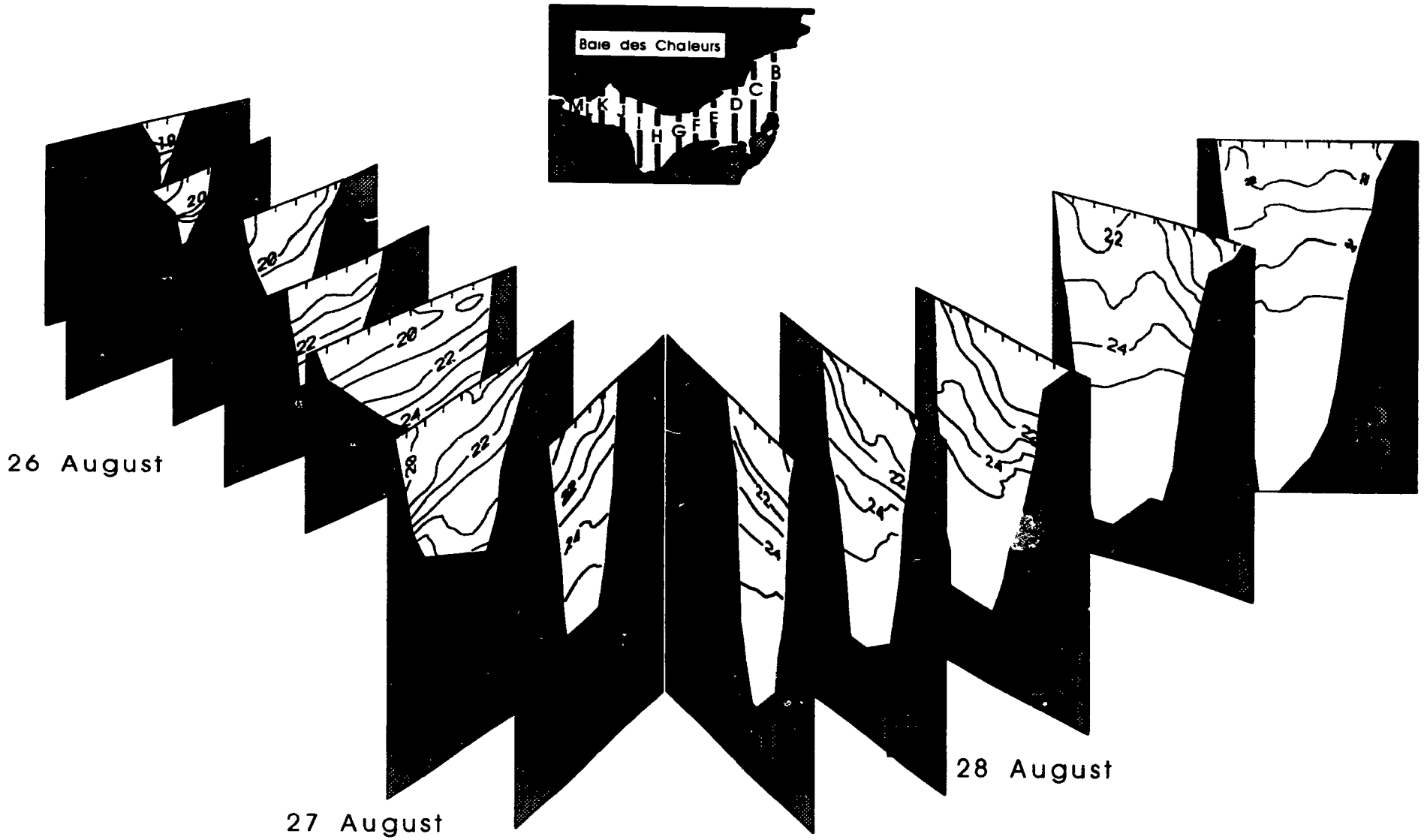

Fig. 36
RH5: 5, 6, 7 September 1991

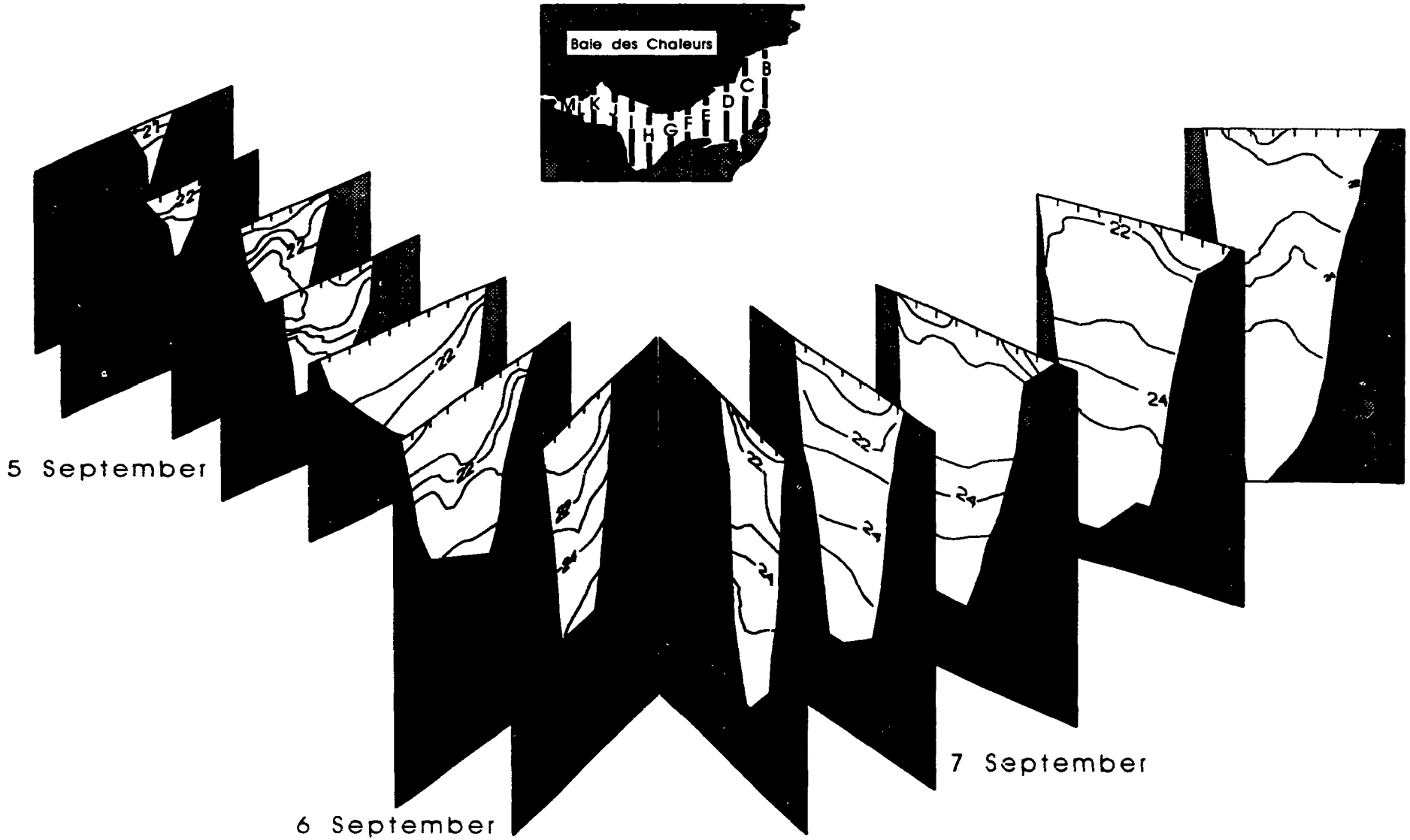

Fig. 37
RH6: 15, 16 September 1991

Fig. 38
RH8: 29, 30 September, 1 October 1991

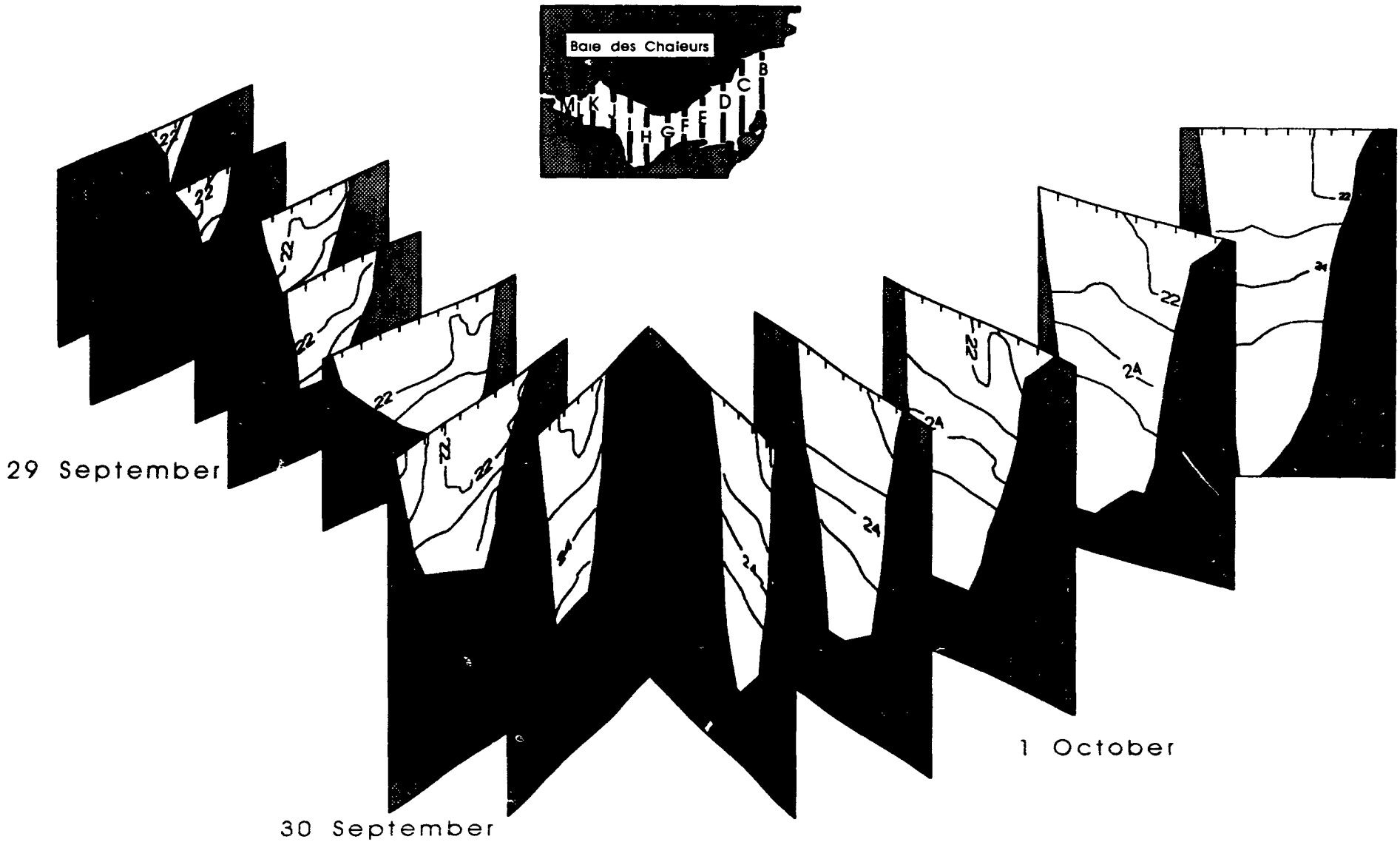

Fig. 39
RH9: 8, 9, 10 October 1991

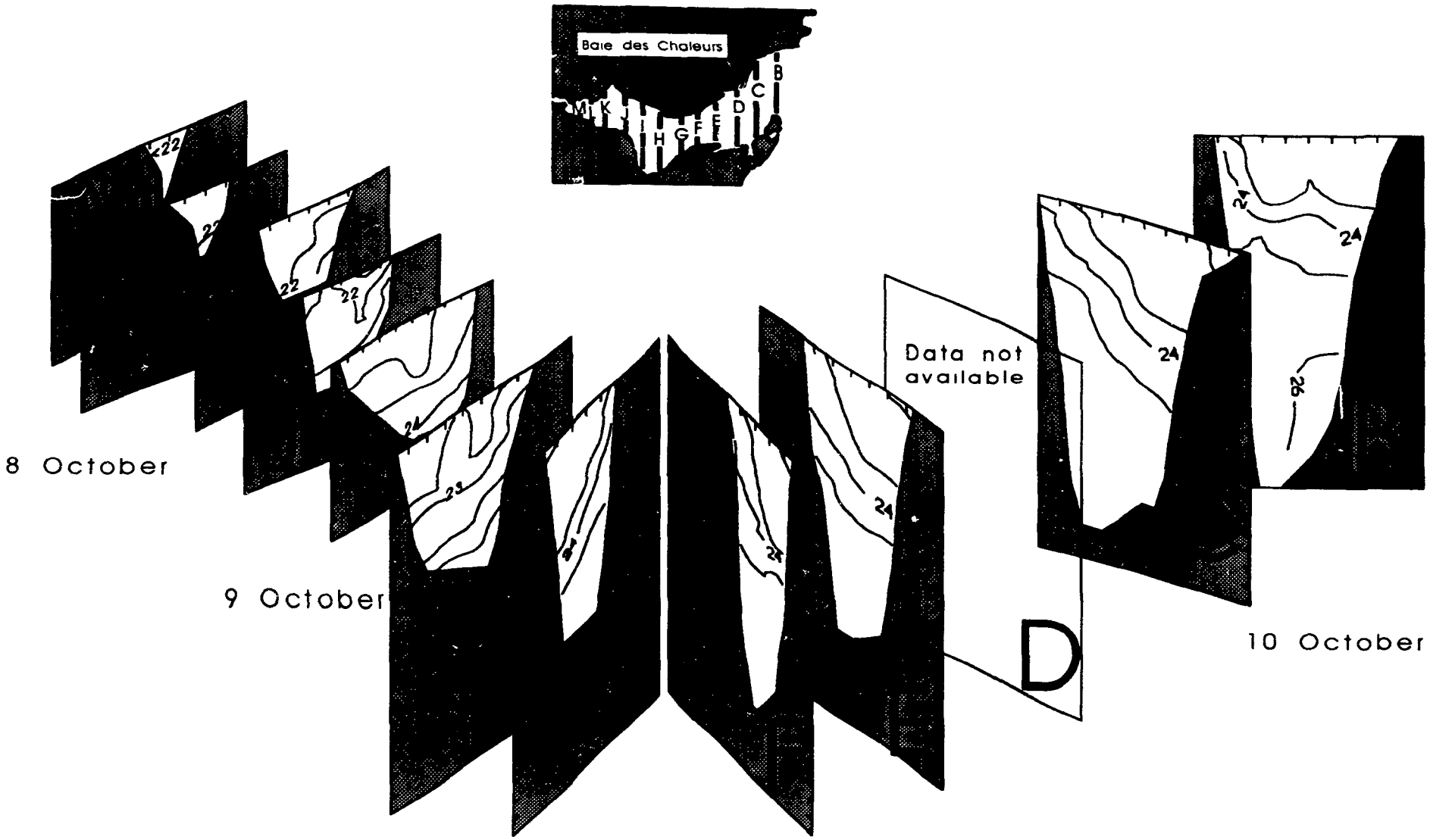

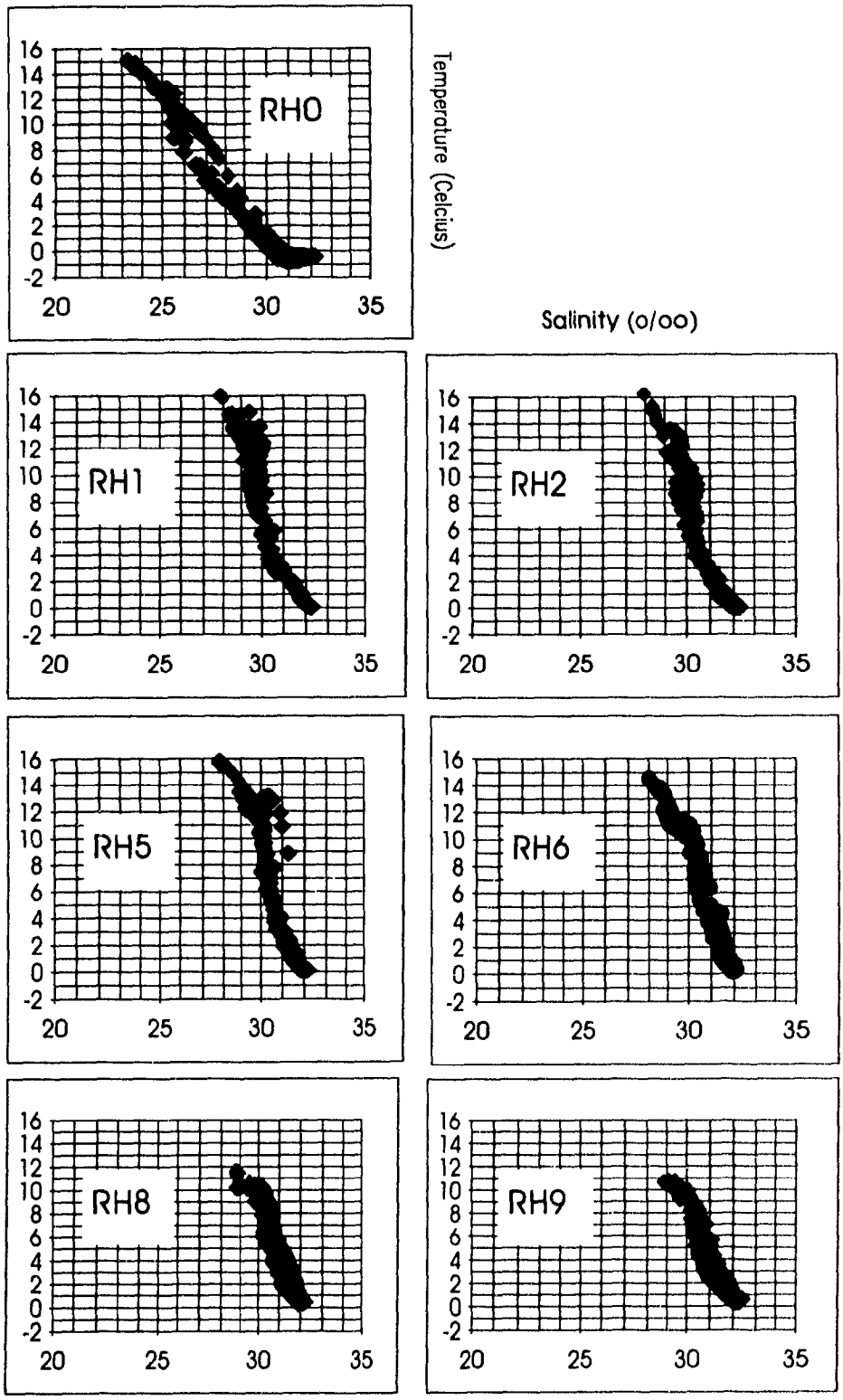
RH0
RH1
RH2
RH5
RH6
RH8
RH9
Temperature (Celcius)
Salinity (o/oo)
16
14
12
10
8
6
4
2
0
-2
20
25
30
35

Fig. 40

BAIE DES CHALEURS
Weekly CTD profiles
1991

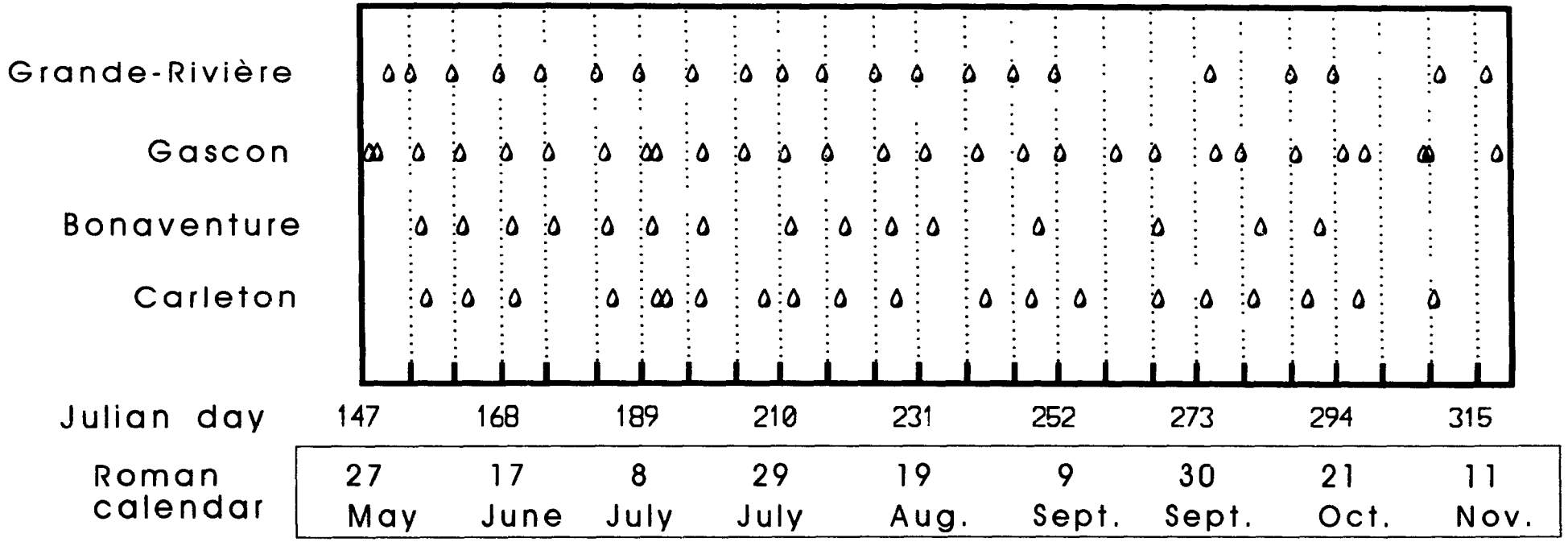

Fig. 41

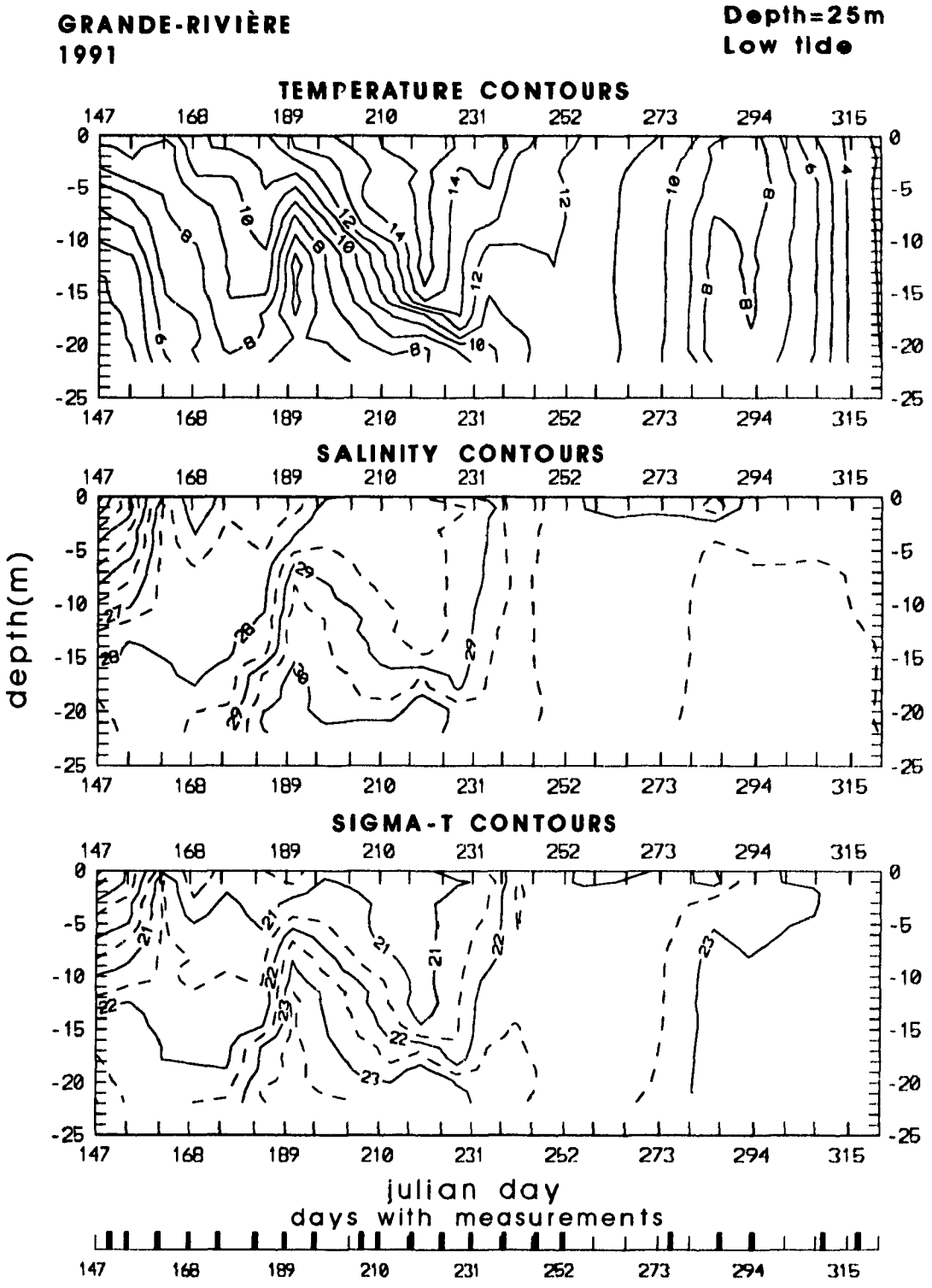
GRANDE-RIVIÈRE
1991
Depth=25m
Low tide
TEMPERATURE CONTOURS
SALINITY CONTOURS
SIGMA-T CONTOURS
depth(m)
julian day
days with measurements
147
168
189
210
231
252
273
294
315
0
-5
-10
-15
-20
-25

Fig. 42

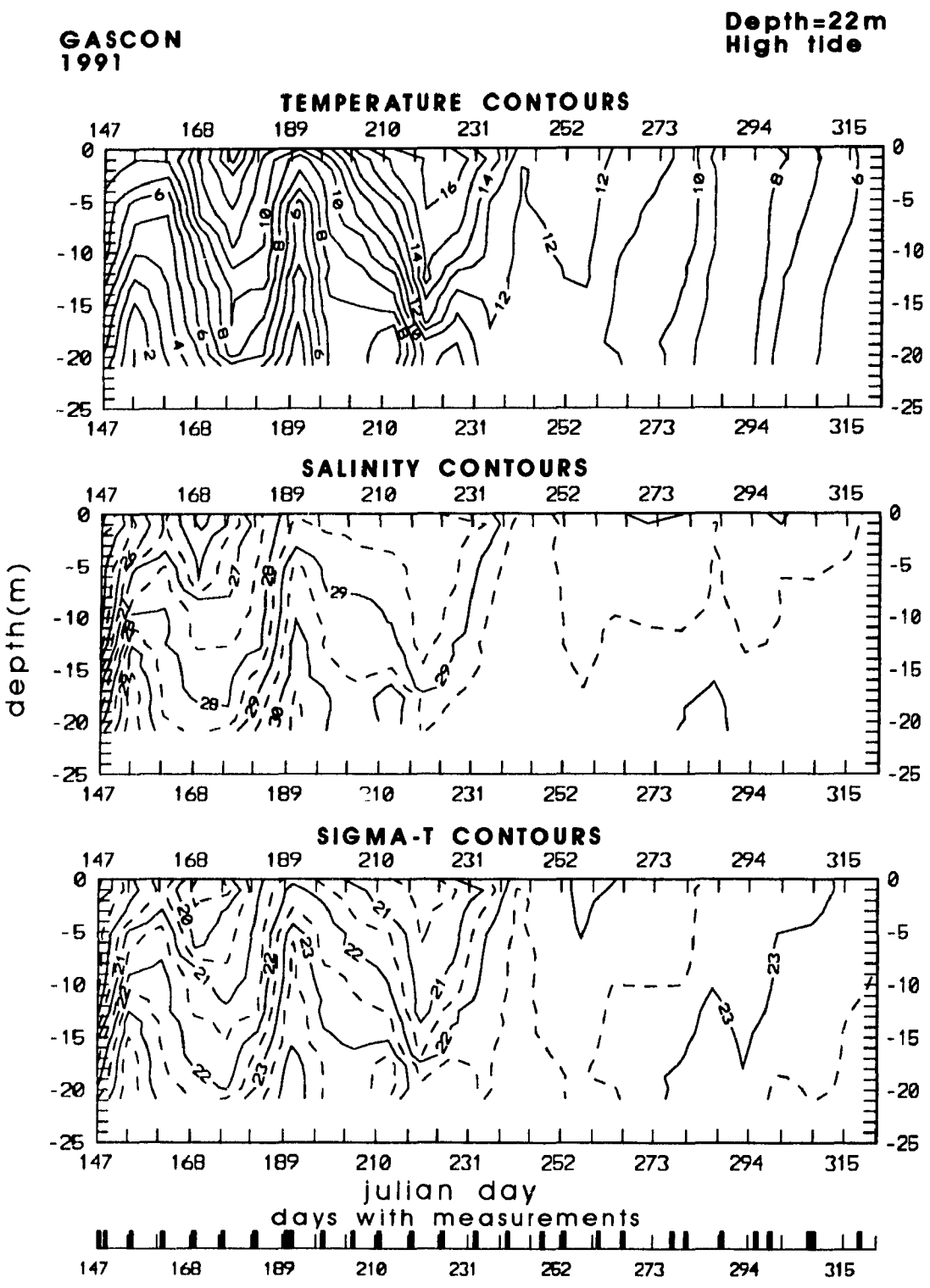
GASCON
1991
Depth=22m
High tide
TEMPERATURE CONTOURS
SALINITY CONTOURS
SIGMA-T CONTOURS
depth(m)
147 168 189 210 231 252 273 294 315
0 -5 -10 -15 -20 -25
julian day
days with measurements

Fig. 43

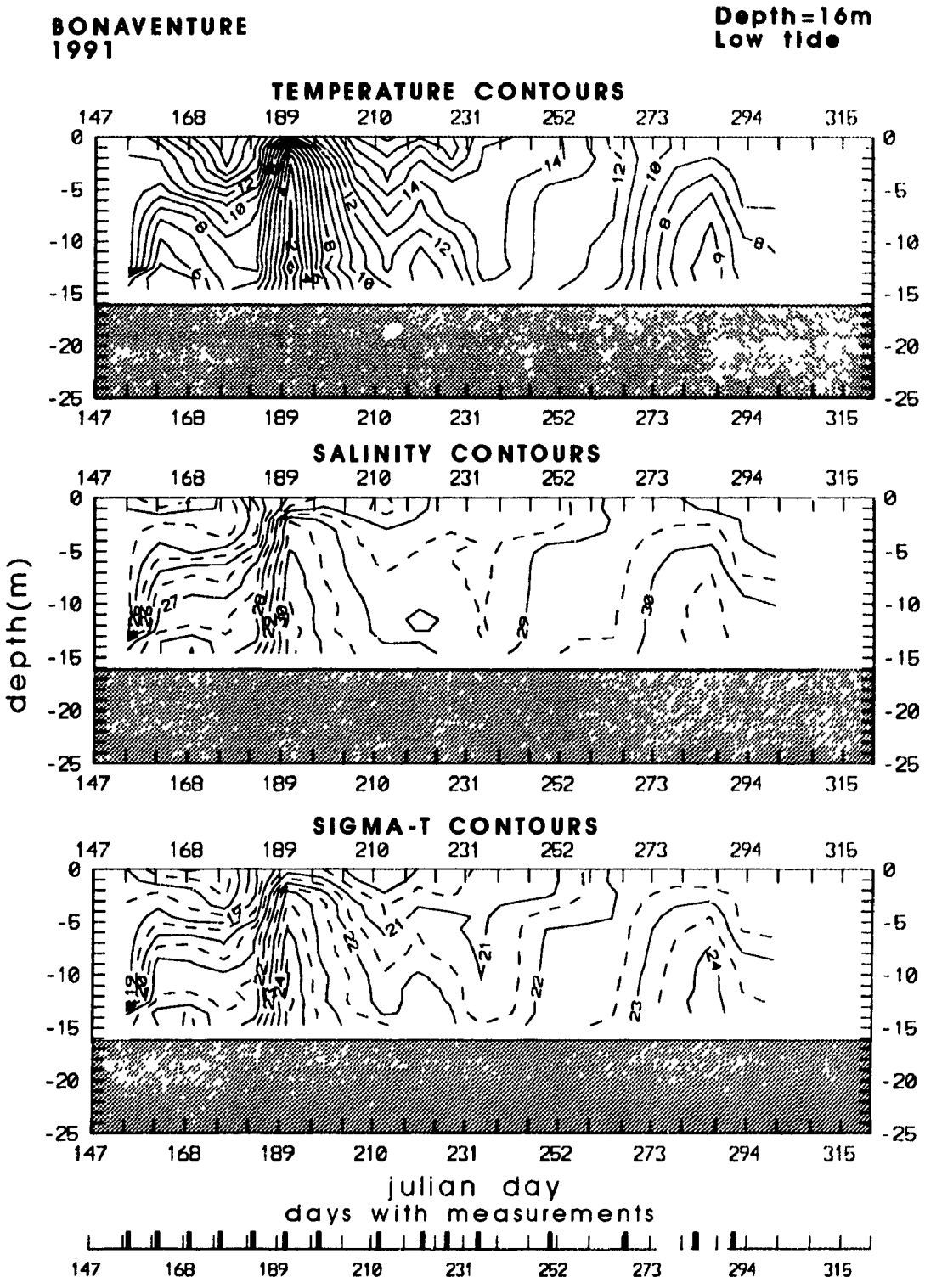
BONAVENTURE
1991
Depth=16m
Low tide
TEMPERATURE CONTOURS
SALINITY CONTOURS
SIGMA-T CONTOURS
depth(m)
julian day
days with measurements
147
168
189
210
231
252
273
294
315
0
-5
-10
-15
-20
-25

Fig. 44

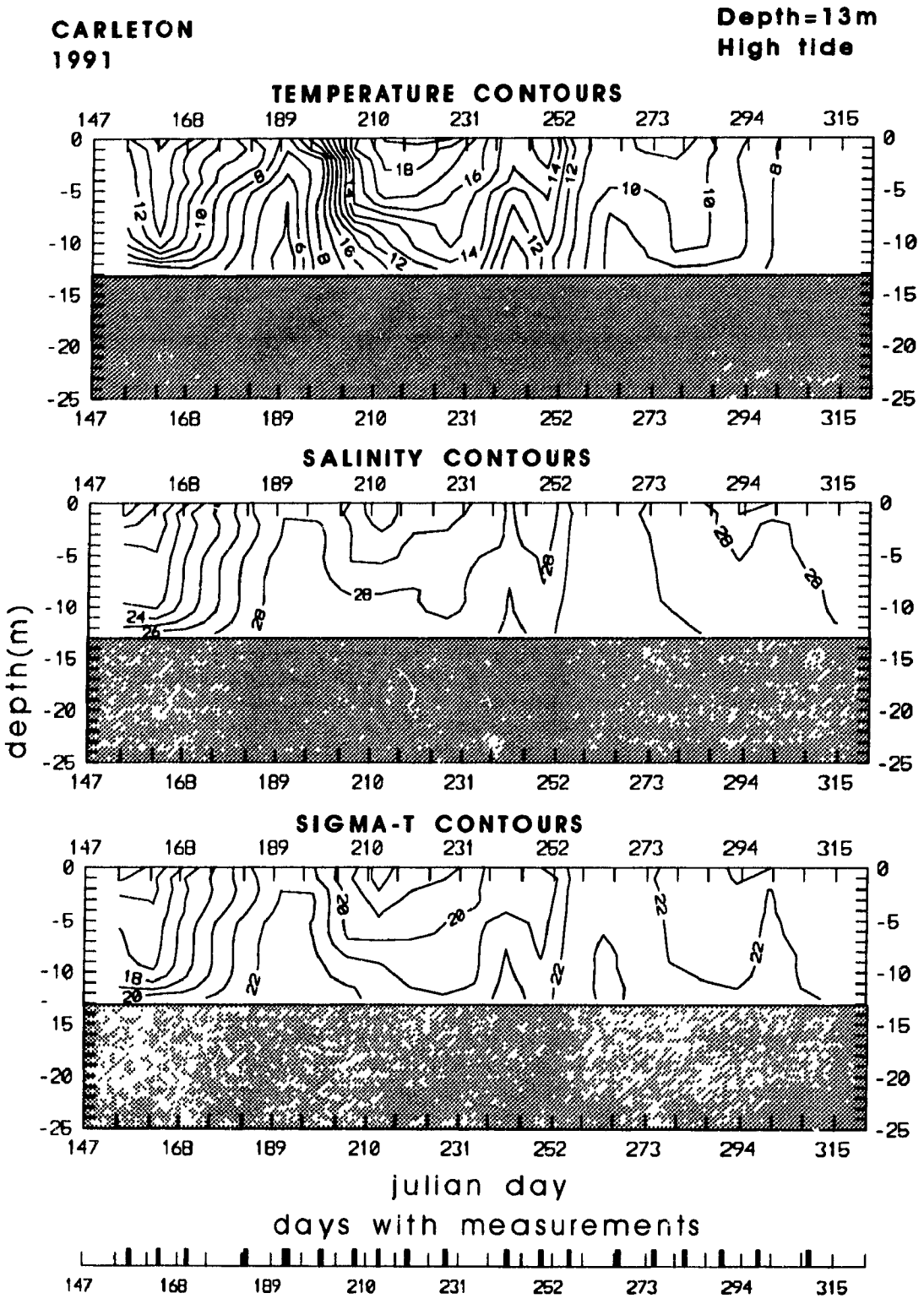
CARLETON
1991
Depth=13m
High tide
TEMPERATURE CONTOURS
SALINITY CONTOURS
SIGMA-T CONTOURS
depth(m)
julian day
days with measurements
147
168
189
210
231
252
273
294
315
0
-5
-10
-15
-20
-25

Fig. 45

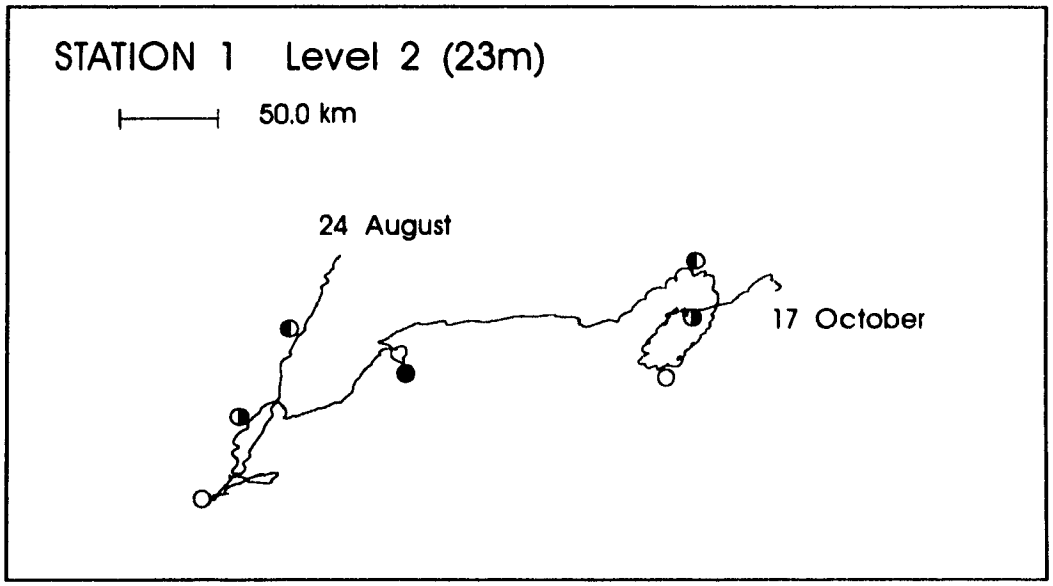
STATION 1 Level 2 (23m)
50.0 km
24 August
17 October

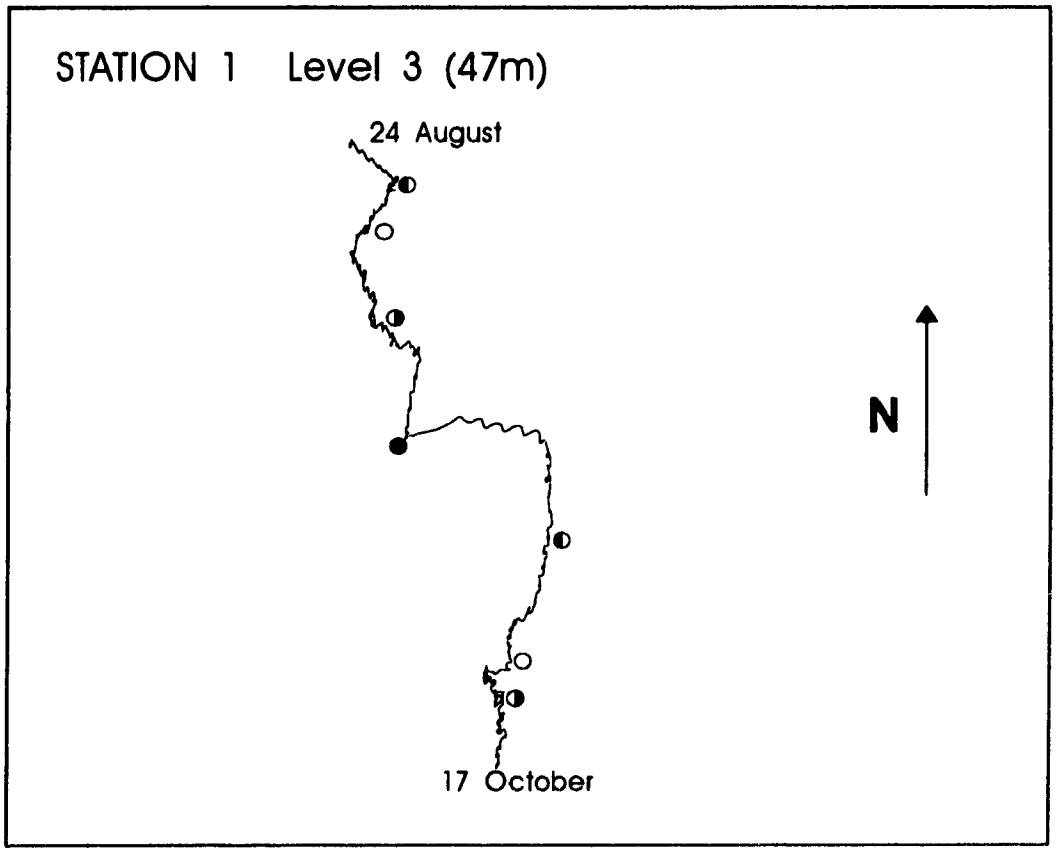
STATION 1 Level 3 (47m)
24 August
17 October
N

Fig. 46

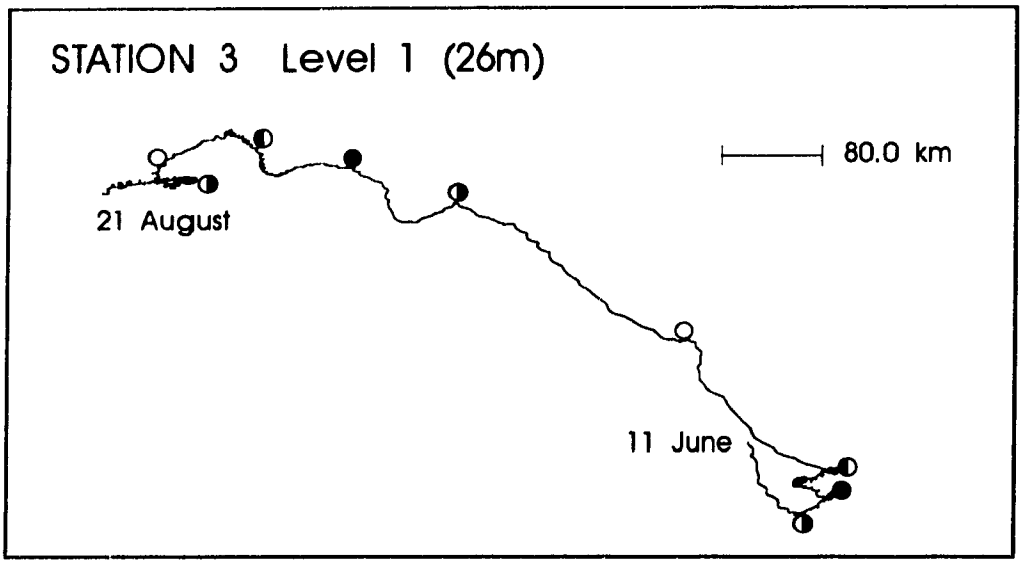
STATION 3 Level 1 (26m)
80.0 km
21 August
11 June

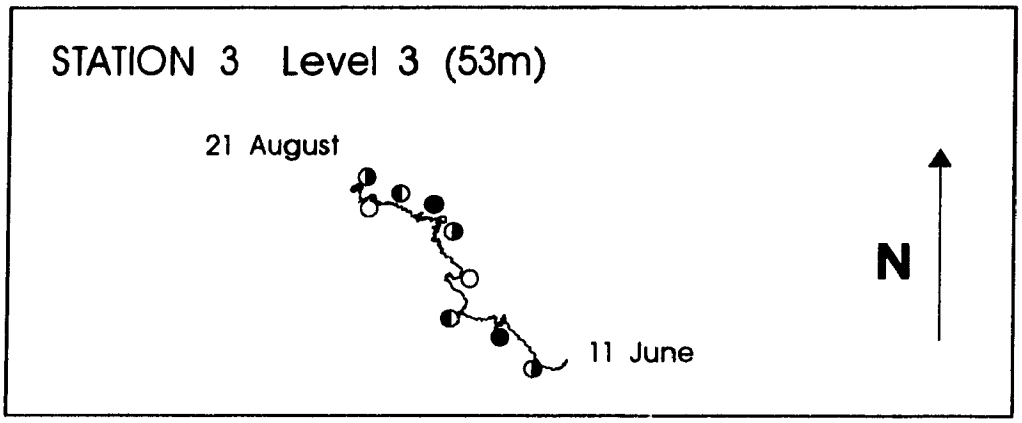
STATION 3 Level 3 (53m)
21 August
11 June
N

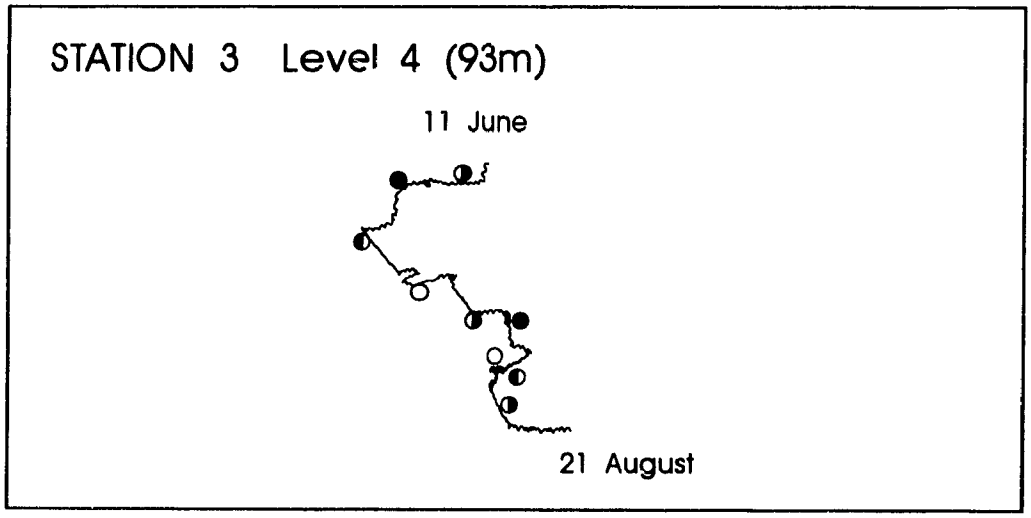
STATION 3 Level 4 (93m)
11 June
21 August

Fig. 47

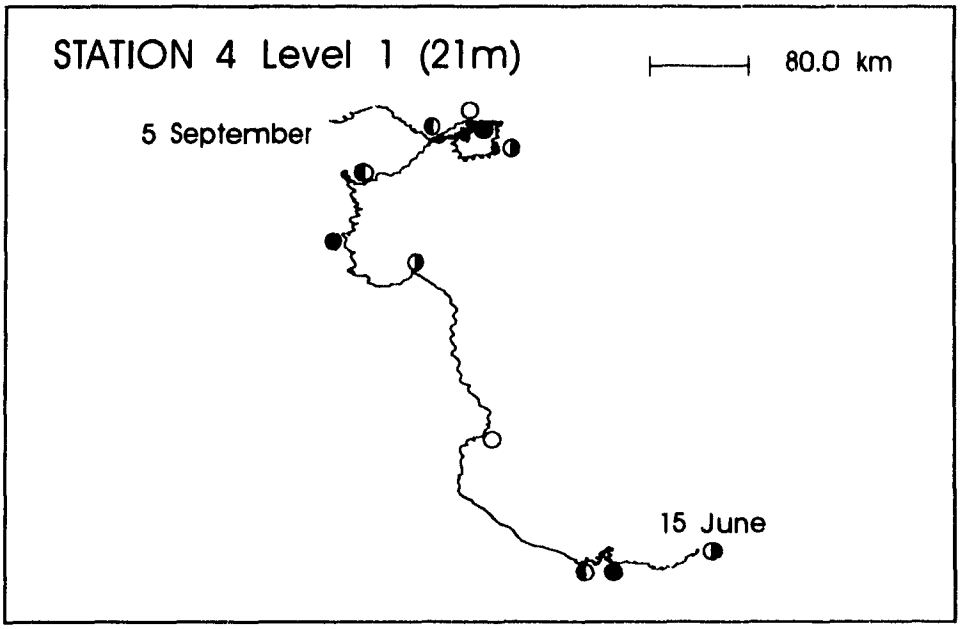
STATION 4 Level 1 (21m)
80.0 km
5 September
15 June

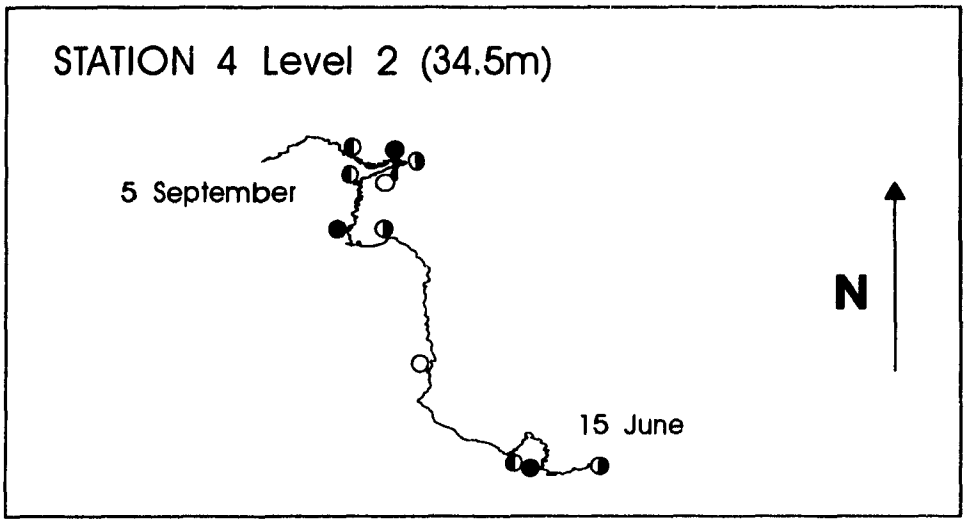
STATION 4 Level 2 (34.5m)
5 September
N
15 June

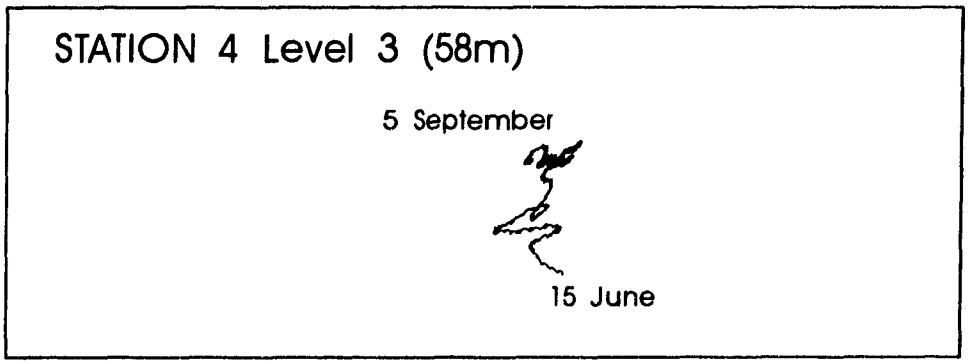
STATION 4 Level 3 (58m)
5 September
15 June

Fig. 48

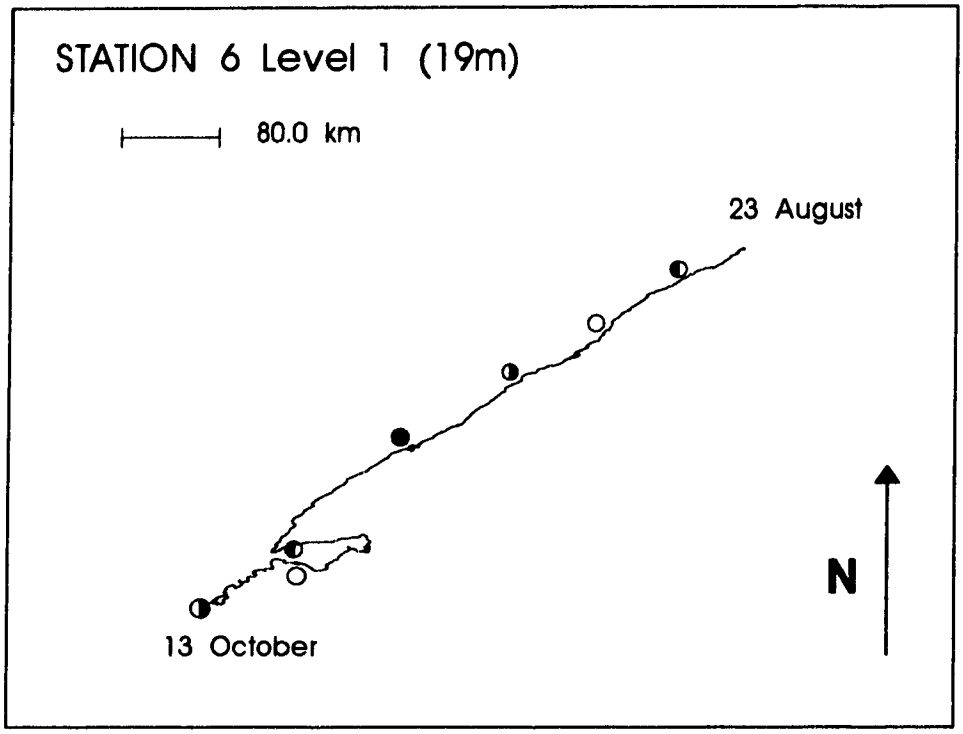
STATION 6 Level 1 (19m)
80.0 km
23 August
13 October
N

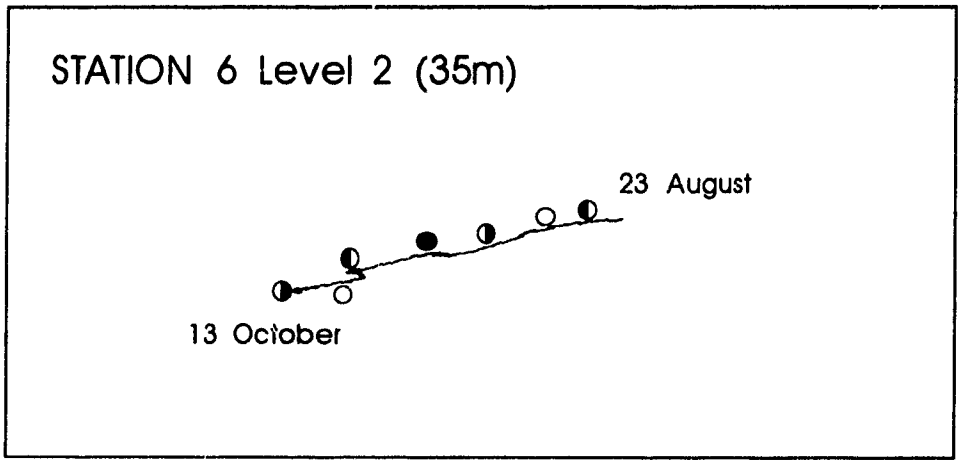
STATION 6 Level 2 (35m)
23 August
13 October

Fig. 49

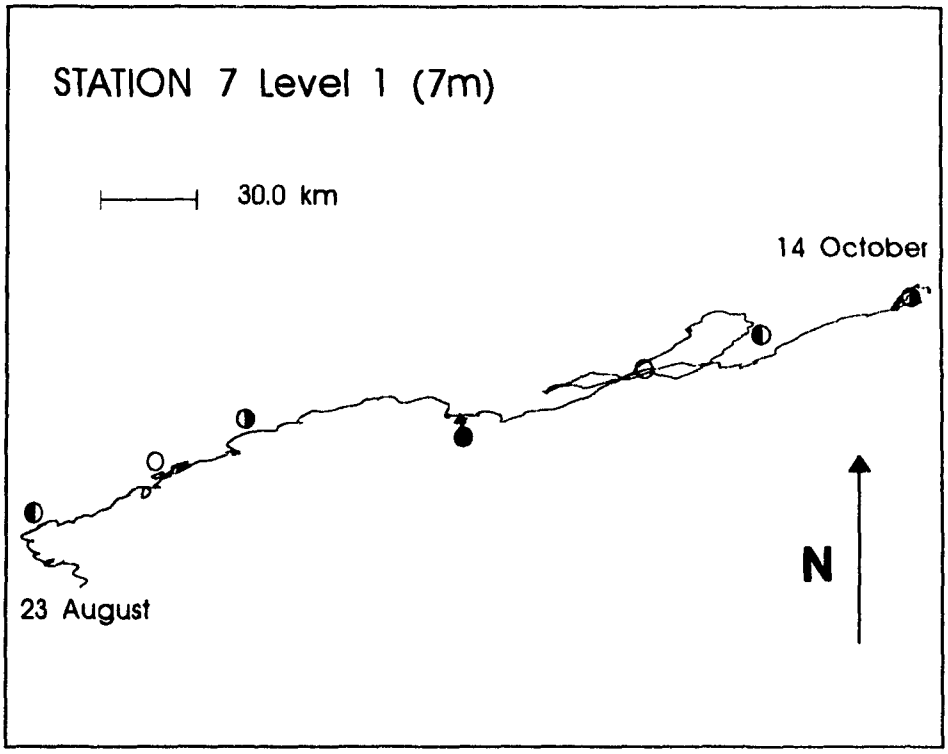
STATION 7 Level 1 (7m)
30.0 km
14 October
23 August
N

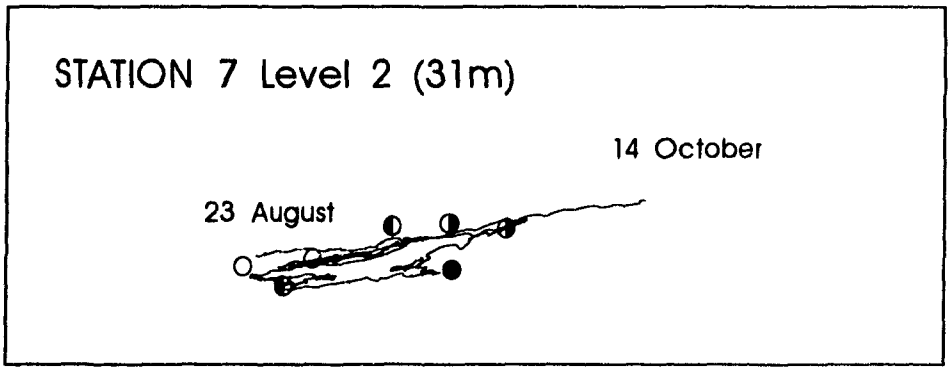
STATION 7 Level 2 (31m)
14 October
23 August

Fig. 50

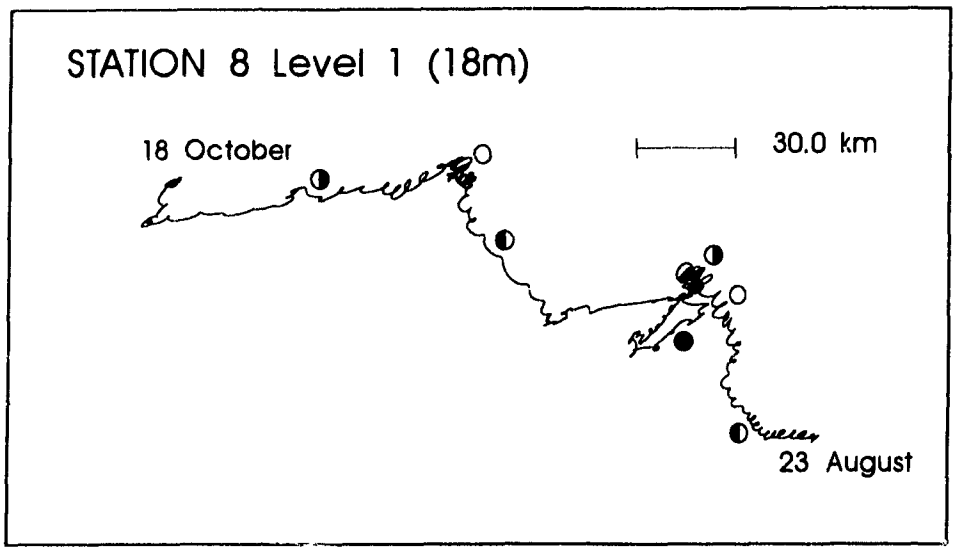
STATION 8 Level 1 (18m)
18 October
30.0 km
23 August

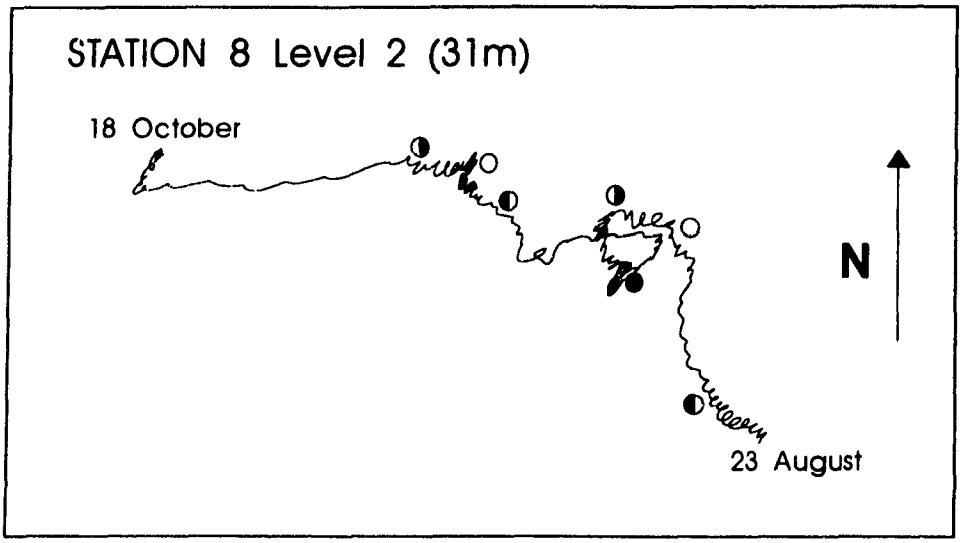
STATION 8 Level 2 (31m)
18 October
N
23 August

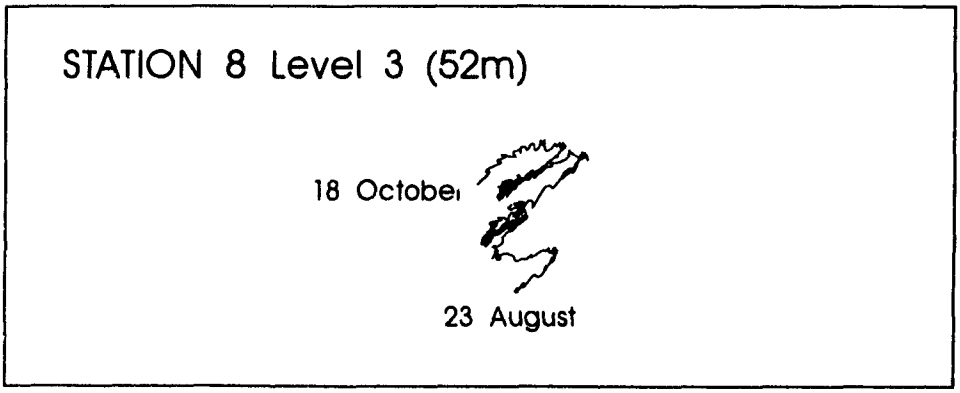
STATION 8 Level 3 (52m)
18 October
23 August

Fig. 51

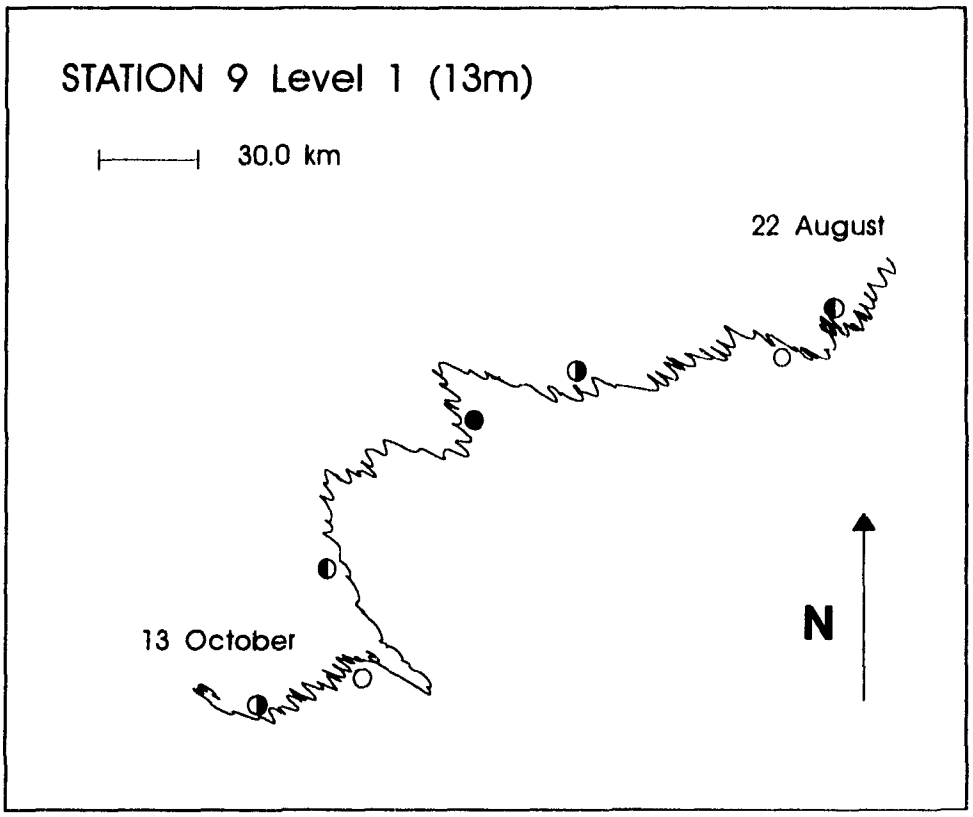

Fig. 52

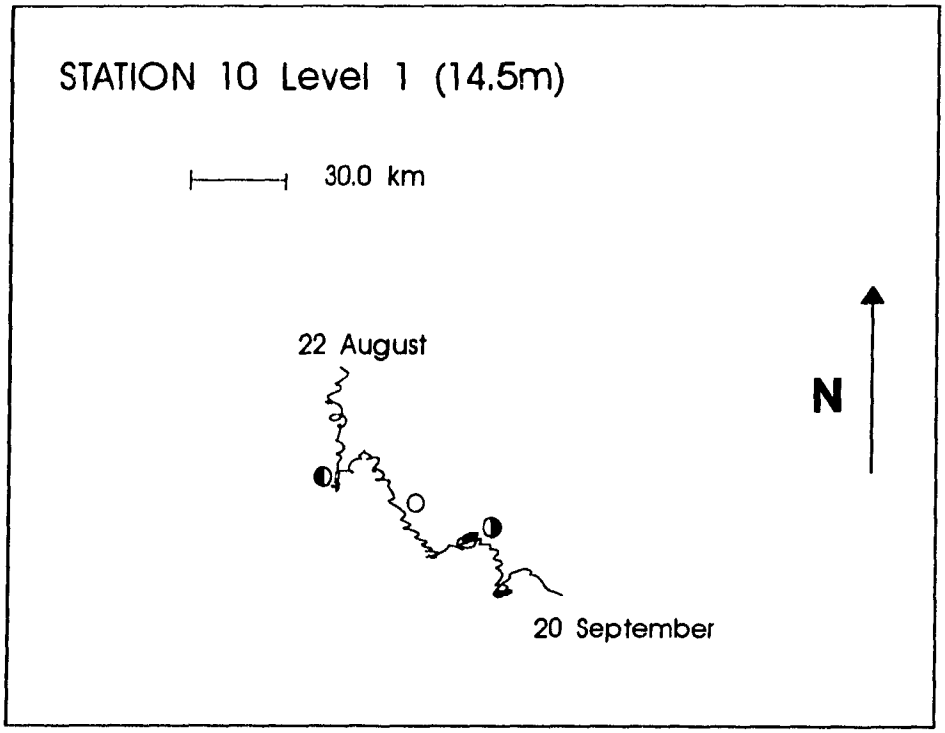

Fig. 53

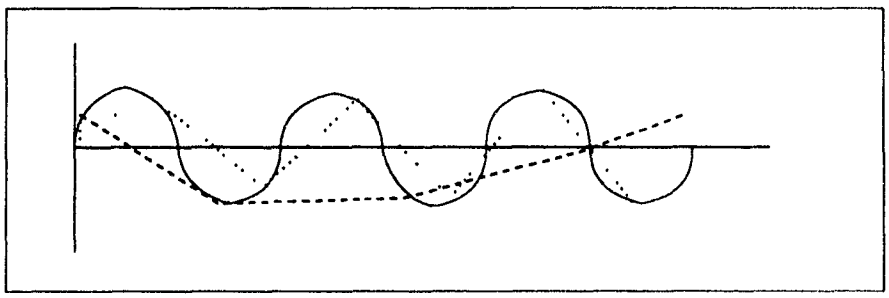

Fig. 54

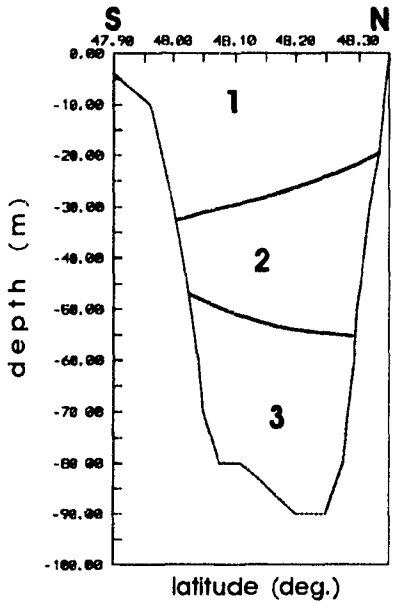
S
N
47.90
48.00
48.10
48.20
48.30
0.00
-10.00
-20.00
-30.00
-40.00
-50.00
-60.00
-70.00
-80.00
-90.00
-100.00
1
2
3
depth (m)
latitude (deg.)

Fig. 55

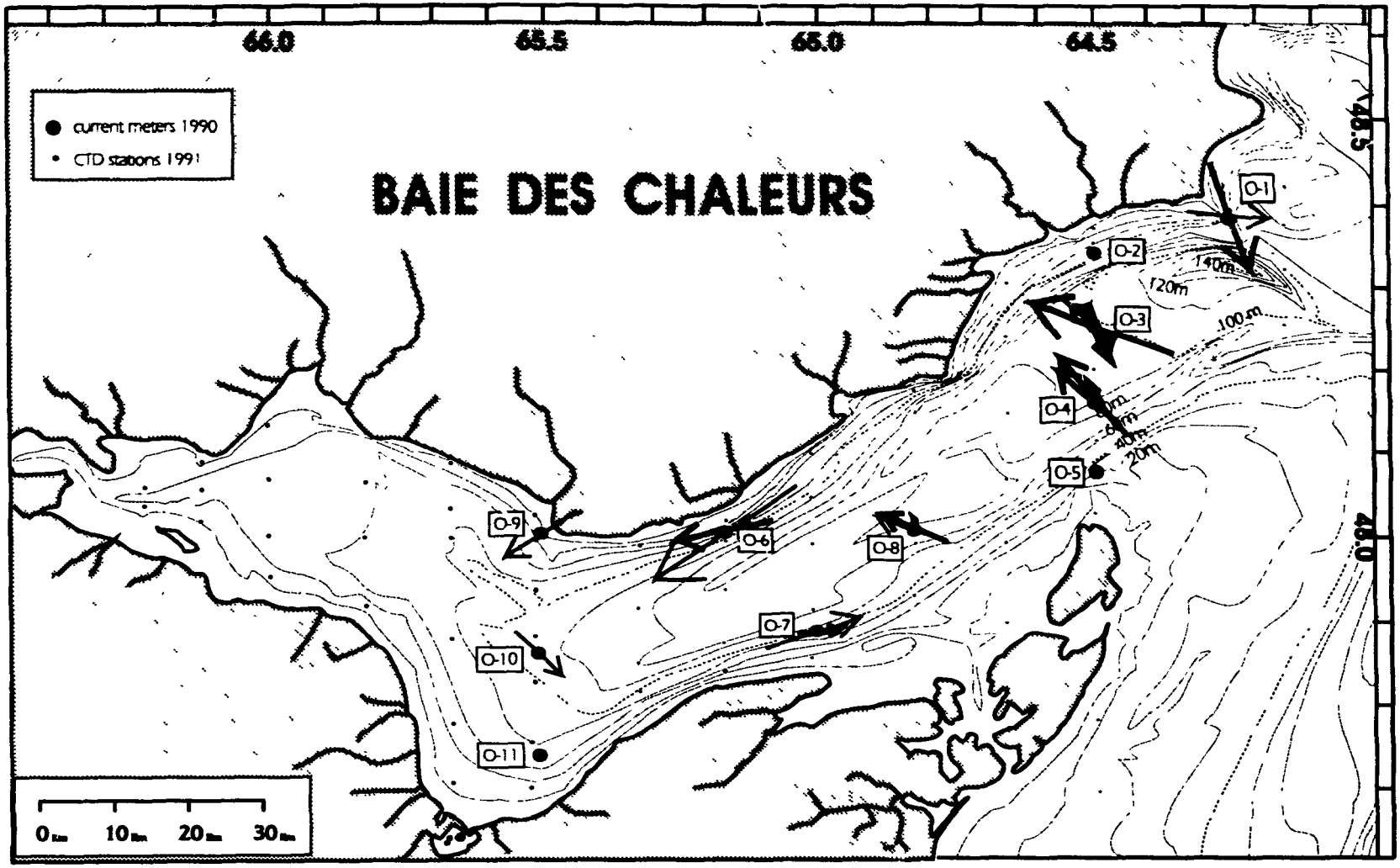
66.0
65.5
65.0
64.5
48.5
48.0
current meters 1990
CTD stations 1991
BAIE DES CHALEURS
O-1
O-2
O-3
O-4
O-5
O-6
O-7
O-8
O-9
O-10
O-11
140m
120m
100m
60m
40m
20m
0km
10km
20km
30km

Fig. 56

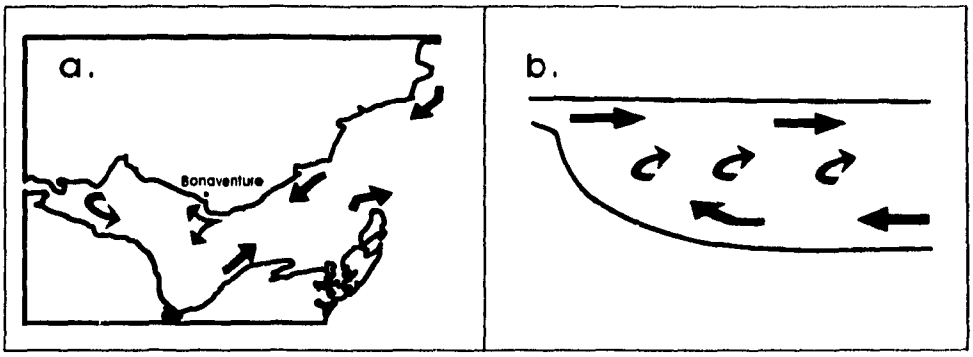

Fig. 57